

Dark Dust and single-cloud sightlines in the ISM

R. Siebenmorgen¹, J. Krełowski², J. Smoker³, G. Galazutdinov^{4,5}, and S. Bagnulo⁶

¹ European Southern Observatory, Karl-Schwarzschild-Str. 2, 85748 Garching, Germany. email: Ralf.Siebenmorgen@eso.org

² Rzeszów University, al. T. Rejtana 16c, 35-959, Rzeszów, Poland

³ European Southern Observatory, Alonso de Cordova 3107, Vitacura, Santiago, Chile

⁴ Instituto de Astronomía, Universidad Católica del Norte, Av. Angamos 0610, Antofagasta, Chile

⁵ Pulkovo Observatory, Pulkovskoe Shosse 65, Saint-Petersburg 196140, Russia

⁶ Armagh Observatory and Planetarium, College Hill, Armagh BT61 9DG, UK

Received: January 15, 2019 / Accepted: June 15, 2020

ABSTRACT

The precise characteristics of clouds and nature of dust in the diffuse ISM can only be extracted by inspecting the rare cases of single-cloud sightlines, which may be identified by the lack of significant Doppler splitting of interstellar lines observed at resolving power $\lambda/\Delta\lambda \gtrsim 75,000$. We have searched for such sightlines using high-resolution spectroscopy towards reddened OB stars for which far UV extinction curves are known. We have compiled a sample of 186 spectra with 100 obtained specifically for this project with UVES. From our sample we identified 66 single-cloud sightlines, about half of which were previously unknown. We have used the CH/CH⁺ line ratio of our targets to establish if the sightlines are dominated by warm or cold clouds. We found that CN is detected in all cold ($\text{CH}/\text{CH}^+ > 1$) clouds, but is frequently absent in warm clouds. We inspected the WISE (3 – 22 μm) observed emission morphology around our sightlines and excluded a circumstellar nature for the observed dust extinction. We found that most sightlines are dominated by cold clouds that are located far away from the heating source. For 132 stars, we derived the spectral type and the associated spectral type – luminosity distance. We also applied the interstellar Ca II distance scale, and compared both these distance estimates with GAIA parallaxes, finding that these distance estimates scatter by $\sim 40\%$. By comparing spectrophotometric distances with GAIA we detected for 9 sightlines a hidden dust component amounting to a few mag of extinction. This *Dark Dust* is populated by $\gtrsim 1\mu\text{m}$ large grains and appears predominantly in the field of the cold ISM.

Key words. ISM: clouds – ISM: lines and bands – Line: profiles – Stars: early-type – (ISM) dust, extinction

1. Introduction

The major physical and chemical characteristics of the ISM are obtained by studying: a) interstellar extinction (reddening), caused by solid particles of submicron size (Trumpler 1930); b) interstellar polarisation (Hong & Greenberg 1980), caused by non-spherical dust particles when they are oriented for instance by the magnetic field; c) spectral lines of interstellar atomic gas, see, e.g., the UV survey by Field (1974), who proved that in the ISM, heavy elements are strongly depleted in comparison to their abundances in stellar atmospheres, that is, they are hidden in dust grains; d) rotational emission features that have been detected for many (~ 200) complex molecules with a dipole momentum; e) bands of simple molecules or radicals, e.g. $\cdot\text{CH}$, CH^+ , $\cdot\text{OH}$, OH^+ , $\cdot\text{SH}$, $\cdot\text{NH}$, $\cdot\text{CN}$, C_2 , C_3 ; f) diffuse interstellar bands (DIBs), discovered by Heger (1922). A more complete list of interstellar and circumstellar diatomics and molecules is available at Wikipedia. Currently, the list of known DIBs exceeds 550 entries (Fan et al. 2019), and the majority of them are very shallow; g) cosmic rays, which ionise parts of the ISM. As evidenced by Krelowski et al. (1992); Fitzpatrick & Massa (2007), and others, the above described interstellar absorption spectra differ from cloud-to-cloud, and large variations in the dust properties are observed (Chini & Kruegel 1983; Krelowski et al. 2019b). These differences demonstrate that all components mentioned above are interdependent, i.e. variations of extinction and/or polarisation curves are accompanied with various strength ratios of atomic and/or molecular features.

One can resolve individual Doppler components in interstellar atomic and/or molecular lines by means of high resolution spectroscopy while extinction and continuum polarisation are necessarily averaged along any sightline. Profiles of interstellar features observed at extremely high resolving power of $\lambda/\Delta\lambda \sim 10^6$ with the UHRF (Diego et al. 1995) or the McDonald (Tull et al. 1995) instruments reveal multiple Doppler components, (e.g. Crane et al. (1995); Barlow et al. (1995); Price et al. (2000); Crawford (2002); Welty & Hobbs (2001); Welty et al. (2003)). Strictly speaking, only very few and nearby sightlines can be considered genuine single-cloud sightlines that do not display fine structures in the Doppler profiles of IS lines. Clouds however, are not static entities. Dynamically they may be colliding, merging or disrupted. Velocity shears, shells, bubbles, and filamentary structures are observed. Cloud structures are impacted by cosmic rays changing the ionization structures of the atoms and molecules. Magneto-hydrodynamical waves generate small-scale cloud structures (Falle & Hartquist 2002). Shocks propagating through the ISM can ablate or destroy the clouds (Klein et al. 1994). In some clouds self-gravitation is at work forming cloudlets (Wada 2008), which are observed as time-variable IS absorption lines (Falgarone et al. 1991; Lauroesch et al. 2000; Price et al. 2000; Welty & Fitzpatrick 2001; Crawford 2002). Fractal cloud structures (Elmegreen 2002) arise from typically subsonic ($\lesssim 0.7\text{ km/s}$) turbulent motions (Barlow et al. 1995; Welty & Hobbs 2001).

Our project is tailored to study global dust characteristics in clouds and we do not consider local small-scale variations in the

detailed cloud morphology. We take that a cloud has about similar physical dust parameters in grain material, abundance, sizes, and that grain alignment might be triggered by the global magnetic field structure. On the contrary, these dust parameters are supposed to vary on a large scale, when clouds are well by several 10 - 100 pc. Therefore in this paper we use the term single-cloud sightline when the observed interstellar line profiles show in high resolution spectra at resolving power $\lambda/\Delta\lambda \sim 75,000$ (FWHM ~ 4 km/s) one dominating Doppler component, that accounts for about half of the observed column density. Of course in some of those "single-cloud sightlines" there may be two or more fine structure components with slightly different radial velocities.

Siebenmorgen et al. (2018) have demonstrated that when observing sightlines that intersect different components (likely not resembling each other), the pristine nature of the extinction and polarisation curve of each individual cloud cannot be recovered. One loses the possibility to investigate the relation between the physical parameters of the dust and the observational characteristics of the extinction and polarisation. The only way to investigate such relations is to inspect sightlines dominated by single clouds. The Large Interstellar Polarisation Survey (LIPS) (Bagnulo et al. 2017) allowed us to simultaneously fit the extinction and polarisation curves of 59 sightlines. Siebenmorgen et al. (2018) applied a dust model composed of silicate and carbon grains, finding that large (>6 nm) spheroidal silicate particles, that are of prolate shape, account for the observed polarisation curves. For 32 sightlines we complemented LIPS data set with UVES archive high-resolution spectra. This enabled us to extract a small number of eight single-cloud dominated sightlines. In that study several correlations between the observed extinction and polarisation characteristics and the physical parameters of the dust were confirmed, and several previously unknown correlations that are significant in single-cloud sightlines only were found, demonstrating the validity of our approach. They observed that interstellar polarisation from multiple-clouds is depolarised hence smaller than that from single-cloud sightlines. We found large variations of the dust characteristics from cloud-to-cloud. However, when a number of clouds are averaged, a similar "mean" of the dust parameters is retrieved representing of what is called the Milky Way mean extinction curve; actually an ill-defined average.

In this paper we present a high-resolution (HR) spectroscopic search for such single-cloud sightlines in the few kpc distance of the solar neighbourhood and for which the far UV extinction curve is known.

2. Observations

Our target selection is aimed at identifying a sample of single-cloud sightlines that are suited for detailed studies of variations of dust properties in the diffuse ISM. For these single-cloud sightlines we need the knowledge of the wavelength-dependence of extinction and polarisation. Therefore we started by considering all 544 sightlines for which the far UV extinction curves between 0.33 – 0.09 μm were derived from IUE (Fitzpatrick & Massa 2007; Valencic et al. 2004) and/or FUSE (Gordon et al. 2009) satellite data. For these stars we performed an extensive search of available optical, high-resolution (HR) spectra ($\lambda/\Delta\lambda \gtrsim 40,000$), which enables the study of the interstellar line profiles. We found archive spectra for 87 sightlines and conducted new observations for 100 sightlines with the UVES spectrometer (Dekker et al. 2000; Smoker et al. 2009).

There are 136 sightlines that have HR spectra with a broad wavelength coverage appropriate for a detailed analysis. They are catalogued in Table 1, where we specify (1) the identification number (ID) used in this paper, the target name for which we favour (2) the HD identifier and if different provide the (3) main name as used in SIMBAD, (4) the V band magnitude, (5) the reddening $E(B-V)$, (6) the extinction A_V , (7) the total-to-selective extinction R_V , (8) the previous classification of the spectral type with its literature reference, (9) our spectral classification based on the HR spectroscopy (Sect. 3.1), and (10) the instrument used to obtain HR spectroscopy. The uncertainties for A_V , $E(B-V)$ and R_V given in Table 1 take into account the scattering between different estimates found in the literature (Wegner 2003; Fitzpatrick & Massa 1990; Valencic et al. 2004; Gordon et al. 2009) for the same star. We add a systematic error of 0.05, 0.02 and 0.2 magnitudes to the uncertainties for A_V , $E(B-V)$ and R_V , respectively. For these stars we examined mid-IR imaging.

We found accompanying UVES spectra of 50 stars that were observed with limited wavelength coverage but include the K α line at 7699 Å. The K α line, as we will see, is a good indicator for classifying a sightline to be dominated by a single or multiple velocity components. These stars (IDs 137 – 186) are listed separately in Table 2 together with the ESO program ID as reference and fit parameters of the K α line profile.

2.1. New UVES observations

We performed UVES observations of 100 stars using the standard "390+760" setting that led to a wavelength range of approximately 3270 – 4450 Å in the blue arm, 5700 – 7520 Å in the lower red arm, and 7660 – 9460 Å in the red upper arm with some gaps between the spectral orders. The setting was chosen to cover the Na α lines at 3302.4, 3303, 5890, and 5895.9 Å Ca α H and K doublet at 3933.7 and 3968.5 Å, K α at 7699 Å, the strong DIBs at 5780 and 5797 Å, as well as a host of other interstellar lines such as, when our signal-to-noise ratio (S/N) is sufficient, Ti α 3383.8 Å, CH 4300.3 Å, CH $^+$ 4232.5 Å, and CN 3874.6 Å. The typical S/N per pixel for the reduced data was 130 around Ca α (3933.6 Å) and 200 around Na α (5890 Å). The slit width was set to 0.5'', that provided a spectral resolution (as measured from telluric lines) of $\lambda/\Delta\lambda \sim 75,000$. We note that Welty et al. (1994, 1996) detected Ca α and Na α components separated by as little as 0.5 km/s, components that would remain unresolved in our data.

We processed UVES raw data and measured line profiles in the reduced spectra with our interactive analysis software DECH¹. The automatic data reduction of the UVES spectra by the ESO pipeline may show several shortcomings which potentially affect the quality of the extracted spectra. We noticed: *i*) imperfection of the algorithm that automatically finds the position of the spectral orders, *ii*) a sub-optimal setting of the integration limits, *iii*) a robust but simplified algorithm that averages different spectra of the same star in which low quality data are not excluded. In two out of 126 UVES spectra, the unsupervised automatic extraction with default parameters failed. In Fig. 1 we demonstrate the benefit of performing an interactive data analysis as compared to an automatic reduction.

For the DECH data reduction, we averaged bias images for subsequent correction of flat-field, wavelength calibration, and stellar spectra. The scattered light was determined as a complex shaped two-dimensional surface function, which is individually

¹ available upon request to G. Galazutdinov.

Table 1. Study sample sorted by HD number . The meaning of the columns is: 1) Identification number, (2) HD identifier, (3) if different the main name of the star as used in SIMBAD, (4) V magnitude, (5) reddening E(B-V), (6) visual extinction A_V , (7) total-to-selective extinction R_V , (8) spectral type from previous literature, (9) spectral type as derived in this work, and (10) instrument used to obtain high-resolution spectroscopy.

| 1 ID | 2 Name | 3 SIMBAD | 4 V mag | 5 $E_{(B-V)}$ | 6 A_V mag | 7 R_V | 8 Spectral Type literature | 9 Spectral Type this work | 10 Instrument |
|---------|-----------|-------------|---------------|------------------|-------------------|-----------------|----------------------------------|---------------------------------|-------------------|
| 1 | HD 023180 | * omi Per | 3.83 | 0.29 ± 0.03 | 0.91 ± 0.08 | 3.14 ± 0.31 | B1IV ^F | B4IV | UVES ^b |
| 2 | HD 024263 | * 31 τ | 5.69 | 0.21 ± 0.06 | 0.72 ± 0.22 | 3.44 ± 0.65 | B5V ^V | B4IV + binary | UVES ^a |
| ... | | | | | | | | | |
| 135 | HD 326333 | V* V920 Sco | 9.62 | 0.45 ± 0.03 | 1.52 ± 0.08 | 3.38 ± 0.28 | B1V ^F | B1V + cloud | UVES ^a |
| 136 | HD 326364 | | 9.60 | 0.62 ± 0.03 | 1.80 ± 0.08 | 2.91 ± 0.25 | B0IV ^F | B3IV + cloud | UVES ^a |

Notes: Cols. 5–7 extracted from Gordon et al. (2009), Fitzpatrick & Massa (2007), with uncertainties revised as explained in the text. Spectral types as derived by: ^F Fitzpatrick & Massa (2007), ^G Gordon et al. (2009), ^H Houk (1982), ^{HS} Houk & Swift (1999), and ^V Valencic et al. (2004). Spectroscopic data from: *a*: this work; *b*: Cox et al. (2017); *c*: UVES prog ID 096.D-0008(A) (unpublished ESO archive); *d*: UVES prog ID 099.C-0637(A) (unpublished ESO archive); *e*: Bagnulo et al. (2013); *f*: Sembach et al. (1993); *g*: Welty & Crowther (2010); *h*: Tolstoy et al. (2003); *i*: Krelowski et al. (2010); *j*: SAO 1.0 m; *k*: SOPHIE archive; *l*: ELODIE archive. For the complete list see Table A.1.

Table 2. UVES archive spectra covering the K₁ line. The meaning of the columns is: 1) Identification number, (2) HD identifier, (3) ESO program ID, and (4–5) fit parameters of the K₁ line profile. Single-cloud sightlines are highlighted in boldface.

| 1 ID | 2 Star | 3 Prog. ID | 4 v_{\odot} km/s | 5 $\log(N)$ cm ⁻² |
|---------|------------------|---------------|--|--|
| 137 | CPD 592600 | 071.C-0513(C) | -17.71±0.90 -4.67±0.11 1.81±0.03 | 10.62±0.08 11.00±0.02 11.66±0.01 |
| 138 | CPD 573509 | 094.D-0355(A) | -3.25±0.04 9.22±0.31 | 11.86±0.01 11.14±0.05 |
| 186 | Walker 67 | 092.C-0019(A) | 26.84±0.03 | 11.66±0.01 |

Notes: For the complete list see Table A.2.

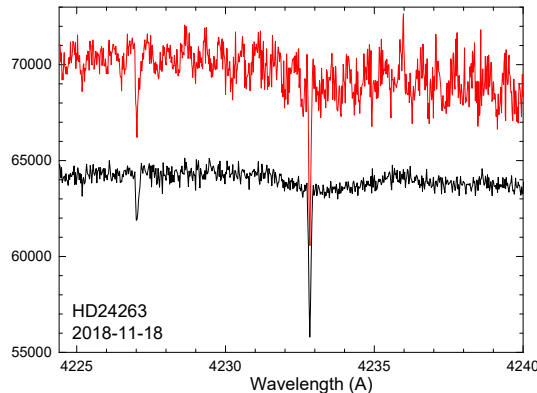


Fig. 1. A small region of the spectrum of the HD 24263 sightline obtained with the aid of UVES pipeline (upper line in red colour) and with our own DECH interactive analysis system DECH (lower line in black colour). The weak feature shortward of the CH⁺ line is the feature of ¹³CH⁺.

calculated for each stellar and flat-field frame by a cubic-spline approximation over manually selected areas of minima between the spectral orders. Then, the pixel-to-pixel variations across the CCD was corrected by dividing all stellar frames by the averaged and normalized flat-field frame. One-dimensional stellar spectra were extracted by simple summation in the cross-dispersion direction along the width of each spectral order. The extracted spectra of the same object observed in the same night were averaged to achieve the highest S/N ratio. Fiducial continuum normalization was based on a cubic spline interpolation over the

interactively selected anchor points. The wavelength scale of the spectra was calculated on the basis of a polynomial:

$$\lambda(x, m) = \sum_{i=0}^k \sum_{j=0}^n a_{ij} x^i m^j, \quad (1)$$

where a_{ij} are polynomial coefficients, x^i the pixel position in dispersion direction, and m^j the order number, respectively. Depending on the spectrograph's arm typically 700 and up to 1200 lines of the Thorium lamp were used in the final wavelength solution. The rms residual error between the fit and the position of the lines is usually $\leq 0.003\text{Å}$, i.e. much lower than 1 km s^{-1} . Due to the fact that the wavelength calibration was not taken directly after the observations, but in the morning after, the absolute error will be somewhat larger. Radial velocities and equivalent width (EW) were measured using Voigt multi-component profile fits and the direct integration methods available in the DECH code.

2.2. Archive HR spectra

In addition to the 100 stars observed by us with UVES we have found HR spectra of 87 other sightlines. There are 17 UVES spectra taken in the context of the EDIBLES survey (Cox et al. 2017), which covers almost the entire optical wavelength range from 320 to 1000 nm with S/N exceeding 500 per pixel. One spectrum was taken from existing data (co-author Galazutdinov) of both the 1.0 m Zeiss Special Astrophysical Observatory of the Russian Academy of Sciences, and the 1.8 m Bohyunsan Optical Astronomy Observatory in Korea. Eighteen spectra were taken from ELODIE (Moultaka et al. 2004), FEROS (Kaufer et al. 1999), SOPHIE² and ESO UVES archives, or their single or multiple cloud status was determined by a literature search using SIMBAD. These 36 sightlines with archive spectra are provided in Table 1. We have found additional public available UVES spectra for 50 stars which were observed with sparse wavelength coverage but include the K₁ line and are presented in Table 2.

2.3. WISE mid-IR imaging

In addition to optical HR spectroscopy, we searched for mid-IR data which provide dust emission signatures of the clouds. Mid-IR imaging is obtained with the Wide-field Infrared Survey Explorer (WISE, Wright et al. 2010) for all sources of Table 1. WISE³ mapped the sky at 3.4, 4.6, 12, and 22 μm (W1, W2, W3,

² atlas.obs-hp.fr/sophie

³ images available at: <https://irsa.ipac.caltech.edu/applications/wise/>

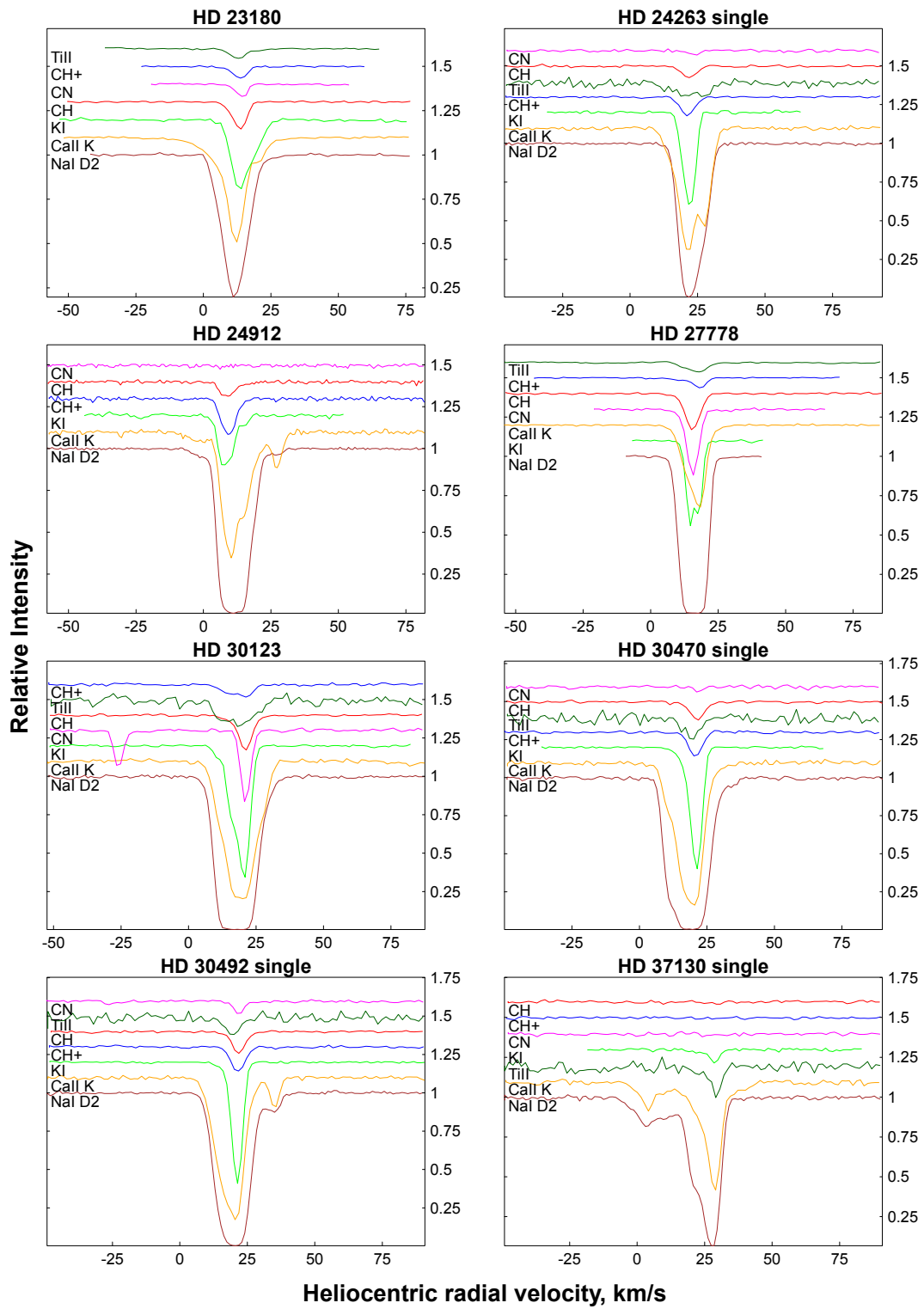


Fig. 2. UVES derived heliocentric velocity profiles in Ti II 3383.8 Å (dark green), CN 3874.6 Å (magenta), CH 4300.3 Å (red), CH^+ 4232.5 Å (blue), K I 7699 Å (green), Ca II K 3933.7 Å (orange), Na I D2 5889 Å (brown). Single-cloud sightlines are marked “single”. For the remaining spectra see Fig. A.1 to Fig. A.16.

W4) in 2010 with an angular resolution of 6.1'', 6.4'', 6.5'', and 12.0'' in the four bands, respectively. WISE achieved 5σ point source sensitivities better than 0.08, 0.11, 1 and 6 mJy.

Table 3. Result summary. The meaning of the columns is: (1) Identification number as of Table 1, (2) HD identifier, equivalent width (EW) of (3) Ca II K and (4) Ca II H doublet used for (5) distance estimate (Megier et al. (2009)). Distances obtained from (6) GAIA parallax and (7) spectral type-to-luminosity ratio. Appearance of single (S) or multi (M) velocity components of profiles for (8) Ca II H and K, (9) Na I, (10) K I lines. Fit parameters of the K I line profile: (11) position, (12) column density, and (13) derived equivalent width. (14) Classification of cloud environment as cold (c) or warm (w) with or without CN I detection. (15) Infrared morphology of WISE (W4) image. Single-cloud sightlines are highlighted in boldface.

| 1 ID | 2 Target | 3 Ca II | 4 | 5 Ca II | 6 GAIA | 7 Sp/L | 8 Ca II K | 9 Na I | 10 K I | 11 v _∞ (km/s) | 12 log N (10 ⁹ /cm ²) | 13 EW (mÅ) | 14 Environ. | 15 WISE |
|---------|------------------|---------------|---------------|--------------------------------------|--------------------------------------|-----------|--------------|-----------|-----------|--------------------------------|--|------------------|----------------|------------|
| | | EW(K) (mÅ) | EW(H) (mÅ) | Ca II (pc) | | | | | | | | | class | class |
| 1 | HD 023180 | 86±2 | 47±1 | 340 ⁺²⁰ ₋₁₅ | 256 ⁺⁷² ₋₄₇ | 320 | S | S | M | 13.08 | 464±11 | 69.1±1.6 | c+CN | a |
| 2 | HD 024263 | 129±3 | 84±2 | 670 ⁺⁶⁵ ₋₅₀ | 222 ⁺⁸ ₋₈ | 210 | M | S | S | 21.93 | 706±10 | 90.6±1.2 | - | a |
| ... | | | | | | | | | | | | | | |
| 135 | HD 326333 | 391±16 | 260±13 | 1980 ⁺⁴⁶⁰ ₋₂₂₀ | 1500 ⁺¹³⁴ ₋₁₁₄ | 1960 | M | M | M | -10.64 | 237±12 | 39.1±1.9 | c+CN | a |
| | " | | | | | | | | | 1.64 | 570±7 | 76.9±0.9 | w-CN | |
| 136 | HD 326364 | 378±23 | 196±13 | 1597 ⁺³⁷⁹ ₋₂₃₃ | 1679 ⁺¹⁴⁹ ₋₁₂₇ | 1859 | M | M | M | -8.67 | 437±7 | 64.3±1.2 | c+CN | a |
| | " | | | | | | | | | 1.69 | 945±8 | 106.9±0.9 | w-CN | |

Notes: ^LR low resolution spectrum has insufficient resolving power for classification as single-cloud sightline, ^s saturated line, ^v: ignored because lines have different velocities, ^e: WISE image shows artifact. For the complete list see Table A.3.

3. Analysis of spectroscopic data and mid-IR imaging

In this Section we present our spectral classification (Sect. 3.1) of the sample (Table 1), measurements of radial velocities and equivalent widths (Sect. 3.2). In Sect. 3.3 we derive column densities from the K I profile and identify the single-cloud sightlines. We then use the CH/CH⁺ line ratio to classify the environment of the clouds to be either cold or warm (Sect. 3.4), and in Sect. 3.5 we analyse WISE mid-IR images of our sightlines to constrain the location of the dust emission. We apply three different methods to estimate distances to the targets (Sect. 4.1).

HD 164747A and HD 164747B are separated by 3.4'' and not resolved by IUE. Both stars are covered in our UVES image. They are of same spectral type and show a different Doppler structure of Ca II lines. The intensities of DIBs are identical and thus one can assume that extinction curves are also identical. We remove from our analysis HD 123335 (ID 59), HD 134591 (ID 62), HD 147331 (ID 70) and HD 151346 (ID 79) because of contamination of the lines. We spectroscopically classified 136 stars of Table 1 and carried out the remaining analysis on 132 stars with results summarised in Table 3.

3.1. Spectral classification

The knowledge of the spectral type is important for estimating the reddening and spectrophotometric distance of a star. Our high resolution spectra allow accurate measures of line intensities and profiles. We apply a two-step approach by estimating the spectral class of the stars following the procedure described and exemplified by Krełowski et al. (2018). The first step is based on the measured ratios of H I, He I and Mg II line strengths as suggested by Walborn & Fitzpatrick (1990) and by the Stony Brook catalogue⁴. The position of OB standard stars in the Mg II/He I versus H I/He I plane is shown and tabulated by Krełowski et al. (2018). For example, in that scheme a B6 star has Mg II/He I ~ 0.9 and H I/He I ~ 20, while a B9.5 star shows Mg II/He I ~ 2.6 and H I/He I ≥ 70, respectively. The second step includes confirmation or correction of our initial spectral type classification through careful inspection of the high resolution spectra of the considered stars. This includes interpretation of possible incompatibilities. In this second step, we inspect various line profiles

of H I, He I, He II, C IV, Mg II, Si II, Si III, and Si IV. The detection of He II and C IV lines point to O type stars while the presence of Si IV to an early B star. Higher strength ratio of the He I 4471 in comparison to Mg II 4481 provides another indication for early B type stars. At mid B, the intensity of Si IV 4089 and Si III 4552 lines relative to that of Si II 4128-30 is the defining characteristic, while for late B, it is the intensity of Mg II 4481 relative to that of He I 4471, following Walborn (2008). Hydrogen Balmer line profiles provide evidence of a dwarf or a high luminosity star. The similarity of lines such as the series of He I at 3965, 4009, 4026, 4121, 4144, 4169, 4388, 4437, 4713, 4923 and 5876 Å is characteristic for B type stars if He II lines are absent. We also checked for signatures of multiple stellar components and binarity as apparent from the profile shapes. Intensities of weak stellar lines in fast rotators or in binaries are hard to estimate and create uncertainties in Sp/L determinations.

Our newly estimated spectral types, as well as those previously given in the literature, are listed in cols. 7 and 8 of Table 1, respectively. For 89 out of the 136 stars both estimates agree to within one subclass. Eighteen stars were previously classified as B0-V while we identified them as O type stars with 12 as O9 and the other between spectral type O6-8. Twenty two stars of our sample appear as spectroscopic binary stars, and 13 are in SIMBAD associated to a cloud. In the following paragraphs we discuss the discrepant cases and why we decided on a binary classification for some objects.

The typical signature of O type star is the presence of both C IV 5801.3 and C IV 5811 lines that are not seen in B type stars. In O7 stars, the He I line near 4471.5 is as deep as He II 4541.6. In even hotter stars, He II feature becomes stronger, while in late O type stars the He I line becomes dominant. For example in Herschel 36 we classify it as O8V, the C IV lines are detected while Mg II is barely seen, and He I is stronger than He II.

The luminosity class of a star can be estimated by the H I lines profile. Our classifications were done by comparing the spectra of our targets with those given as standards by Walborn & Fitzpatrick (1990). Supergiants and bright giants (class I and II) show narrow H I lines such as HD 46711 and HD 91943. Main sequence stars (class IV and V) show broad H lines such as HD 37903, HD 108927 and HD 147196.

Spectral types of several objects may be uncertain if they belong to a binary system, and the apparent binarity is revealed by double, blended profiles that are difficult to separate in the two

⁴ http://www.astro.sunysb.edu/fwalter/SMARTS/spstds_f2.html

components. We classify HD 315032 as early B0 star because Mg II is barely seen. HD 156247 appears as a binary in He I, Mg II and C II lines. The He I line profile appears likely blended in HD 315033 and in HD 161653, for which broad wings of H I lines and many O⁺ lines are detected. We classify HD 161653 as B3 II although it was classified as B0.5 III by Valencic et al. (2004), and as B2 II by Houk (1982). The classification is uncertain because this star is apparently binary and the "red" component of He I seems broader than in Mg II. Hydrogen lines have broad wings, which is characteristic for dwarfs. However, if the star is of class IV, the Sp/L distance becomes only ~ 660 pc, while GAIA and Ca II measurements put it further than 1 kpc away. In our class II the Sp/L distance of HD 161653 becomes 1230 pc very consistent with the other distance estimates (cmp. Table 3).

3.2. Radial velocity and equivalent width measurements

We converted the spectra of Table 1 into normalised intensity versus heliocentric velocity for the profiles of the following spectral lines: Ti II 3383.8 Å, CN 3874.6 Å, Ca II K 3933.7 Å, CH 4300.3 Å, CH⁺ 4232.5 Å, Na I 5890 Å, and K I 7699 Å. (see Fig. 2 and Figs. A.1 – A.16). We note that the profiles of Ti II and Ca II K lines often appear similar (see Hunter et al. 2006) as do Na I and K I. Apart from these seven lines, we inspected other lines like Ca I 4227 Å and DIBs covered in the observed wavelength range of our observations, finding that they had often low S/N or, like Na I 5895.9 Å are frequently saturated. In addition to the heliocentric velocities, for the seven lines listed above we also measured the equivalent widths for the Ca II H and K doublets as given in cols. 3 and 4 of Table 3. Interstellar lines often do not show the same radial velocities and appear in three distinct families. Usually radial velocity of a) K I and CH coincide nearly perfectly and likely also with CN, while b) CH⁺ frequently shows a shift. c) Ca II lines are quite frequently of very complex Doppler structure in contrast to other IS lines while Ca II and Ti II show similar profiles. DIBs seem to originate in clouds following K I (Galazutdinov et al. 2000).

3.3. Identification of single-cloud sightlines

We classified the appearance of the radial velocity profiles of Ca II K, Na I, and K I as single (S) or multi (M) components sightlines. The results are given in cols. 8 – 10 of Table 3. Saturated Na I lines for which a classification was not possible are marked by a hyphen. We find that the K I line is particularly suited for the S or M classification. The K I profile is fit by a multi-component Voigt function using position, column density as free parameters; in order to estimate the column density, we applied the apparent optical depth method described by Savage & Sembach 1991 as implemented in DECH. The best-fit parameters to the K I profiles are given in col. 4 (position) and col. 5 (column density) in Table 2 and in col. 11 and col. 12 in Table 3, respectively. We found that for 80 of the 132 sightlines of Table 3 that allowed us to perform this analysis, the fit to the K I profile required multiple components, while 52 of these stars were fit by a single component model. In addition we found that 14 of the 52 stars of Table 2 are dominated by a single component.

A number of objects have been observed in the K I and Ca I surveys by Welty & Hobbs (2001) and Welty et al. (2003), who utilized the UHFR or McDonald spectrographs. These observations are consistent with our classifications of multi-component sightlines. For example, the multi-component sight-

line HD 23180 shows in UVES a very asymmetric K I profile and reveals in the spectra by Welty et al. (2003) four components between 10.5–14.9 km/s. HD 27778 shows in UVES a double peak in K I which is confirmed in the spectrum by Welty & Hobbs (2001) showing four about equally strong components between 14.1–18.6 km/s. More interestingly there are HD 207198 and HD 209975 that show multiple components in the Welty & Hobbs (2001) and Welty et al. (2003) spectra whereas these lines appear in ELODIE and SOPHIE spectra as single component. Both of the latter instruments have about half the resolving power provided by UVES, obviously insufficient for characterization as single-cloud sightline. There are 8 similar low resolution spectra in our sample that therefore cannot be classified. These stars are marked LR in Table 3. There are four stars with decent signal to noise spectra by Welty & Hobbs (2001) and Welty et al. (2003) that are in common to our single-cloud sightlines: HD 147165, HD 147889, HD 147933, and HD 149757. All of them show within ± 1.5 km/s a single dominating component which is a factor of 2 - 3 stronger in column density than 3 - 4 accompanying fine structure components. The ultra-high resolution spectra confirm of what we call a single-cloud sightline when observed with UVES.

In total, we found that 66 of the 186 stars of this investigation may be classified as single-cloud sightlines, with 31 of them already previously identified as such (Sembach et al. 1993; Ensor et al. 2017; Siebenmorgen et al. 2018).

3.4. Cloud environment

Diffuse clouds show significant variations in their physical conditions depending on their density, strength of the radiation field, cosmic ray intensity, and whether shocks are present or not. The strength of simple radicals such as CN, CH, CH⁺ as well as DIBs are known to vary from cloud to cloud (Krełowski & Walker 1987). The presence of CH⁺ gives particular insights into the environmental condition of the clouds. CH⁺ is produced in warm shock wave or strong UV field heated media, and rapidly destroyed by collisions with H, H₂, and e⁻ (Morris et al. 2016). The carriers of broad DIBs like the 5780 Å band are more abundant when simple radicals are destroyed. This seems to happen in strongly irradiated warm clouds where CN is often not seen. Regions showing weak ionization with line intensity ratios CH/CH⁺ $\gtrsim 1$, seem to be connected to low irradiated cold environments (Krełowski et al. 2019a), and there the CN line is detected. We show this result in Fig. 3 for HD 112607, HD 110715, and HD 30123 where CN is detected and the cloud is cold (CH/CH⁺ $\gtrsim 1$), and in Fig. 4 for HD 146285, HD 148579, and HD 287150 where CN is not detected and the cloud environment is warm (CH/CH⁺ < 1). This finding has been reported for five of our stars⁵ by Pan et al. (2005), where CH and CN column densities for moderately high density gas ($n > 30 \text{ cm}^{-3}$) correlate and no CN is detected in low density regions showing CH⁺.

The strength of the lines and DIBs is further discussed by Weselak et al. (2008); Krełowski et al. (2019a). In this work we have inspected the CH A-X 4300.3 Å, CH⁺ 4232.5 Å and the CN 3874.6 Å line in spectra of our sample (see Fig. 2, and Figs. A.1 – A.16). The wavelength ranges of these lines are included in the spectra of 109 of our sample of stars. Thirteen of them have in CH and CN low S/N. In five stars, the CH lines were not detected. Three multi-component sightlines show significant velocity shifts between the lines and were excluded from the anal-

⁵ HD 147888, HD 147933, HD 204827, HD 206267, and HD 207198

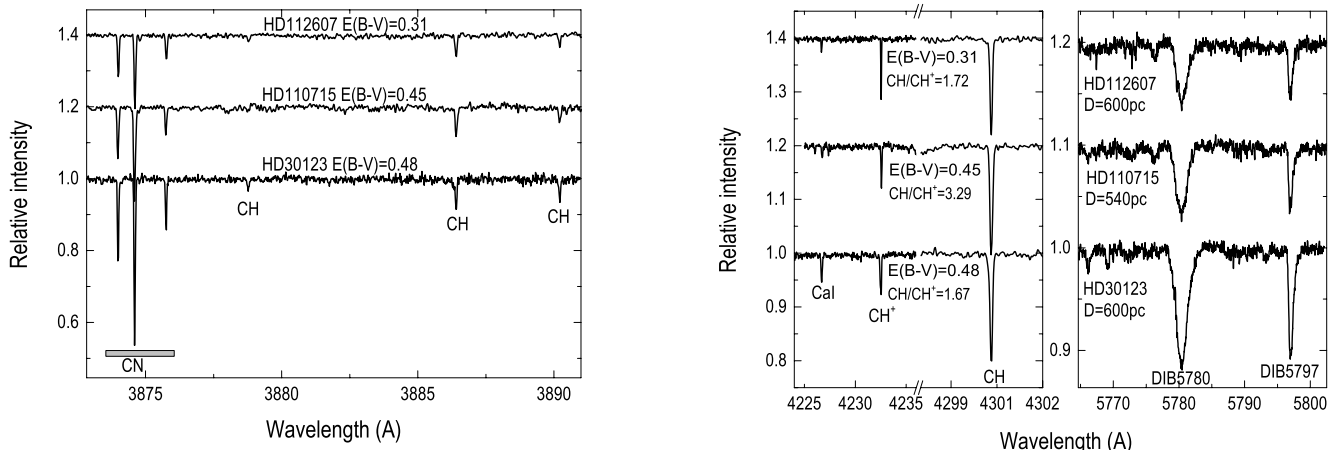


Fig. 3. Spectral features of the rotational R1, R0, and P1 transitions of Cyanogen (CN) near 3875Å (left), CH⁺ 4232.5Å and CH A-X 4300.3Å transition (middle), and DIBs at 5780Å and 5797Å (right panel) for three single-cloud sightlines HD 112607, HD 110715, and HD 30123. The CH/CH⁺ line intensity ratio, $E_{(B-V)}$, distance, and some other lines are labelled.

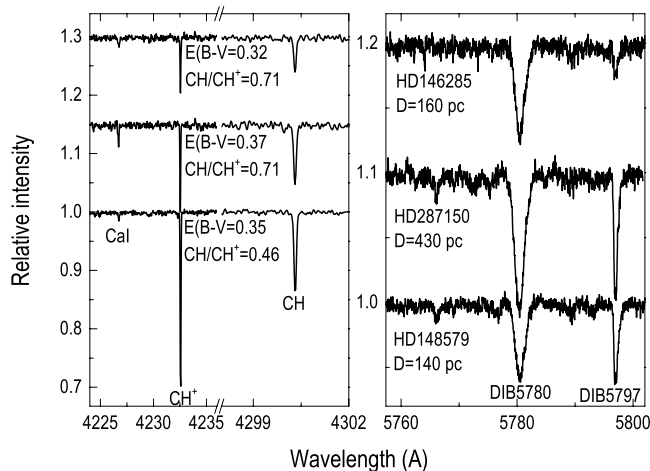


Fig. 4. Spectra of CH⁺ 4232.5Å and CH 4300.3Å transition (left) and DIBs at 5780Å and 5797Å (right panel) for three single-cloud sightlines HD 146285, HD 148579, and HD 287150. The CH/CH⁺ ratio, $E_{(B-V)}$ reddening, distance, and Ca I line are labelled.

ysis. This leaves us with 88 spectra. In six of them CH and CN split in two clearly separated velocity components, and because of multi-component sightlines we were able to measure 97 ratios of CH/CH⁺ with or without detection of CN lines. For them we report in col. 14 of Table 3: 39 warm clouds ($CH/CH^+ < 1$) where the CN line is not detected, labelled w-CN; 54 cold clouds ($CH/CH^+ \gtrsim 1$) where the CN line is detected, labelled c+CN; and only four warm clouds where CN is detected, labelled w+CN. The CN line is detected in all clouds assigned as “cold”.

Data in CH and CN bands are available in 39 out of 52 single-cloud sightlines with spectra covering these features (Table 3). For them CN is detected in 23 out of 38 single-clouds classified as cold. Except HD 156247, CN is missing in all other 14 single-clouds classified as warm. In case that the cloud is close to the OB star it should be warm. Clouds of single-cloud sightlines are cold and are predominantly located far away from the star in the cold ISM.

3.5. Analysis of mid-IR imaging

We complemented our spectroscopic analysis by using archive mid-IR imaging, to assess the nature of the cloud environment. Dust is heated by UV and optical stellar light and re-emits the absorbed energy at infrared (IR) wavelengths. Inspecting the appearance of our sources in the mid-IR may allow us to constrain the location of the dust cloud(s) along the sightline that is either nearby the star in a circumstellar envelope or further away in the diffuse ISM. We studied the connection of star and dust emission along the sightlines by inspecting the morphology of mid-IR images provided by WISE, in a $5' \times 5'$ field centred on our stars.

The observed mid-IR fluxes are dominated either by star or dust emission. If the flux is dominated by dust emission, it is likely resolved in the WISE W3 and W4 bands. This can be demonstrated by computing the dust emission of a circumstellar dust envelope of a mixture of large 600 nm sized carbon and silicate grains that are heated by a typical B type star of our target list. The star has a luminosity of $10^4 L_\odot$ and temperature of 20,000 K. The shell has an inner boundary set by dust evaporation at temperature ~ 1500 K and an outer radius of 1 pc. For a dust envelope with a constant density and dust mass of $0.8 M_\odot$ the total optical depth $\tau_V = 1$. In this shell dust becomes warmer than 80 K up to distances of a few 10^{17} cm. This envelope may be detected with the spatial resolution of WISE⁶ up to 1 kpc distance, and more so if the emission, for example in W3, is dominated by very small (nanometre) particles such as PAHs (Siebenmorgen (1993); Krügel (2008)). One may consider that dust clouds have much higher optical depth than estimated adopting the A_V of the sightline to the star (Table 1). In this case, the clouds could be heated by embedded stars. As such stars are unseen in the near-IR, but in the mid-IR the optical depth must be very high ($A_V \geq 10$ mag) making such a scenario for the A_V of our sightlines unlikely.

We classified the morphology of the WISE images and distinguished the following cases:

a) absence of dust emission signatures. The WISE image at the position of the star appears point-like, and is brighter in W1

⁶ A $6''$ beam has at 1115 pc a linear scale of 10^{17} cm.

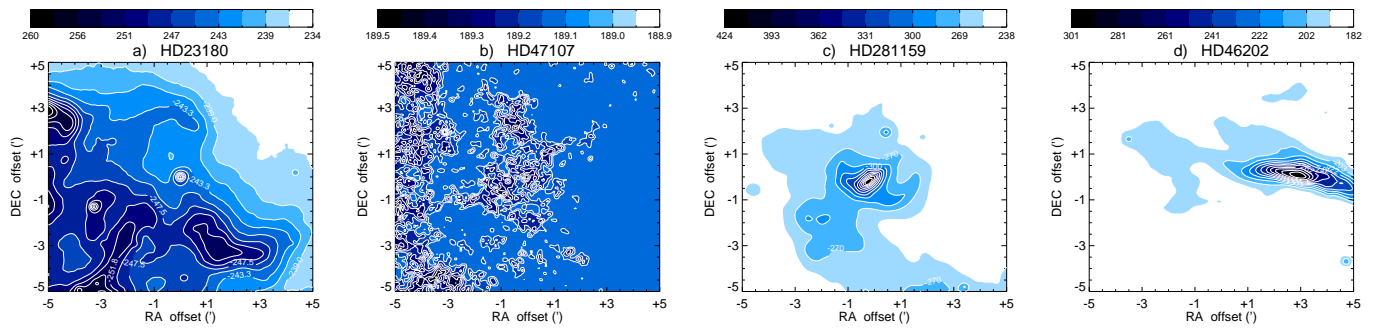


Fig. 5. WISE images in filter W4 ($\sim 22 \mu\text{m}$) centred on stars of different morphological types. From left to right: HD 23180 (type a), HD 47107 (type b), HD 281159 (type c), HD 46202 (type d). Fluxes levels are measured in mJy.

and W2 than in W3 and W4, where the star is sometimes not even detected.

b) background is enhanced. The emission near the star shows in W3 and more so in W4 a somewhat enhanced, diffuse background component.

c) cloud is detected. The star is located in or seems within less than $1'$ associated to a bright extended and often ellipsoidal shaped dust cloud. The clouds are often brighter in the W3 and more so in the W4 band than in the W1 and W2 bands.

d) distant dust lane or cloud is detected more than $1'$ away from the star, and is likely not associated with the star. The dust lane often extends over the full WISE image. The dust lane or cloud is often brighter in W3 and more so in W4 than in W1 and W2.

Typical examples of our classification of the emission morphology as seen by WISE in filter W4 are shown in Fig. 5 for HD 23180 (case a), HD 47107 (case b), HD 281159 (case c), and HD 46202 (case d). In the W4 ($22 \mu\text{m}$) image of HD 23180, two point sources are detected and one at the position of the star. In HD 47107 the star is detected and surrounded by some diffuse enhanced background. HD 281159 is detected near the center of a cloud and surrounded by a structure which is bright in W4, visible in W1 and W2 but not detected in W3. The star HD 46202 is not detected but a cloud $2'$ W of it is visible. Other remarkable structures are seen for HD 172028 that is inside a cloud which is bright in all bands. HD 155756 shows a nearby cloud $1'$ NE that is likely not associated with the star. HD 200775 showing two bright dust clouds and one around the star. From 132 objects with WISE classification in col. 15 of Table 3 there are 84 (63 %) in category a, 20 (15 %) in category b, 14 (11 %) in category c, and 14 (11 %) in category d, respectively. For the 52 single-cloud sightlines the distribution is similar: there are WISE images for all of such stars, and 33 (63 %) of them are in category a, 9 (15 %) in category b, 2 (4 %) in category c, and 9 (17 %) in category d, respectively.

An extended dust halo or circumstellar shell which might give a significant contribution to the total dust column density along the sightline is detected in a minority of our sample. This is category c which are only 10 % of the stars. Therefore dust along our sightlines seems predominantly (90 %) located in the diffuse ISM, at least the clouds are not detected by dust emission within a $1'$ neighbourhood to the stars.

4. Discussion

4.1. Distance estimates

We have derived the distances of our sample of early type stars using three different methods: *i*) GAIA parallax (D_{GAIA}); *ii*) spectral type and luminosity (D_{SpL}); and *iii*) the amount of interstellar matter derived from the Ca II (H, K) doublet ($D_{\text{Ca II}}$) as proposed by Megier et al. (2005).

i) The geometric distances D_{GAIA} were taken from Bailer-Jones et al. (2018). They are based on the second GAIA data release, where an inference procedure is used, which does not consider physical properties of the stars. Furthermore, the uncertainty of parallax measurements increases more and more with increasing distance to the star.

ii) The spectroscopic distances D_{SpL} were obtained from the spectral type and luminosity using the spectral classification of Sect. 3.1 and dust extinction given in Table 1. Spectroscopic distances depend on the correct identification of spectral type and luminosity class of a star. A difference of one spectral subclass in OB stars changes the derived stellar temperature already by 10 % implying an error in the distance of 40 %. This method requires also a correction of dust extinction with its own uncertainties (Krügel 2009; Scicluna & Siebenmorgen 2015). Unresolved binaries, common among early-type stars, result in errors of the spectral type and affects the estimate of the spectroscopic distance.

iii) Distance estimates $D_{\text{Ca II}}$ were obtained using the relation between interstellar absorption to distance studied already by Struve (1928) and more recently by Smoker et al. (2006). This method works well when the absorbing material is relatively uniformly distributed, and within the Galactic plane. Galazutdinov (2005) showed that the Ca II is a better distance indicator than K I, Na I or the reddening $E_{(B-V)}$. Megier et al. (2009) find a simple relation between the equivalent width of Ca II (H, K) doublet and the distance $D_{\text{Ca II}}$. Large-scale structures and dependencies on galactic latitude, local enhancements in the Ca II column density, likely related to stellar clusters and associations, and a frequent saturation of the Ca II line limit the accuracy of the method. Therefore we have used our EW measurements of the Ca II (H, K) doublet (cols. 3-4 of Table 3) and utilized the formulae of Megier et al. (2009) to compute the distance $D_{\text{Ca II}}$. Distance estimates derived from the three methods for the 132 stars of our sample are given in columns 5-7 of Table 3.

The relationships between the distance estimates D_{GAIA} , $D_{\text{Ca II}}$, and D_{SpL} , derived in Sect. 4.1, are shown in Fig. 6. Binaries and stars associated to clouds are ignored. For reasonable $D_{\text{Ca II}}$ estimate the ratio of the equivalent width of the Ca II

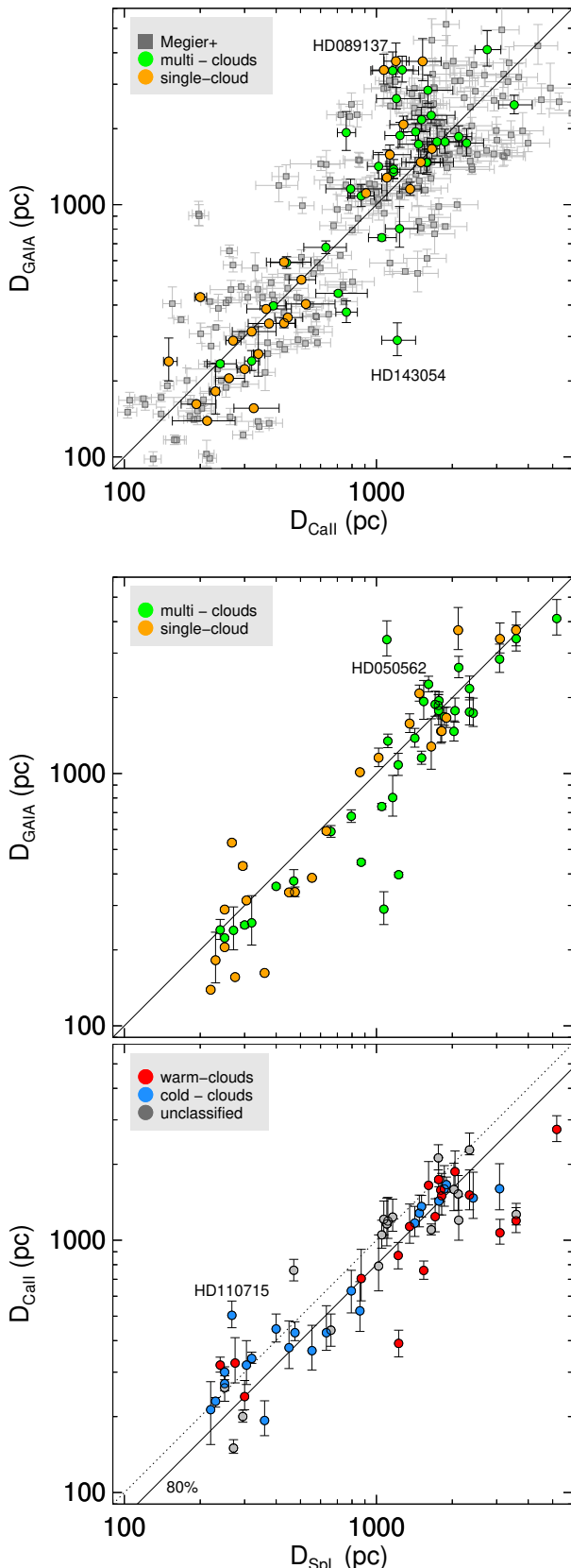


Fig. 6. Relation between distance estimates using GAIA parallax D_{GAIA} (Bailer-Jones et al. 2018), spectral type and luminosity D_{SpL} , and Ca II H, K doublet, $D_{\text{Ca II}}$. Squares (grey) give Ca II distances by Megier et al. (2009) and circles indicate distances as of Table 3 with sightlines dominated by single-cloud (orange), multi-clouds (green), cold (blue) and warm (red) clouds as labelled.

H and K doublet shall be $EW(H)/EW(K) > 1.32$. We consider stars with all three estimates measured at $> 3\sigma$ confidence and exclude binaries. This gives samples including 59 pairs of distance estimates that correlate with Pearson's coefficient $\rho(D_{\text{GAIA}}, D_{\text{Ca II}}) \sim 0.74$, $\rho(D_{\text{GAIA}}, D_{\text{SpL}}) \sim 0.89$, and $\rho(D_{\text{Ca II}}, D_{\text{SpL}}) \sim 0.82$, respectively. At short distances, $D_{\text{GAIA}} \leq 2$ kpc, there are 48 pairs, which correlate stronger ($\rho \gtrsim 0.87$), while at larger distance, $D_{\text{GAIA}} > 2$ kpc, 11 pairs remain and the correlation with GAIA distances breaks down.

In Fig. 6 we also show 232 distance estimates derived from the Ca II H, K doublet measurements at $> 3\sigma$ confidence and $EW(H)/EW(K) > 1.32$ by Megier et al. (2009). They show similar scatter and their $D_{\text{Ca II}}$ estimates correlate at $D_{\text{GAIA}} < 6$ kpc with $\rho = 0.7$, and a subsample at $D_{\text{GAIA}} \leq 2$ kpc correlates with $\rho = 0.83$. In the Megier et al. (2009) and our sample there are 17 stars in common. The EW of the Ca II H, K generally agree to better than 4% with three exceptions: HD 27778, HD 99872, and HD 141318. For these stars the EW show larger variations so that the derived Ca II distances differ by more than 20%. Whenever available we use the UVES derived $D_{\text{Ca II}}$ estimates as this instrument provides the highest resolving power. Megier et al. (2009) applied HIPPARCOS (ESA 1997) data for deriving their $D_{\text{Ca II}}$ formulae. In both data samples that are shown in top panel of Fig. 6 we do not notice a significant trend in the EW of the Ca II (H, K) doublet with the parallax distance estimates that would reduce the observed scatter.

Overall one notices a strong variation of about a factor of two when comparing different distance estimates of the same star. Within that scatter $D_{\text{Ca II}} \sim D_{\text{GAIA}}$ while $D_{\text{Ca II}} \sim 0.8 \times D_{\text{SpL}}$, however the sparse statistics avoids firm conclusions. As shown in Fig. 6 the variation in the distances remain when building subsamples of sightlines dominated by single or multiple clouds and warm or cold cloud environments. The reddening of our sample is also not correlated with the GAIA distance ($\rho(E_{\text{B-V}}, D_{\text{GAIA}}) = 0.2$).

We mark in Fig. 6 cases where the SpL and Ca II distances agree but the GAIA distance at small and large value of the parallax is off by more than a factor of three. For example HD 50562 is located by GAIA far away at 3.4 kpc while $D_{\text{Ca II}} \sim D_{\text{SpL}} \sim 1.1$ kpc are a factor three closer. On the other hand HD 143054 is predicted to be at 300 pc nearby when using GAIA while $D_{\text{Ca II}} \sim D_{\text{SpL}} \gtrsim 1.1$ kpc which is a factor four further away. Distances of HD 24263 derived from GAIA and SpL are at ~ 220 pc while $D_{\text{Ca II}}$ estimates are at 670 pc or finally HD 110715 shows $D_{\text{Ca II}} \sim D_{\text{SpL}} \sim 530$ pc while $D_{\text{SpL}} \sim 270$ pc. Further discrepancies can be identified in Table 3. For an individual star one cannot favour ad-hoc one against the other method for deriving distances.

5. Dark dust

The distance D of a star, its apparent m_V and absolute magnitude M_V , and the dust extinction along the sightline is connected by the photometric equation. Dust absorbs relatively more blue than red photons so that the interstellar extinction is often exchanged by the term “reddening” and simplified to be given by $A_V = R_V \times E_{\text{B-V}}$. However, it was never proved that it is allowed to neglect any additional constant extinction that represents some neutral, grey or as we call it *dark dust*. Indeed, in the original form of the photometric equation by Trumpler (1930) there is

beside the wavelength dependent selective interstellar extinction also such a constant C_{Dark} representing dark dust

$$m_V - M_V = 5 \log D - 5 + R_V \times E_{B-V} + C_{\text{Dark}} \quad (2)$$

Trumpler (1930) estimated $C_{\text{Dark}} \sim 0.2 \text{ mag/kpc}$ which appears today as a crude underestimate. He proposed “meteoric bodies” and we claim grains of sizes larger than the wavelength of the obscured light for explaining dark dust extinction. Indeed a number of studies claim the detection of a dark dust component populated by $\gtrsim 1 \mu\text{m}$ large grains. Dark dust is frequently found around circumstellar shells (Strom et al. 1971; Sitko et al. 1994; Lanz et al. 1995) or evolved stars (Apruzese 1974; Andriesse et al. 1978; Jura et al. 2001; Scicluna et al. 2015). Such dark dust goes often in hand with a total-to-selective extinction larger than what is applied as “canonical” value of Milky Way dust of $R_V \gtrsim 3.1$ (Fitzpatrick et al. 2019). More recently Krełowski et al. (2016) find that Ca II as well as VLBI parallax distances of the Orion Trapezium star HD 37020 differs from spectrophotometric distance by a factor 2.5. They interpret it as being due to $A_{\text{Dark}} = 1.8 \text{ mag}$ dark dust extinction in front of the star. Dark dust has also been detected in the general field by Skórzyński et al. (2003). They find that towards some OB stars located within 400 pc of the solar neighbourhood the intrinsic absolute magnitudes are too faint so that the derived spectrophotometric distances are significantly overestimated when compared to Hipparcos distances. This discrepancy is explained by a few mag of dark dust extinction in the ISM.

We consider stars of Table 3 at GAIA distances $\lesssim 2 \text{ kpc}$, measured at $> 4\sigma$ confidence, and exclude binaries as reported in Table 1. For 10 out of 77 of such stars the spectrophotometric distance differs significantly by more than $\pm 50\%$ from the GAIA distance. In that interval there are nine stars with $D_{\text{SpL}} \gtrsim 1.5 \times D_{\text{GAIA}}$ (Table 4) and one peculiar star HD 112954 for which $D_{\text{GAIA}} \sim 2.25 D_{\text{SpL}}$. Excluding these 10 stars the scatter in $D_{\text{SpL}}/D_{\text{GAIA}}$ is reduced to $\sim 22\%$. We find that:

i) Dark dust sightlines appear most frequently in the field. In our sample there is only one star HD 37903 for which a dust cloud can be associated in WISE imaging (Sect. 3.5). This star is illuminating the bright reflection nebula NGC 2023 in Orion and shows vibrationally excited interstellar H₂, indicative of a photodissociation region around the star (Meyer et al. 2001; Gnatciński 2011).

ii) The extinction of light by dark dust occurs in the cold ISM. At least all dark dust sightlines detected by us are associated to cold cloud environments (Sect. 3.4).

iii) Dark dust sightlines show predominantly flat extinction curves. There are 6 stars at $R_V \gtrsim 3.8$. Flat extinction curves are associated to large grains.

We estimate the amount of dark extinction postulating that the GAIA distance is precise and the luminosity L of the star is correctly derived by our spectral classification. The observed flux is given by

$$\frac{L e^{-\tau}}{4\pi D_{\text{SpL}}^2} = \frac{L e^{-(\tau+\tau_{\text{dark}})}}{4\pi D_{\text{GAIA}}^2} \quad (3)$$

hence $\tau_{\text{dark}} = \ln(D_{\text{SpL}}^2/D_{\text{GAIA}}^2)$ which amounts to typically 1 – 3 mag of dark dust extinction (Table 4). High precision extinction measurements in the near IR or at even longer wavelength are required for a clear identification of large particles that remain hidden in the dark dust component of the ISM.

Table 4. Dark dust detections. The meaning of the columns is: (1) counter, (2) HD identifier, (3) total-to-selective extinction R_V , (4) spectrophotometric distance, (5) GAIA distance, (6) visual extinction, and (7) dark dust extinction A_{Dark} .

| 1 | 2 | 3 | 4 | 5 | 6 | 7 |
|---|-----------|---------|------------------------|-------------------------|-----------|--------------------------|
| | Name | R_V^a | D_{SpL} pc | D_{GAIA} pc | Av mag | A_{Dark} mag |
| 1 | HD 037130 | 5.5 | 765 | 400 | 1.3 | 1.4 |
| 2 | HD 037903 | 4.1 | 1225 | 397 | 1.5 | 2.4 |
| 3 | HD 096675 | 3.8 | 360 | 162 | 1.1 | 1.7 |
| 4 | HD 143054 | 2.8 | 1070 | 290 | 1.5 | 2.8 |
| 5 | HD 146285 | 3.8 | 275 | 156 | 1.2 | 1.2 |
| 6 | HD 147196 | 3.1 | 220 | 139 | 0.8 | 1.0 |
| 7 | HD 147888 | 4.1 | 185 | 92 | 2.0 | 1.5 |
| 8 | HD 169582 | 3.0 | 3500 | 1681 | 2.6 | 1.6 |
| 9 | HD 294264 | 5.5 | 870 | 445 | 2.8 | 1.5 |

Notes: ^a Table A.1, ^a Bailer-Jones et al. (2018)

6. Summary and Conclusions

In this paper we have argued that our interpretation of the extinction and polarisation of the interstellar medium is strongly biased by the fact that multiple interstellar clouds may be present along any line of sight. Recently, we have shown that, when the analysis is limited to what we call single-cloud sightlines, new relationships appear between the observing characteristics of extinction and polarisation and the physical properties of the dust. Such relations are hidden in multiple-cloud sightlines where interstellar lines are Doppler-split, while single-cloud sightlines are suitable to investigate the pristine nature of interstellar material. Unfortunately, while hundreds of extinction and polarisation curves have been measured for the ISM, the number for single-cloud sightlines that have been investigated is still very limited. Siebenmorgen et al. (2018) argued that data for detailed dust modelling are available just for eight sightlines. To overcome this observational bias we have performed an extensive survey of high resolution (HR) spectra of reddened OB stars for which the (far) UV extinction curve has been measured by IUE or FUSE. We have compiled a sample of 186 HR spectra of such stars, 100 of which were observed by us using the UVES instrument of the ESO VLT. Archive spectra with a broad wavelength coverage for another 36 sightlines were retrieved from various archives as well as 50 accompanying UVES narrow band archive spectra that include the K I line. All sightlines for which UVES raw data were available were reprocessed by us with our interactive analysis package DECH.

Dust properties are supposed to vary on a large scale, typically when dust clouds are separated by several 10-100 pc whereas within a single cloud the mean characteristics of dust remains. This paper is tailored to detect single-clouds that can be used for further investigations of the dust characteristics in the diffuse ISM. In that context we assign the term single-cloud sightline when the observed interstellar lines observed at $\lesssim 4 \text{ km/s}$ (FWHM) resolution shows one dominating Doppler component. Whereby, we recognize that IS lines come in families of distinct radial velocities with K I coinciding with CH, while CH+ is often shifted, and Ca II and Ti II showing similar and more complex structures. Such offsets in the velocity profiles as well as local, small-scale variations, and details in the cloud morphology are not considered. Comparisons of our stars that are in common with previous ultra-high resolution spectra e.g. by Welty & Hobbs (2001); Welty et al. (2003) confirm our assignment in

single- or multi-component sightlines. Nevertheless, the comparison also demonstrates that lower resolution spectra at > 4 km/s (FWHM) are insufficient for such a classification. From the 186 HR spectra we identified a sample of 66 single-cloud sightlines, the majority of which were previously unknown.

In 97 sightlines we detected CH and CH^+ , and we used their strength ratio for the classification as warm (line ratio $\text{CH}/\text{CH}^+ < 1$) or cold ($\text{CH}/\text{CH}^+ > 1$) clouds. In all 52 cold clouds we detected CN, while we did not detect it in 33 out of 37 warm clouds. Most of the clouds are cold, and located sufficiently far away from the heating source in the cold diffuse ISM. We inspected the WISE 3 – $22\mu\text{m}$ emission morphology of our clouds. They appear predominantly stellar while dust emission that is associated with the star is detected in only 10% of the cases. Therefore we exclude a circumstellar nature of the observed reddening for most cases and the extinction towards our stars is due to dust located in the diffuse ISM.

The high resolving power of our data has allowed us to accurately measure the $\text{Mg II}/\text{He I}$ and $\text{He I}/\text{H I}$ line intensity ratios, which beside other features are used to revisit the spectral classification of our targets. In most cases (89/136) we confirmed previous assignments found in the literature, but for 47/136 stars our revision of spectral type was substantial. In 22 sightlines we identified binary systems. We used our revised classification to compute the spectral type–luminosity distance of the stars. We also measured the equivalent width of the Ca II H and K doublet and estimated the spectroscopic distance of the stars. We compared both distance estimates to the GAIA parallaxes. Overall the scatter in the distance estimates is large $\sim 40\%$. There are cases where only one of the three distances is heavily discrepant from the others. Sometimes, to agree with Gaia, spectroscopic estimates requires unacceptably low luminosity of the stars. One cannot favour ad-hoc one against the other method for deriving distances.

Finally, we have detected a hidden dust population amounting to a 1 – 3 mag extinction in the ISM that we hence called *dark dust*. For these stars the spectrophotometric distances are significantly larger than what is derived by GAIA. Dark dust appear predominantly in the cold ISM with flat extinction curves. Dark dust does in the optical not show a wavelength dependent absorption of stellar light. It is presumably made of very large $\gtrsim 1\mu\text{m}$ sized grains. For direct identification of such dark dust particles high precision extinction measurements in the near IR or at even longer wavelength are required.

In an accompanying paper we detail our stellar classifications. We will use the sample of 66 single cloud sightlines presented in this paper to investigate the polarisation properties of the interstellar medium, and we will search for correlations between diffuse interstellar bands, atomic and molecular lines, and other properties of ISM dust such as the reported dark dust component.

Acknowledgements. We are greatful to the referee for pointing us to the UHRF data. This research is based on data obtained from the ESO Science Archive Facility and in particular on observations collected under ESO observing programme ID 0102.C-0040. Additionally, data from the following ESO programme IDs was used in this paper: 065.I-0526(A), 065.N-0378(A), 066.B-0320(A), 071.C-0513(C), 073.C-0337(A), 073.D-0024(A), 076.C-0431(A), 096.D-0008(A), 099.C-0637(A), 194.C-0833(A). We also used spectra retrieved from the ELODIE and SOPHIE archives at Observatoire de Haute-Provence (OHP), available at atlas.obs-hp.fr/elodie and atlas.obs-hp.fr/sophie. This research has also made use of the SIMBAD database, operated at the CDS, Strasbourg, France. GAG and JK acknowledge the financial support of the Chilean fund CONICYT grant REDES 180136. JK acknowledge the financial support of the Polish National Science Centre, Poland (2017/25/B/ST9/01524) for the period 2018 — 2021.

References

- Andriesse, C. D., Donn, B. D., & Viotti, R. 1978, MNRAS, 185, 771
 Apruzese, J. P. 1974, ApJ, 188, 539
 Bagnulo, S., Cox, N. L. J., Cikota, A., et al. 2017, A&A, 608, A146
 Bailer-Jones, C. A. L., Rybizki, J., Fouesneau, M., Mantelet, G., & Andrae, R. 2018, AJ, 156, 58
 Barlow, M. J., Crawford, I. A., Diego, F., et al. 1995, MNRAS, 272, 333
 Chini, R. & Kruegel, E. 1983, A&A, 117, 289
 Cox, N. L. J., Cami, J., Farhang, A., et al. 2017, A&A, 606, A76
 Crane, P., Lambert, D. L., & Sheffer, Y. 1995, ApJS, 99, 107
 Crawford, I. A. 2002, MNRAS, 334, L33
 Dekker, H., D'Odorico, S., Kaufer, A., Delabre, B., & Kotzlowski, H. 2000, in Society of Photo-Optical Instrumentation Engineers (SPIE) Conference Series, Vol. 4008, Proc. SPIE, ed. M. Iye & A. F. Moorwood, 534–545
 Diego, F., Fish, A. C., Barlow, M. J., et al. 1995, Monthly Notices of the Royal Astronomical Society, 272, 323
 Elmegreen, B. G. 2002, ApJ, 564, 773
 Ensor, T., Cami, J., Bhatt, N. H., & Soddu, A. 2017, ApJ, 836, 162
 ESA. 1997, The HIPPARCOS and TYCHO catalogues. Astrometric and photometric star catalogues derived from the ESA HIPPARCOS Space Astrometry Mission, Vol. 1200 (<https://ui.adsabs.harvard.edu/abs/1997ESASP1200....E>)
 Falgarone, E., Phillips, T. G., & Walker, C. K. 1991, ApJ, 378, 186
 Falle, S. A. E. G. & Hartquist, T. W. 2002, MNRAS, 329, 195
 Fan, H., Hobbs, L. M., Dahlstrom, J. A., et al. 2019, ApJ, 878, 151
 Field, G. B. 1974, ApJ, 187, 453
 Fitzpatrick, E. L. & Massa, D. 1990, ApJS, 72, 163
 Fitzpatrick, E. L. & Massa, D. 2007, ApJ, 663, 320
 Fitzpatrick, E. L., Massa, D., Gordon, K. D., Bohlin, R., & Clayton, G. C. 2019, ApJ, 886, 108
 Galazutdinov, G. 2005, Journal of Korean Astronomical Society, 38, 215
 Galazutdinov, G. A., Krelowski, J., & Musaev, F. A. 2000, MNRAS, 315, 703
 Gnaciński, P. 2011, A&A, 532, A122
 Gordon, K. D., Cartledge, S., & Clayton, G. C. 2009, ApJ, 705, 1320
 Heger, M. L. 1922, Lick Observatory Bulletin, 10, 141
 Hong, S. S. & Greenberg, J. M. 1980, A&A, 88, 194
 Houk, N. 1982, Michigan Catalogue of Two-dimensional Spectral Types for the HD stars (Harvard 1975 MCTS Book)
 Houk, N. & Swift, C. 1999, Michigan Spectral Survey, 5, 0
 Jura, M., Webb, R. A., & Kahane, C. 2001, ApJ, 550, L71
 Kaufer, A., Stahl, O., Tubbesing, S., et al. 1999, The Messenger, 95, 8
 Klein, R. I., McKee, C. F., & Colella, P. 1994, ApJ, 420, 213
 Krelowski, J., Beletsky, Y., Galazutdinov, G. A., et al. 2010, ApJ, 714, L64
 Krelowski, J., Galazutdinov, G., & Bondar, A. 2019a, MNRAS, 486, 3537
 Krelowski, J., Galazutdinov, G. A., Bondar, A., & Beletsky, Y. 2016, MNRAS, 460, 2706
 Krelowski, J., Snow, T. P., Seab, C. G., & Papaj, J. 1992, MNRAS, 258, 693
 Krelowski, J., Strobel, A., Galazutdinov, G. A., Bondar, A., & Valyavin, G. 2019b, MNRAS, 486, 112
 Krelowski, J., Strobel, A., Galazutdinov, G. A., Musaev, F., & Bondar, A. 2018, Acta Astron., 68, 285
 Krelowski, J. & Walker, G. A. H. 1987, ApJ, 312, 860
 Krügel, E. 2008, An introduction to the physics of interstellar dust (IOP)
 Krügel, E. 2009, A&A, 493, 385
 Lanz, T., Heap, S. R., & Hubeny, I. 1995, ApJ, 447, L41
 Lauroesch, J. T., Meyer, D. M., & Blades, J. C. 2000, ApJ, 543, L43
 Megier, A., Strobel, A., Bondar, A., et al. 2005, ApJ, 634, 451
 Megier, A., Strobel, A., Galazutdinov, G. A., & Krelowski, J. 2009, A&A, 507, 833
 Meyer, D. M., Lauroesch, J. T., Sofia, U. J., Draine, B. T., & Bertoldi, F. 2001, ApJ, 553, L59
 Morris, P. W., Gupta, H., Nagy, Z., et al. 2016, ApJ, 829, 15
 Moultsaka, J., Illovaisky, S. A., Prugniel, P., & Soubiran, C. 2004, PASP, 116, 693
 Pan, K., Federman, S. R., Sheffer, Y., & Andersson, B. G. 2005, ApJ, 633, 986
 Price, R. J., Crawford, I. A., & Barlow, M. J. 2000, MNRAS, 312, L43
 Savage, B. D. & Sembach, K. R. 1991, ApJ, 379, 245
 Scicluna, P. & Siebenmorgen, R. 2015, A&A, 584, A108
 Scicluna, P., Siebenmorgen, R., Wesson, R., et al. 2015, A&A, 584, L10
 Sembach, K. R., Danks, A. C., & Savage, B. D. 1993, A&AS, 100, 107
 Siebenmorgen, R. 1993, ApJ, 408, 218
 Siebenmorgen, R., Voshchinnikov, N. V., Bagnulo, S., et al. 2018, A&A, 611, A5
 Sitko, M. L., Halbedel, E. M., Lawrence, G. F., Smith, J. A., & Yanow, K. 1994, ApJ, 432, 753
 Skórzyński, W., Strobel, A., & Galazutdinov, G. A. 2003, A&A, 408, 297
 Smoker, J., Haddad, N., Iwert, O., et al. 2009, The Messenger, 138, 8
 Smoker, J. V., Lynn, B. B., Christian, D. J., & Keenan, F. P. 2006, MNRAS, 370, 151
 Strom, K. M., Strom, S. E., & Yost, J. 1971, ApJ, 165, 479
 Struve, O. 1928, ApJ, 67, 353

- Tolstoy, E., Venn, K. A., Shetrone, M., et al. 2003, AJ, 125, 707
 Trumpler, R. J. 1930, PASP, 42, 214
 Tull, R. G., MacQueen, P. J., Sneden, C., & Lambert, D. L. 1995, PASP, 107, 251
 Valencic, L. A., Clayton, G. C., & Gordon, K. D. 2004, ApJ, 616, 912
 Wada, K. 2008, ApJ, 675, 188
 Walborn, N. R. 2008, in Revista Mexicana de Astronomia y Astrofisica Conference Series, Vol. 33, 5–14
 Walborn, N. R. & Fitzpatrick, E. L. 1990, PASP, 102, 379
 Wegner, W. 2003, Astronomische Nachrichten, 324, 219
 Welty, D. E. & Crowther, P. A. 2010, MNRAS, 404, 1321
 Welty, D. E. & Fitzpatrick, E. L. 2001, ApJ, 551, L175
 Welty, D. E. & Hobbs, L. M. 2001, ApJS, 133, 345
 Welty, D. E., Hobbs, L. M., & Kulkarni, V. P. 1994, ApJ, 436, 152
 Welty, D. E., Hobbs, L. M., & Morton, D. C. 2003, ApJS, 147, 61
 Welty, D. E., Morton, D. C., & Hobbs, L. M. 1996, ApJS, 106, 533
 Weselak, T., Galazutdinov, G. A., Musaev, F. A., & Krelowski, J. 2008, A&A, 484, 381
 Wright, E. L., Eisenhardt, P. R. M., Mainzer, A. K., et al. 2010, AJ, 140, 1868

Appendix A: Tables and Figures

Complete entries of Table 1, Table 2, and Table 3 are provided in Table A.1, Table A.2, and Table A.3, respectively. Remaining figures of UVES derived velocity profiles are displayed in Fig. A.1 to Fig. A.16.

Table A.1. Study sample sorted by HD number. The meaning of the columns is: 1) Identification number, (2) HD identifier, (3) if different the main name of the star as used in SIMBAD, (4) V magnitude, (5) reddening $E(B-V)$, (6) visual extinction A_V , (7) total-to-selective extinction R_V , (8) spectral type from previous literature, (9) spectral type as derived in this work, and (10) instrument used to obtain high-resolution spectroscopy.

| 1 ID | 2 Name | 3 SIMBAD | 4 V mag | 5 $E'_{(B-V)}$ | 6 A_V' mag | 7 R_V' mag | 8 SpTy literature | 9 SpTy ^a this work | 10 Instrument |
|---------|-----------|-------------|---------------|-------------------|--------------------|--------------------|-------------------------|-------------------------------------|---------------------|
| 1 | HD 023180 | * omi Per | 3.83 | 0.29±0.03 | 0.91±0.08 | 3.14±0.31 | B1IV ^F | B1III | UVES ^b |
| 2 | HD 024263 | * 31 τ | 5.69 | 0.21±0.06 | 0.72±0.22 | 3.44±0.65 | B5VV | B3.5V + binary | UVES ^a |
| 3 | HD 024912 | ksi Per | 4.02 | 0.35±0.06 | 1.00±0.26 | 2.86±0.71 | O7VV | O8III | ELODIE ⁱ |
| 4 | HD 027778 | 62 τ | 6.36 | 0.39±0.10 | 1.09±0.09 | 2.79±0.59 | B3V ^F | B3V | UVES ^b |
| 5 | HD 030123 | | 8.61 | 0.48±0.03 | 1.58±0.08 | 3.30±0.27 | B8III ^F | B5IV + cloud | UVES ^a |
| 6 | HD 030470 | | 9.47 | 0.35±0.03 | 1.08±0.08 | 3.09±0.29 | A0V ^F | B9.5V + cloud | UVES ^a |
| 7 | HD 030492 | | 8.96 | 0.40±0.04 | 1.17±0.11 | 2.93±0.35 | A0IV ^F | B9.5V + cloud | UVES ^a |
| 8 | HD 037130 | | 9.97 | 0.23±0.03 | 1.26±0.11 | 5.50±0.44 | B8-9IV ^{HS} | B8V + cloud | UVES ^a |
| 9 | HD 037903 | | 7.83 | 0.36±0.11 | 1.49±0.11 | 4.11±0.64 | B1.5V ^F | B0V | UVES ^b |
| 10 | HD 038023 | | 8.86 | 0.52±0.03 | 1.64±0.08 | 3.16±0.26 | B4V ^F | B2V | UVES ^a |
| 11 | HD 046056 | | 8.15 | 0.50±0.10 | 1.41±0.13 | 2.83±0.40 | O8V(n) ^F | O8V | UVES ^a |
| 12 | HD 046106 | | 7.92 | 0.43±0.03 | 1.26±0.08 | 2.92±0.27 | B1V ^F | O9.7V | UVES ^a |
| 13 | HD 046149 | | 7.60 | 0.46±0.03 | 1.29±0.08 | 2.81±0.26 | O8.5V ^F | O8.5V | UVES ^a |
| 14 | HD 046202 | | 8.18 | 0.49±0.11 | 1.53±0.13 | 3.13±0.43 | O9V ^F | O9V | UVES ^a |
| 15 | HD 046223 | | 7.28 | 0.54±0.06 | 1.48±0.19 | 2.73±0.35 | O5V ^V | O4V | UVES ^c |
| 16 | HD 046485 | | 8.26 | 0.61±0.03 | 1.83±0.08 | 3.00±0.25 | O7Vn(e) ^F | O7V | UVES ^a |
| 17 | HD 046660 | | 8.04 | 0.56±0.03 | 1.65±0.08 | 2.95±0.25 | B1V ^F | O9V | UVES ^a |
| 18 | HD 046711 | | 9.09 | 1.05±0.03 | 3.36±0.08 | 3.20±0.23 | B3II ^F | B3I + binary | UVES ^a |
| 19 | HD 046883 | | 7.78 | 0.63±0.03 | 1.93±0.08 | 3.06±0.25 | B0.5V ^F | B3II | UVES ^a |
| 20 | HD 047107 | | 8.01 | 0.23±0.03 | 0.69±0.08 | 3.00±0.33 | B1.5Ia ^F | B1.5V | UVES ^a |
| 21 | HD 047382 | | 7.14 | 0.44±0.03 | 1.37±0.08 | 3.12±0.27 | B0III ^F | B3II | UVES ^a |
| 22 | HD 050562 | | 8.60 | 0.26±0.08 | 0.64±0.24 | 2.45±0.65 | B2III ^V | B3V | UVES ^a |
| 23 | HD 054306 | | 8.78 | 0.23±0.03 | 0.63±0.08 | 2.73±0.32 | B2V ^F | B1.5V | UVES ^a |
| 24 | HD 060479 | | 8.41 | 0.57±0.06 | 1.70±0.20 | 2.98±0.37 | B0II ^V | O9I + binary | UVES ^a |
| 25 | HD 062542 | | 8.04 | 0.36±0.03 | 0.99±0.08 | 2.74±0.28 | B5V ^F | B3V | UVES ^d |
| 26 | HD 068633 | | 8.00 | 0.49±0.03 | 1.78±0.09 | 3.64±0.27 | B5V ^F | B2V + bin | UVES ^a |
| 27 | HD 070614 | | 9.27 | 0.65±0.06 | 1.91±0.20 | 2.94±0.34 | B6 ^F | B3III | UVES ^a |
| 28 | HD 072648 | | 7.61 | 0.34±0.03 | 1.21±0.09 | 3.56±0.30 | B1-2Ib ^F | B3III (II) | UVES ^a |
| 29 | HD 079186 | | 5.04 | 0.40±0.06 | 1.28±0.31 | 3.21±0.76 | B5Ia ^V | B5Ia | UVES ^b |
| 30 | HD 083597 | | 9.20 | 0.34±0.06 | 1.31±0.24 | 3.84±0.51 | B2V ^V | B0Ve | UVES ^a |
| 31 | HD 089137 | | 7.98 | 0.27±0.06 | 0.72±0.18 | 2.68±0.48 | B2II ^V | B2II | UVES ^a |
| 32 | HD 091943 | | 6.73 | 0.25±0.06 | 0.93±0.23 | 3.73±0.62 | B0.5II ^V | B1Ia | UVES ^a |
| 33 | HD 091969 | | 6.53 | 0.23±0.06 | 0.85±0.22 | 3.69±0.61 | B0Ib ^V | B0I + binary | UVES ^a |
| 34 | HD 091983 | | 8.58 | 0.29±0.03 | 0.93±0.08 | 3.20±0.31 | B1III ^F | B2III | UVES ^a |
| 35 | HD 092007 | | 8.94 | 0.32±0.03 | 0.97±0.08 | 3.03±0.29 | B0II ^F | B1III | UVES ^a |
| 36 | HD 092044 | | 8.25 | 0.43±0.03 | 1.42±0.08 | 3.30±0.28 | B0.5II ^F | B1.5II | UVES ^a |
| 37 | HD 093632 | | 8.31 | 0.56±0.07 | 2.33±0.30 | 4.17±0.44 | B0V ^V | O6I | UVES ^a |
| 38 | HD 094663 | | 9.35 | 0.38±0.08 | 1.29±0.30 | 3.38±0.58 | O9.5III ^V | O9.5IV + bin | UVES ^a |
| 39 | HD 096042 | | 8.23 | 0.43±0.09 | 0.87±0.30 | 2.01±0.53 | B1V ^V | B1V + bin | UVES ^a |
| 40 | HD 096675 | | 7.69 | 0.30±0.06 | 1.15±0.24 | 3.83±0.55 | B6IV ^V | B5V | UVES ^a |
| 41 | HD 097484 | V* EM Car | 8.36 | 0.60±0.07 | 1.54±0.21 | 2.57±0.35 | O8V ^V | O8V | UVES ^a |
| 42 | HD 099264 | | 5.58 | 0.27±0.03 | 0.85±0.08 | 3.15±0.32 | B3III ^F | B2V | UVES ^a |
| 43 | HD 099872 | | 6.09 | 0.36±0.03 | 1.06±0.10 | 2.95±0.46 | B3V ^F | B3V | UVES ^a |
| 44 | HD 099890 | | 8.28 | 0.24±0.16 | 0.75±0.11 | 3.11±0.71 | B0.5V ^G | B1IV | UVES ^a |
| 45 | HD 100213 | V* TU Mus | 8.38 | 0.37±0.13 | 1.28±0.14 | 3.47±0.52 | O8VG | O8V(n)z + B0V(n) | UVES ^a |
| 46 | HD 101008 | | 9.15 | 0.27±0.03 | 0.93±0.08 | 3.43±0.33 | O9V ^F | O9V | UVES ^a |
| 47 | HD 104565 | | 9.25 | 0.60±0.06 | 2.06±0.22 | 3.43±0.37 | B0Ia ^V | O9.7II | UVES ^a |
| 48 | HD 108927 | | 7.78 | 0.24±0.03 | 0.74±0.08 | 3.10±0.33 | B5V ^F | B5V | UVES ^a |
| 49 | HD 110336 | | 8.64 | 0.45±0.03 | 1.21±0.08 | 2.69±0.26 | B9IV ^F | B9IV | UVES ^a |
| 50 | HD 110715 | | 8.65 | 0.45±0.03 | 1.31±0.08 | 2.92±0.26 | B9V ^F | B9V | UVES ^a |
| 51 | HD 110863 | | 9.06 | 0.54±0.03 | 1.60±0.08 | 2.97±0.25 | B1Vp ^F | B2II-III | UVES ^a |
| 52 | HD 110946 | V* LN Mus | 9.14 | 0.50±0.03 | 1.60±0.08 | 3.20±0.26 | B1V ^F | B3III | UVES ^a |
| 53 | HD 111973 | *κCru | 5.98 | 0.39±0.07 | 1.39±0.26 | 3.55±0.51 | B5Ia ^V | B5I | UVES ^a |
| 54 | HD 111990 | | 6.80 | 0.41±0.06 | 1.45±0.22 | 3.54±0.45 | B1I ^V | B1.5I + binary | UVES ^a |
| 55 | HD 112607 | | 8.06 | 0.31±0.04 | 0.85±0.10 | 2.73±0.38 | B7-8III ^F | B5IV | UVES ^a |
| 56 | HD 112954 | | 8.37 | 0.57±0.03 | 1.75±0.08 | 3.07±0.25 | B9IV ^F | A0V | UVES ^a |
| 57 | HD 122669 | | 8.96 | 0.60±0.08 | 2.46±0.33 | 4.09±0.45 | B0V ^V | B0Ve | UVES ^a |
| 58 | HD 123008 | | 8.79 | 0.62±0.08 | 2.06±0.29 | 3.32±0.41 | B0V ^V | O9.2Iab | UVES ^a |
| 59 | HD 123335 | V* V883 Cen | 6.34 | 0.23±0.03 | 0.76±0.08 | 3.30±0.34 | B5IV ^F | B3V+B8V | UVES ^a |
| 60 | HD 125288 | * v Cen | 4.36 | 0.28±0.06 | 0.61±0.24 | 2.19±0.55 | B5II ^V | B5II-III | FEROS ⁱ |
| 61 | HD 129557 | V* BU Cir | 5.23 | 0.23±0.09 | 0.53±0.28 | 2.29±0.76 | B2III ^V | B2III | UVES ^e |
| 62 | HD 134591 | | 8.37 | 0.24±0.07 | 0.60±0.21 | 2.51±0.60 | B5III ^F | B8IV | UVES ^a |
| 63 | HD 141318 | | 5.77 | 0.24±0.05 | 0.83±0.18 | 3.44±0.54 | B2II ^V | B2III | UVES ^a |
| 64 | HD 141926 | | 9.13 | 0.80±0.06 | 2.96±0.22 | 3.69±0.32 | B2V ^V | B1V | UVES ^a |
| 65 | HD 143054 | | 9.39 | 0.55±0.03 | 1.54±0.08 | 2.80±0.25 | B2III-III ^F | B2.5V | UVES ^a |
| 66 | HD 146284 | | 6.70 | 0.25±0.03 | 0.77±0.08 | 3.10±0.32 | B8V ^F | B7IV | UVES ^a |
| 67 | HD 146285 | | 7.93 | 0.32±0.03 | 1.23±0.09 | 3.83±0.32 | B8V ^F | B7V | UVES ^a |
| 68 | HD 147165 | *σSco | 2.88 | 0.41±0.03 | 1.48±0.09 | 3.60±0.29 | B1III ^F | B1III + binary | UVES ^b |
| 69 | HD 147196 | | 7.04 | 0.27±0.03 | 0.84±0.08 | 3.10±0.31 | B5V ^F | B7V | UVES ^a |
| 70 | HD 147331 | | 8.75 | 0.59±0.06 | 1.75±0.20 | 2.97±0.36 | B0Ia ^V | O9I + binary | UVES ^a |
| 71 | HD 147701 | | 8.36 | 0.69±0.03 | 2.78±0.09 | 4.03±0.26 | B5V ^F | B5III | UVES ^a |
| 72 | HD 147888 | *ρOph D | 6.74 | 0.48±0.05 | 1.97±0.09 | 4.08±0.39 | B3V ^F | B3V | UVES ^b |
| 73 | HD 147889 | | 7.90 | 1.06±0.03 | 4.44±0.09 | 4.19±0.24 | B2V ^F | B2V | UVES ^b |
| 74 | HD 147933 | *ρOph A | 4.59 | 0.47±0.03 | 2.07±0.09 | 4.41±0.29 | B1.5V ^F | B1V | UVES ^b |
| 75 | HD 148579 | | 7.34 | 0.35±0.03 | 1.40±0.09 | 4.01±0.31 | B9V ^F | B8V | UVES ^a |
| 76 | HD 148594 | | 6.89 | 0.21±0.03 | 0.65±0.08 | 3.10±0.35 | B9V ^F | B5.5V | UVES ^a |
| 77 | HD 149038 | * μ Nor | 4.92 | 0.22±0.07 | 1.08±0.37 | 4.92±1.11 | B0Ia ^V | O9.5Ia | UVES ^b |
| 78 | HD 149757 | * ζOph | 2.57 | 0.31±0.03 | 0.95±0.08 | 3.08±0.30 | O9.5Vnn ^F | O9.2IV | UVES ^b |

Table A.1. – continued –

| 1 ID | 2 Name | 3 SIMBAD | 4 V mag | 5 $E'_{(B-V)}$ | 6 Av ⁱ mag | 7 Rv ⁱ | 8 SpTy literature | 9 SpTy ^a this work | 10 Instrument |
|---------|-------------|-------------|---------------|-------------------|-----------------------------|----------------------|-------------------------|-------------------------------------|---------------------|
| 79 | HD 151346 | | 7.91 | 0.59± 0.03 | 2.25± 0.09 | 3.81± 0.26 | B7p ^F | B8IV | UVES ^a |
| 80 | HD 152096 | | 9.41 | 0.30± 0.09 | 0.94± 0.31 | 3.15± 0.66 | B2Ib ^V | B2I-II + binary | UVES ^a |
| 81 | HD 152245 | | 8.41 | 0.36± 0.06 | 1.08± 0.22 | 2.99± 0.54 | B0Ib ^V | B0V | UVES ^a |
| 82 | HD 152247 | | 7.17 | 0.41± 0.06 | 1.43± 0.22 | 3.49± 0.44 | O9.5Iab ^V | O9.2II | UVES ^e |
| 83 | HD 152560 | | 8.28 | 0.39± 0.03 | 1.27± 0.08 | 3.25± 0.28 | B0.5IV ^F | O9.5IV | UVES ^b |
| 84 | HD 152667 | V* V861 Sco | 6.18 | 0.49± 0.06 | 1.63± 0.21 | 3.33± 0.39 | B0.5Ia ^V | O9I + binary | UVES ^a |
| 85 | HD 155756 | | 9.27 | 0.78± 0.09 | 2.39± 0.31 | 3.07± 0.38 | B0Ia ^V | O9I + binary | UVES ^a |
| 86 | HD 156247 | V* U Oph | 5.91 | 0.25± 0.04 | 0.73± 0.11 | 2.92± 0.43 | B5V ^F | B4V + binary | UVES ^a |
| 87 | HD 161653 | | 7.20 | 0.28± 0.06 | 0.94± 0.22 | 3.37± 0.61 | B0.5Iab ^V | B3II + binary | UVES ^a |
| 88 | HD 162978 | * 63 Oph | 6.20 | 0.34± 0.06 | 1.20± 0.23 | 3.54± 0.54 | O8III ^V | O8II | UVES ^a |
| 89 | HD 163181 | | 6.49 | 0.74± 0.08 | 2.40± 0.37 | 3.24± 0.52 | B0Ia ^V | O9.5lab | UVES ^a |
| 90 | HD 164536 | | 7.12 | 0.25± 0.03 | 0.93± 0.09 | 3.73± 0.35 | O7-8 ^F | O7.5V | UVES ^a |
| 91 | Herschel 36 | | 10.30 | 0.86± 0.13 | 4.48± 0.36 | 5.21± 0.81 | O7.5V(n) ^F | O8V + cloud | UVES ^b |
| 92 | HD 164816 | | 7.11 | 0.31± 0.12 | 0.99± 0.12 | 3.21± 0.68 | B0V ^F | O9.5V | UVES ^a |
| 93 | HD 164863 | | 7.27 | 0.26± 0.03 | 0.87± 0.08 | 3.34± 0.33 | B0V ^F | B0V | UVES ^a |
| 94 | HD 164906 | | 7.47 | 0.43± 0.11 | 2.17± 0.11 | 5.01± 0.65 | B1IV ^G | B1IV + cloud | UVES ^a |
| 95 | HD 164947A | | 9.41 | 0.29± 0.03 | 1.07± 0.09 | 3.70± 0.33 | B2V ^F | B2V + binary | UVES ^a |
| 95 | HD 164947B | | 9.80 | 0.29± 0.03 | 1.07± 0.09 | 3.70± 0.33 | B2V ^F | B2V + binary | UVES ^a |
| 96 | HD 167771 | | 6.54 | 0.42± 0.13 | 1.48± 0.14 | 3.53± 0.52 | O7III ^F | O7III + O8III | UVES ^a |
| 97 | HD 168750 | | 8.27 | 0.36± 0.07 | 1.27± 0.27 | 3.52± 0.58 | B1Ib ^V | B2III | UVES ^a |
| 98 | HD 168941 | | 9.38 | 0.34± 0.09 | 1.23± 0.12 | 3.56± 0.50 | O9.5II ^G | O9III | CES ^f |
| 99 | HD 169582 | | 8.70 | 0.87± 0.06 | 2.60± 0.21 | 2.99± 0.31 | O5V ^V | O6V (Ia,O3-4?) + bin | UVES ^a |
| 100 | HD 170634 | | 9.85 | 0.69± 0.03 | 2.05± 0.08 | 2.97± 0.24 | B7V ^F | B8-9IV | UVES ^a |
| 101 | HD 170740 | | 5.72 | 0.47± 0.03 | 1.37± 0.08 | 2.91± 0.26 | B2V ^F | B2V + binary | UVES ^b |
| 102 | HD 172028 | | 7.83 | 0.78± 0.03 | 2.27± 0.08 | 2.91± 0.24 | B3II ^F | B3II | UVES ^g |
| 103 | HD 172140 | | 9.95 | 0.23± 0.03 | 0.62± 0.08 | 2.71± 0.32 | B0.5III ^F | B0.5III | CES ^f |
| 104 | HD 172175 | | 9.40 | 0.95± 0.06 | 2.63± 0.19 | 2.77± 0.28 | O6VV | O6.5IV | UVES ^a |
| 105 | HD 177989 | | 9.33 | 0.22± 0.03 | 0.63± 0.08 | 2.85± 0.33 | B2II ^F | B2II | CES ^f |
| 106 | HD 180968 | * 2 Vul | 5.43 | 0.21± 0.09 | 0.99± 0.36 | 3.31± 0.86 | B0invar ^F | B3IV + binary | UVES ^h |
| 107 | HD 185418 | | 7.45 | 0.52± 0.09 | 1.39± 0.12 | 2.67± 0.41 | B0.5V ^F | B0.5V | UVES ^b |
| 108 | HD 185859 | | 6.49 | 0.60± 0.06 | 1.65± 0.19 | 2.74± 0.33 | B0.5Ia ^V | B3I + binary | UVES ^b |
| 109 | HD 198478 | * 55 Cyg | 4.83 | 0.57± 0.06 | 1.48± 0.22 | 2.60± 0.39 | B3Ia ^V | B4Ia | SAO1m ^j |
| 110 | HD 200775 | | 7.39 | 0.57± 0.12 | 3.21± 0.10 | 5.61± 0.88 | B2Ve ^G | B2Ve | SOPHIE ^k |
| 111 | HD 203532 | | 6.37 | 0.31± 0.03 | 0.92± 0.08 | 2.96± 0.30 | B3IV ^F | B3.5V | UVES ^b |
| 112 | HD 204827 | | 7.94 | 1.08± 0.03 | 2.64± 0.07 | 2.44± 0.22 | B0V ^F | O8IV | BOE ¹⁷ |
| 113 | HD 206267 | | 5.62 | 0.47± 0.08 | 1.26± 0.12 | 2.66± 0.45 | O6V ^G | O5V | SOPHIE ^k |
| 114 | HD 207198 | | 5.94 | 0.58± 0.08 | 1.54± 0.09 | 2.68± 0.31 | O9II ^G | O8.5II | ELODIE ^l |
| 115 | HD 209975 | * 19 Cep | 5.11 | 0.34± 0.06 | 0.96± 0.23 | 2.82± 0.58 | O9Ib ^V | O9I + binary | SOPHIE ^k |
| 116 | HD 210121 | | 7.67 | 0.31± 0.07 | 0.75± 0.20 | 2.42± 0.49 | B9VV | B3.5V | UVES ^b |
| 117 | HD 218376 | * 1 Cas | 4.85 | 0.23± 0.03 | 0.71± 0.08 | 3.10± 0.33 | B1III ^F | B1III | SOPHIE ^k |
| 118 | HD 259105 | | 9.37 | 0.47± 0.03 | 1.42± 0.08 | 3.02± 0.26 | B2V ^F | B1V | UVES ^a |
| 119 | HD 281159 | | 8.52 | 0.89± 0.03 | 2.79± 0.08 | 3.14± 0.24 | B5V ^F | B5V | SOPHIE ^k |
| 120 | HD 284839 | | 9.69 | 0.33± 0.03 | 0.96± 0.08 | 2.92± 0.29 | B9III ^F | B8-7IV | ELODIE ^l |
| 121 | HD 284841 | | 9.34 | 0.43± 0.03 | 1.28± 0.08 | 2.98± 0.27 | B9II ^F | B6.5V + cloud | UVES ^a |
| 122 | HD 287150 | | 9.28 | 0.37± 0.03 | 1.22± 0.08 | 3.29± 0.29 | A2V ^F | B8V | UVES ^a |
| 123 | HD 292167 | | 9.25 | 0.72± 0.03 | 2.29± 0.08 | 3.18± 0.24 | O9III ^F | O9II | UVES ^a |
| 124 | HD 294264 | | 9.53 | 0.52± 0.03 | 2.85± 0.10 | 5.48± 0.31 | B3Vn ^F | B3V | UVES ^a |
| 125 | HD 294304 | | 10.03 | 0.42± 0.03 | 1.23± 0.08 | 2.92± 0.27 | B8Ve ^F | B8? | UVES ^a |
| 126 | HD 315021 | | 8.59 | 0.34± 0.03 | 1.24± 0.09 | 3.65± 0.31 | B2IVn ^F | B2.5V | UVES ^a |
| 127 | HD 315023 | | 10.09 | 0.36± 0.03 | 1.48± 0.09 | 4.10± 0.31 | B2.5Ve ^F | B3V + cloud | UVES ^a |
| 128 | HD 315024 | | 9.55 | 0.30± 0.04 | 1.20± 0.13 | 3.99± 0.47 | B2.5Ve ^F | B3V + cloud | UVES ^a |
| 129 | HD 315031 | | 8.29 | 0.33± 0.03 | 1.20± 0.09 | 3.64± 0.31 | B2IVn ^F | B0.5IV-V + B1V | UVES ^a |
| 130 | HD 315032 | | 9.18 | 0.28± 0.03 | 1.01± 0.09 | 3.61± 0.33 | B2Vne ^F | B2IVe + cloud | UVES ^a |
| 131 | HD 315033 | | 8.93 | 0.35± 0.03 | 1.56± 0.09 | 4.45± 0.33 | B2Vp ^F | B1V + cloud | UVES ^a |
| 132 | HD 326309 | | 10.00 | 0.51± 0.03 | 1.57± 0.08 | 3.07± 0.26 | B0V ^F | B3IV | UVES ^a |
| 133 | HD 326330 | V* V964 Sco | 9.61 | 0.44± 0.03 | 1.42± 0.08 | 3.23± 0.27 | B0.5V ^F | B1V | UVES ^a |
| 134 | HD 326332 | | 9.66 | 0.51± 0.03 | 1.62± 0.08 | 3.17± 0.26 | B0.5V ^F | B2IVe + cloud | UVES ^a |
| 135 | HD 326333 | V* V920 Sco | 9.62 | 0.45± 0.03 | 1.52± 0.08 | 3.38± 0.28 | B1V ^F | B1V + cloud | UVES ^a |
| 136 | HD 326364 | | 9.60 | 0.62± 0.03 | 1.80± 0.08 | 2.91± 0.25 | B0IV ^F | B1IV + cloud | UVES ^a |

Notes: Cols. 5–7 extracted from Gordon et al. (2009), Fitzpatrick & Massa (2007), with uncertainties revised as explained in the text. Spectral types as derived by: ^F Fitzpatrick & Massa (2007), ^G Gordon et al. (2009), ^H Houk (1982), ^{HS} Houk & Swift (1999), and ^V Valencic et al. (2004). Spectroscopic data from: *a*: this work; *b*: Cox et al. (2017); *c*: UVES prog ID 096.D-0008(A) (unpublished ESO archive); *d*: UVES prog ID 099.C-0637(A) (unpublished ESO archive); *e*: Bagnulo et al. (2013); *f*: Sembach et al. (1993); *g*: Welty & Crowther (2010); *h*: Tolstoy et al. (2003); *i*: Krelowski et al. (2010); *j*: SAO 1.0 m; *k*: SOPHIE archive; *l*: ELODIE archive.

Table A.2. UVES archive spectra covering the K₁ line. The meaning of the columns is: (1) Identification number, (2) HD identifier, (3) ESO programm ID, and (4-5) fit parameters of the K₁ line profile. Single-cloud sight-lines are highlighted in boldface.

| ID | Star | Prog. ID | v _∞ km/s | log(N) cm ⁻² |
|-----|-------------------|---------------|--|--|
| 137 | CPD 592600 | 071.C-0513(C) | -4.35±0.01 4.46±0.08 7.63±0.02 | 10.88±0.12 10.94±0.06 11.54±0.03 |
| 138 | CPD 573509 | 094.D-0355(A) | -3.25±0.04 9.22±0.31 | 11.86±0.03 11.14±0.05 |
| 139 | HD 037022 | 194.C-0833(E) | 19.97±0.05 24.88±0.4 | 10.48±0.18 9.83±0.45 |
| 140 | HD 037023 | 067.C-0281(A) | 20.72±0.02 25.07±0.03 | 10.41±0.24 9.59±0.47 |
| 141 | HD 037041 | 194.C-0833(A) | 19.83±0.03 23.05±0.51 | 10.41±0.18 9.85±0.42 |
| 142 | HD 037367 | 194.C-0833(A) | 13.63±0.13 17.07±0.09 | 11.30±0.09 11.32±0.09 |
| 143 | HD 041117 | 194.C-0833(C) | 10.12±0.13 14.92±0.04 | 11.74±0.09 11.72±0.36 |
| 144 | HD 045314 | 194.C-0833(F) | 3.72±0.26 14.89±0.12 18.81±0.05 24.67±0.05 | 10.33±0.24 11.44±0.09 11.86±0.03 11.01±0.06 |
| 145 | HD 054439 | 194.C-0833(H) | 15.59±0.01 23.19±0.01 28.26±0.01 32.72±0.01 35.18±0.02 | 10.22±0.42 10.59±0.27 10.29±0.03 11.44±0.03 10.85±0.09 |
| 146 | HD 064315 | 082.C-0831(A) | 36.28±0.01 72.56±0.01 | 11.61±0.03 11.49±0.03 |
| 147 | HD 073882 | 194.C-0833(H) | 21.12±0.04 27.70±0.09 34.99±0.31 | 11.35±0.03 10.75±0.06 10.23±0.21 |
| 148 | HD 075309 | 194.C-0833(B) | 18.25±0.03 23.64±0.08 21.60±0.35 | 11.02±0.06 10.50±0.15 11.18±0.06 |
| 149 | HD 091824 | 194.C-0833(B) | -0.79±0.04 8.58±0.25 | 11.56±0.03 10.87±0.15 |
| 150 | HD 093129A | 100.D-0767(A) | -41.78±0.12 -20.32±0.57 -15.32±0.04 | 10.57±0.09 10.49±0.33 11.52±0.03 |
| | | | -6.38±0.63 -1.31±0.16 2.96±0.16 | 10.70±0.30 10.66±0.42 11.55±0.06 |
| 151 | HD 093205 | 194.C-0833(B) | -3.26±0.21 5.82±0.21 8.73±0.15 | 10.63±0.15 11.37±0.09 10.50±0.43 |
| 152 | HD 093222 | 194.C-0833(H) | -23.01±0.22 -7.07±0.04 5.41±0.08 6.74±0.37 -23.85±0.45 -7.18±0.07 5.22±0.16 8.18±4.78 | 10.67±0.06 10.89±0.03 10.78±0.24 10.75±0.27 10.29±0.21 10.77±0.06 10.94±0.47 10.51±0.74 |
| 153 | HD 093250 | 088.D-0424(D) | -27.89±0.23 -15.94±0.06 -3.12±0.25 6.19±0.17 | 10.15±0.21 11.54±0.03 11.10±0.12 11.33±0.06 |
| 154 | HD 093843 | 194.C-0833(F) | -42.49±0.21 -30.53±0.05 -17.72±0.23 -8.42±0.15 | 10.15±0.18 11.54±0.03 11.09±0.09 11.33±0.06 |
| 155 | HD 094493 | 194.C-0833(B) | -10.60±0.23 8.38±0.53 10.08±0.06 | 10.89±0.06 10.65±0.24 10.80±0.15 |
| 156 | HD 101190 | 095.D-0234(A) | -10.72±0.91 2.33±0.11 8.81±0.03 | 10.62±0.24 11.00±0.06 11.66±0.03 |
| 157 | HD 101205 | 080.D-0855(A) | -16.35±0.22 7.88±0.04 | 10.90±0.06 11.49±0.03 |
| 158 | HD 103779 | 194.C-0833(F) | -19.16±0.04 -15.45±0.43 -1.50±0.12 3.15±0.16 | 10.60±0.09 10.54±0.12 10.26±0.12 10.33±0.18 |
| | | | 8.77±0.12 10.59±0.06 | 10.59±0.06 |
| 159 | HD 104705 | 071.C-0513(C) | -24.49±0.01 -16.38±0.02 -6.22±0.07 2.62±0.01 8.01±0.01 | 10.49±0.18 10.52±0.24 9.48±0.55 10.45±0.16 11.10±0.06 |
| 160 | HD 105056 | 266.D-5655(A) | 2.03±0.19 6.91±0.23 11.60±0.25 17.42±0.07 | 10.44±0.15 10.51±0.27 10.49±0.24 10.85±0.06 |

Table A.2. – continued –

| ID | Star | Prog. ID | v _∞ | log(N) |
|-----|------------------|---------------|----------------------------|--------------------------|
| | | | km/s | cm ⁻² |
| 161 | HD 112244 | 089.D-0975(A) | -16.00±0.07 9.12±0.13 | 11.21±0.03 11.07±0.03 |
| 162 | HD 122879 | 194.C-0833(B) | -21.38±0.46 -9.36±0.22 | 10.55±0.15 10.64±0.09 |
| | | | 1.75±0.05 6.98±0.10 | 11.01±0.03 10.53±0.12 |
| | | | 11.71±0.07 | 10.67±0.06 |
| 163 | HD 144470 | 194.C-0833(C) | -10.93±0.01 -7.95±0.01 | 10.96±0.06 10.66±0.12 |
| 164 | HD 148379 | 082.C-0566(A) | -26.35±0.49 -22.19±0.06 | 11.16±0.24 11.71±0.09 |
| | | | -16.26±0.16 -6.90±0.10 | 11.30±0.06 10.83±0.09 |
| | | | 0.40±0.05 | 11.33±0.03 |
| 165 | HD 149408 | 082.C-0566(A) | -22.23±0.07 -11.71±0.22 | 11.68±0.06 11.66±0.09 |
| | | | -7.53±0.45 -3.87±0.10 | 10.58±0.47 11.64±0.06 |
| 166 | HD 151804 | 089.D-0975(A) | -15.62±0.40 -6.50±0.22 | 10.40±0.18 10.93±0.12 |
| | | | 1.44±0.37 -0.21±0.47 | 10.88±0.12 11.42±0.09 |
| 167 | HD 152233 | 079.D-0718(B) | 2.40±0.03 | 11.85±0.03 |
| 168 | HD 152234 | 083.D-0066(C) | -9.86±0.08 1.33±0.04 | 11.54±0.03 11.82±0.03 |
| 169 | HD 152235 | 266.D-5655(A) | -48.57±0.18 -22.81±0.54 | 10.78±0.12 10.26±0.36 |
| | | | -5.14±0.09 0.01±0.09 | 11.75±0.06 11.92±0.06 |
| 170 | HD 152236 | 082.C-0566(A) | -16.52±0.12 -8.82±0.11 | 11.31±0.09 11.69±0.06 |
| | | | 0.12±0.07 | 11.82±0.06 |
| 171 | HD 152249 | 082.C-0566(A) | -39.46±0.01 -16.00±0.01 | 10.93±0.15 10.47±0.27 |
| | | | -9.53±0.01 -4.92±0.01 | 10.85±0.15 10.78±0.18 |
| 172 | HD 153919 | 194.C-0833(F) | -33.36±0.65 -29.42±0.58 | 11.07±0.39 10.69±0.43 |
| | | | -24.44±0.63 -4.36±0.10 | 10.88±0.36 11.69±0.06 |
| | | | 3.41±0.15 | 11.02±0.15 |
| 173 | HD 154445 | 082.C-0566(A) | -15.95±0.01 | 11.55±0.03 |
| 174 | HD 164073 | 194.C-0833(D) | -0.38±0.01 3.07±0.02 | 10.92±0.09 9.82±0.47 |
| 175 | HD 164402 | 079.D-0567(A) | -25.92±0.01 -5.97±0.01 | 10.30±0.06 11.39±0.03 |
| | | | -3.28±0.01 | 9.89±0.45 |
| 176 | HD 166734 | 073.D-0609(A) | -10.90±0.14 -2.66±0.16 | 12.12±0.03 11.66±0.12 |
| | | | 7.58±0.23 | 11.50±0.06 |
| 177 | HD 167264 | 194.C-0833(A) | -10.09±0.01 6.35±0.01 | 10.44±0.24 11.57±0.18 |
| | | | 6.02±0.01 | 10.48±0.18 |
| 178 | HD 167838 | 194.C-0833(F) | -24.92±0.24 -16.52±0.04 | 10.43±0.18 11.42±0.03 |
| | | | -12.01±0.03 | 11.45±0.06 |
| | | | -7.10±0.66 | 10.95±0.24 |
| | | | 1.97±0.14 | 10.72±0.21 |
| | | | 8.81±0.78 | 10.92±0.18 |
| | | | 11.06±0.07 | 10.99±0.18 |
| 179 | HD 167971 | 087.D-0264(F) | -12.14±0.05 -0.47±0.12 | 11.89±0.03 11.64±0.06 |
| | | | 10.99±0.06 | 11.83±0.03 |
| 180 | HD 168075 | 083.D-0066(C) | -12.40±0.22 -9.60±0.12 | 12.00±0.09 11.63±0.21 |
| | | | 6.85±0.07 | 11.65±0.03 |
| 181 | HD 168076 | 071.C-0513(C) | -17.07±0.28 -12.86±0.06 | 11.90±0.45 11.68±0.36 |
| | | | -8.76±0.14 7.27±0.40 | 11.85±0.47 11.06±0.47 |
| | | | 7.54±0.51 | 11.63±0.39 |
| 182 | HD 168137 | 090.D-0600(A) | -11.58±0.04 2.10±0.14 | 12.13±0.03 11.54±0.24 |
| | | | 9.14±3.56 | 11.08±0.45 |
| 183 | HD 169454 | 194.C-0833(F) | -26.06±0.01 -18.56±0.02 | 10.54±0.18 10.66±0.18 |
| | | | -14.02±0.02 | 11.45±0.03 |
| | | | -9.19±0.01 | 12.12±0.03 |
| | | | 0.48±0.01 | 10.84±0.15 |
| | | | 7.11±0.02 | 10.70±0.15 |
| | | | 12.00±0.02 | 10.70±0.18 |
| 184 | HD 175156 | 079.D-0567(A) | -5.65±0.01 -27.37±0.69 | 11.97±0.03 10.77±0.09 |
| 185 | HD 303308 | 194.C-0833(D) | -9.85±0.14 6.47±0.17 | 10.35±0.12 11.46±0.06 |
| | | | 10.48±0.05 | 11.09±0.15 |
| 186 | Walker 67 | 092.C-0019(A) | 26.20±0.01 | 11.66±0.03 |

Table A.3. Result summary. The meaning of the columns is: (1) Identification number as of Table 1, (2) HD identifier, equivalent width (EW) of (3) Ca II K and (4) Ca II H doublet used for (5) distance estimate (Megier et al. (2009)). Distances obtained from (6) GAIA parallax and (7) spectral type-to-luminosity ratio. Appearance of single (S) or multi (M) velocity components of profiles for (8) Ca II H and K, (9) Na I, (10) K I lines. Fit parameters of the K I line profile: (11) position, (12) column density, and (13) derived equivalent width. (14) Classification of cloud environment as cold (c) or warm (w) with or without CN I detection. (15) Infrared morphology of WISE (W4) image. Single-cloud sight-lines are highlighted in boldface.

| 1 | 2 | 3 | 4 | 5 | 6 | 7 | 8 | 9 | 10 | 11 | 12 | 13 | 14 | 15 |
|----|------------------|---------------|---------------|--------------------------------------|--|------|------------|------|-----|--------------------------|--|-------------|----------------|-------|
| ID | Target | Ca II | | Distance | | | Components | | | K I | | | Environ. | WISE |
| | | EW(K) (mÅ) | EW(H) (mÅ) | Ca II | GAIA | Sp/L | Ca II K | Na I | K I | v _∞ (km/s) | log N (10 ⁹ /cm ²) | EW (mÅ) | class | class |
| 1 | HD 023180 | 86±2 | 47±1 | 340 ⁺²⁰ ₋₁₅ | 256 ⁺⁷² ₋₄₇ | 320 | S | S | M | 13.08 | 464 ± 11 | 69.1 ± 1.6 | c+CN | a |
| 2 | HD 024263 | 129±3 | 84±2 | 670 ⁺⁶⁵ ₋₅₀ | 222 ⁺⁴⁸ ₋₃₈ | 210 | M | S | S | 21.93 | 706 ± 10 | 90.6 ± 1.2 | - | a |
| 3 | HD 024912 | 121±6 | 73±5 | 540 ⁺¹⁵⁰ ₋₈₅ | 1134 ⁺¹¹⁴ ₋₆₀₅ | 650 | M | M | M | 7.27 | 239 ± 17 | 36.8 ± 2.6 | w-CN | a |
| | " | | | | | | | | | 10.61 | 103 ± 12 | 16.7 ± 1.9 | | |
| | " | | | | | | | | | 15.00 | 39 ± 13 | 6.7 ± 2.2 | | |
| 4 | HD 027778 | 62±1 | 36±1 | 300 ⁺¹⁵ ₋₂₀ | 223 ⁺³ ₋₅ | 250 | S | - | M | 11.87 | 596 ± 4 | 86.8 ± 0.6 | c+CN | a |
| 5 | HD 030123 | 177±4 | 127±3 | 1145 ⁺¹¹⁰ ₋₁₁₅ | 594 ⁺²⁰ ₋₁₉ | 500 | S | S | M | 15.86 | 316 ± 3 | 45.1 ± 0.4 | c+CN | a |
| 6 | HD 030470 | 149±6 | 112±4 | 1120 ⁰ ₋₁₈₅ | 778 ⁺⁶⁰ ₋₅₃ | 440 | S | S | S | 20.98 | 1002 ± 8 | 112.8 ± 1.0 | - | a |
| 7 | HD 030492 | 156±7 | 117±4 | 1160 ⁰ ₋₁₉₀ | 597 ⁺³³ ₋₃₉ | 390 | S | S | S | 21.24 | 893 ± 6 | 100.8 ± 0.7 | c+CN | a |
| 8 | HD 037130 | 100±7 | 57±5 | 410 ⁺¹¹⁰ ₋₇₅ | 400 ⁺⁸ ₋₇₉ | 765 | S | - | S | 28.57 | 67 ± 7 | 11.3 ± 1.1 | no CH | a |
| 9 | HD 037903 | 101±4 | 55±3 | 390 ⁺⁵⁰ ₋₄₅ | 397 ⁺⁹ ₋₉ | 1225 | M | M | M | 23.47 | 29 ± 3 | 4.9 ± 0.6 | w+CN | c |
| | " | | | | | | | | | 27.42 | 33 ± 4 | 5.6 ± 0.7 | | |
| 10 | HD 038023 | 141±9 | 78±7 | 525 ⁺¹⁶⁰ ₋₁₄₀ | 404 ⁺⁷ ₋₁₄ | 860 | M | S | S | 23.03 | 562 ± 6 | 73.2 ± 0.8 | c+CN | a |
| 11 | HD 046056 | 279±14 | 193±9 | 1590 ⁺⁴³⁰ ₋₂₈₀ | 1469 ⁺¹⁴⁸ ₋₁₂₄ | 2030 | M | M | M | 17.64 | 371 ± 4 | 52.7 ± 0.6 | - | c |
| | " | | | | | | | | | 24.07 | 636 ± 5 | 79.2 ± 0.6 | | |
| | " | | | | | | | | | 29.95 | 198 ± 5 | 31.7 ± 0.8 | | |
| 12 | HD 046106 | 279±13 | 202±7 | 1810 ⁰ ₋₂₉₀ | 1623 ⁺²⁸⁷ ₋₂₁₄ | 1540 | M | M | M | 5.20 | 24 ± 8 | 4.1 ± 1.3 | w-CN | b |
| | " | | | | | | | | | 17.55 | 233 ± 5 | 36.8 ± 0.8 | | |
| | " | | | | | | | | | 24.76 | 346 ± 5 | 52.0 ± 0.7 | | |
| | " | | | | | | | | | 29.90 | 291 ± 5 | 44.6 ± 0.7 | | |
| 13 | HD 046149 | 264±13 | 182±7 | 1500 ⁺³⁴⁰ ₋₂₄₀ | 1473 ⁺¹⁷² ₋₁₄₀ | 1815 | M | S | S | 26.12 | 975 ± 25 | 136.1 ± 3.4 | w-CN | a |
| | " | | | | | | | | | 13.88 | 74 ± 19 | 12.7 ± 3.1 | | |
| 14 | HD 046202 | 290±23 | 202±21 | 1680 ⁰ ₋₄₈₀ | 1347 ⁺³⁸³ ₋₂₄₇ | 1805 | M | S | S | 23.84 | 717 ± 29 | 99.7 ± 4.0 | - | d |
| 15 | HD 046223 | 297±5 | 204±3 | 1660 ⁺¹²⁰ ₋₁₁₀ | 1663 ⁺¹⁶⁹ ₋₁₄₁ | 1895 | M | S | S | 26.36 | 1314 ± 18 | 178.0 ± 2.4 | c+CN | b |
| 16 | HD 046485 | 251±12 | 175±8 | 1470 ⁺³⁹⁰ ₋₂₅₀ | 1735 ⁺¹³⁵ ₋₁₉₉ | 2420 | M | S | M | 21.42 | 147 ± 6 | 24.2 ± 1.0 | c+CN | a |
| | " | | | | | | | | | 24.20 | 332 ± 4 | 46.6 ± 0.6 | | |
| | " | | | | | | | | | 28.32 | 995 ± 7 | 111.1 ± 0.8 | | |
| 17 | HD 046660 | 286±7 | 184±5 | 1360 ⁺¹⁴⁵ ₋₁₂₅ | 1153 ⁺⁷³ ₋₆₀ | 1510 | M | S | M | 19.66 | 1788 ± 9 | 175.6 ± 0.9 | c+CN | a |
| 18 | HD 046711 | 387±32 | 289±22 | 2730 ⁺⁸⁵ ₋₈₂₀ | 1740 ⁺¹⁹⁵ ₋₁₃₃ | 2130 | M | M | M | 22.20 | 1462 ± 21 | 163.2 ± 2.3 | c+CN | a |
| | " | | | | | | | | | 28.52 | 1015 ± 13 | 107.9 ± 1.4 | w-CN | |
| | " | | | | | | | | | 33.87 | 202 ± 10 | 31.8 ± 1.5 | | |
| 19 | HD 046883 | 198±8 | 138±5 | 1170 ⁺¹⁹² ₋₁₃₅ | 1381 ⁺¹²⁹ ₋₁₀₉ | 1420 | M | M | M | 17.37 | 516 ± 3 | 67.4 ± 0.4 | c+CN | a |
| | " | | | | | | | | | 22.48 | 875 ± 4 | 97.8 ± 0.4 | | |
| 20 | HD 047107 | 260±12 | 167±9 | 1235 ⁺²²⁰ ₋₁₅₀ | 803 ⁺¹⁸⁰ ₋₁₂₅ | 1160 | M | - | M | 4.49 | 18 ± 4 | 3.2 ± 0.8 | no CH | b |
| | " | | | | | | | | | 9.39 | 53 ± 6 | 9.0 ± 0.9 | | |
| | " | | | | | | | | | 19.98 | 78 ± 6 | 13.2 ± 1.1 | | |
| | " | | | | | | | | | 26.62 | 80 ± 7 | 13.5 ± 1.1 | | |
| 21 | HD 047382 | 290±9 | 197±5 | 1570 ⁺²¹⁰ ₋₁₆₀ | 4063 ⁺¹⁶¹⁶ ₋₁₀₀₀ | 1410 | M | M | M | 19.63 | 343 ± 32 | 55.3 ± 5.2 | - | a |
| | " | | | | | | | | | 27.70 | 703 ± 34 | 104.5 ± 5.1 | | |
| 22 | HD 050562 | 305±15 | 178±14 | 1160 ⁺³¹⁰ ₋₂₁₀ | 3395 ⁺⁶³⁴ ₋₄₇₀ | 1100 | M | M | M | 23.97 | 14 ± 6 | 2.5 ± 1.0 | no CH | a |
| | " | | | | | | | | | 31.43 | 31 ± 5 | 5.3 ± 0.9 | | |
| | " | | | | | | | | | 39.43 | 66 ± 8 | 11.3 ± 1.3 | | |
| | " | | | | | | | | | 47.59 | 49 ± 4 | 8.3 ± 0.6 | | |
| | " | | | | | | | | | 52.01 | 42 ± 4 | 7.1 ± 0.7 | | |
| | " | | | | | | | | | 72.21 | 24 ± 7 | 4.1 ± 1.2 | | |
| 23 | HD 054306 | 198±5 | 114±4 | 759 ⁺⁶⁸ ₋₅₉ | 1930 ⁺⁴⁰⁸ ₋₂₉₀ | 1540 | M | M | M | 21.21 | 25 ± 7 | 4.3 ± 1.3 | w-CN | a |
| | " | | | | | | | | | 33.64 | 141 ± 9 | 23.3 ± 1.5 | | |
| 24 | HD 060479 | 353±43 | 253±23 | 2200 ⁰ ₋₇₂₀ | 3419 ⁺⁶⁰² ₋₄₅₀ | 4000 | M | M | M | 35.42 | 2150 ± 15 | 219.6 ± 1.5 | - ^y | a |
| | " | | | | | | | | | 45.49 | 690 ± 9 | 96.8 ± 1.3 | | |
| 25 | HD 062542 | 53±2.3 | 36.7±2.3 | 365 ⁺⁹⁵ ₋₅₀ | 386 ⁺⁵ ₋₄₃ | 555 | M | S | S | 13.65 | 497 ± 5 | 70.6 ± 0.7 | c+CN | a |
| 26 | HD 068633 | 96±3 | 68±3 | 630 ⁺¹³⁰ ₋₁₁₅ | 677 ⁺⁴³ ₋₃₇ | 795 | M | M | M | 9.29 | 594 ± 5 | 74.7 ± 0.6 | c+CN | a |
| | " | | | | | | | | | 19.09 | 333 ± 5 | 48.2 ± 0.7 | c+CN | |
| 27 | HD 070614 | 272±18 | 187±12 | 1530 ⁰ ₋₃₄₀ | 1868 ⁺¹³⁷ ₋₁₂₀ | 1400 | S | S | M | 22.52 | 527 ± 10 | 71.3 ± 1.4 | - | c |
| | " | | | | | | | | | 30.64 | 259 ± 16 | 42.2 ± 2.6 | | |
| 28 | HD 072648 | 476±17 | 347±10 | 3360 ⁰ ₋₄₆₀ | 1233 ⁺⁶⁶ ₋₆₀ | 825 | M | S | M | 21.61 | 528 ± 8 | 76.6 ± 1.1 | w-CN | b |
| | " | | | | | | | | | 44.40 | 54 ± 6 | 9.3 ± 1.1 | | |
| 29 | HD 079186 | 223±3 | 145±2 | 1100 ⁺⁶⁰ ₋₂₈₀ | 1279 ⁺³⁶⁹ ₋₂₃₉ | 1650 | M | M | S | 11.75 | 439 ± 3 | 57.3 ± 0.4 | - | a |
| 30 | HD 083597 | 247±11 | 160±9 | 1200 ⁺²⁰⁰ ₋₂₀₀ | 2631 ⁺²³⁸ ₋₂₃₄ | 2120 | M | M | M | 7.86 | 91 ± 14 | 15.6 ± 2.4 | - | a |
| | " | | | | | | | | | 16.64 | 331 ± 7 | 48.8 ± 1.1 | | |
| 31 | HD 089137 | 253±8 | 154±6 | 1070 ⁺¹⁴⁰ ₋₁₃₅ | 3417 ⁺⁵³⁴ ₋₄₁₂ | 3090 | M | M | S | 8.70 | 106 ± 5 | 17.5 ± 0.9 | w-CN | c |
| 32 | HD 091943 | 296±6 | 182±6 | 1265 ⁺¹³⁵ ₋₁₁₅ | 3422 ⁺⁴³⁵ ₋₃₆₃ | 3585 | M | S | M | -10.91 | 477 ± 5 | 64.0 ± 0.7 | - | a |
| | " | | | | | | | | | -3.26 | 81 ± 5 | 13.6 ± 0.9 | | |
| | " | | | | | | | | | 8.43 | 68 ± 9 | 11.6 ± 1.5 | | |
| 33 | HD 091969 | 307±16 | 188±12 | 1300 ⁺³³⁰ ₋₂₃₀ | 2567 ⁺³⁷⁴ ₋₂₉₂ | 2290 | M | - | M | -12.30 | 29 ± 11 | 5.0 ± 1.9 | no CH | a |
| | " | | | | | | | | | -3.83 | 97 ± 10 | 16.2 ± 1.6 | | |
| | " | | | | | | | | | 2.25 | 110 ± 10 | 18.2 ± 1.6 | | |
| | " | | | | | | | | | 9.04 | 102 ± 10 | 17.0 ± 1.6 | | |
| 34 | HD 091983 | 308±11 | 202±8 | 1525 ⁺²⁸⁰ ₋₂₁₀ | 3698 ⁺⁸⁵³ ₋₇₁₇ | 2110 | M | S | S | -3.01 | 437 ± 6 | 62.0 ± 0.8 | - | a |
| 35 | HD 092007 | 283±12 | 195±10 | 1600 ⁺²⁸⁰ ₋₂₈₀ | 2841 ⁺⁴³⁷ ₋₃₂₅ | 3080 | M | M | M | -3.51 | 445 ± 6 | 61.2 ± 0.8 | c+CN | b |
| | " | | | | | | | | | 6.34 | 130 ± 8 | 21.8 ± 1.4 | | |
| 36 | HD 092044 | 238±7 | 173±6 | 1570 ⁰ ₋₂₂₀ | 2852 ⁺⁵³⁹ ₋₃₉₇ | 2880 | M | M | S | -4.28 | 531 ± 10 | 67.7 ± 1.3 | c+CN | b |

Table A.3. – continued –

| 1 | 2 | 3 | 4 | 5 | 6 | 7 | 8 | 9 | 10 | 11 | 12 | 13 | 14 | 15 | |
|----|-------------------------|---------------|---------------|--------------------------------------|---------------------------------------|------|------------|---|------|--------|-----------------------|-----------------------------------|------------|-------|-------|
| ID | Target | Ca II | | Distance | | | Components | | | K I | | | Environ. | WISE | |
| | | EW(K) (mÅ) | EW(H) (mÅ) | Ca II | GAIA | Sp/L | Ca II | K | Na I | K I | v_{\odot} (km/s) | log N ($10^9 / \text{cm}^2$) | EW (mÅ) | class | class |
| 37 | HD 093632 | 795±31 | 511±19 | 3520 ⁺⁶³⁰ ₋₄₇₀ | 2486 ⁺²³⁰ ₋₁₉₅ | 3465 | M | M | M | -17.88 | 234 ± 7 | 35.6 ± 1.1 | w-CN | d | |
| " | | | | | | | | | | -12.18 | 90 ± 7 | 14.9 ± 1.1 | | | |
| " | | | | | | | | | | -1.81 | 66 ± 11 | 11.2 ± 1.9 | | | |
| " | | | | | | | | | | 7.29 | 119 ± 7 | 19.5 ± 1.2 | | | |
| 38 | HD 094663 | 415±36 | 292±19 | 2440 ⁰ ₋₆₁₀ | 3311 ⁺³⁸⁵ ₋₃₁₄ | 4040 | M | M | M | -10.20 | 505 ± 9 | 64.4 ± 1.2 | - | d | |
| " | | | | | | | | | | -6.68 | 555 ± 24 | 86.0 ± 3.8 | | | |
| " | | | | | | | | | | 6.95 | 147 ± 13 | 24.2 ± 2.2 | | | |
| 39 | HD 096042 | 459±32 | 326±19 | 2760 ⁰ ₋₆₅₀ | 4007 ⁺⁶⁴⁹ ₋₄₉₇ | 1080 | M | M | M | -12.88 | 183 ± 7 | 29.0 ± 1.1 | - | c | |
| " | | | | | | | | | | -5.85 | 330 ± 7 | 48.3 ± 1.1 | | | |
| " | | | | | | | | | | -0.47 | 513 ± 8 | 69.2 ± 1.1 | | | |
| " | | | | | | | | | | 9.68 | 97 ± 9 | 16.4 ± 1.6 | | | |
| 40 | HD 096675 | 32±3 | 19±5 | 193 ⁺³⁸ ₋₂₅ | 162 ⁺² ₋₂ | 360 | S | S | S | 14.97 | 418 ± 4 | 57.1 ± 0.5 | c+CN | a | |
| 41 | HD 097484 | 396±24 | 295±11 | 2770 ⁰ ₋₅₅₀ | 2760 ⁺³⁸⁷ ₋₃₀₄ | 2575 | M | S | M | -8.38 | 332 ± 9 | 51.4 ± 1.5 | c+CN | b | |
| " | | | | | | | | | | -0.79 | 1823 ± 16 | 194.0 ± 1.7 | | | |
| 42 | HD 099264 | 50±2 | 28±2 | 240 ⁺³⁸ ₋₂₇ | 234 ⁺⁶ ₋₆ | 300 | M | S | M | 7.06 | 21 ± 4 | 3.7 ± 0.7 | w-CN | a | |
| " | | | | | | | | | | 14.00 | 155 ± 6 | 25.2 ± 1.0 | | | |
| 43 | HD 099872 | 59±2 | 37±2 | 320 ⁺²⁴ ₋₂₀ | 240 ⁺²⁴ ₋₂₀ | 240 | S | S | M | 8.81 | 72 ± 5 | 12.3 ± 0.8 | w+CN | a | |
| " | | | | | | | | | | 13.43 | 292 ± 4 | 42.9 ± 0.5 | | | |
| 44 | HD 099890 | 458±13 | 294±9 | 2120 ⁺²⁷⁰ ₋₂₂₀ | 1861 ⁺¹⁹² ₋₁₆₀ | 1760 | M | M | M | -18.53 | 153 ± 5 | 24.9 ± 0.9 | no CH | b | |
| " | | | | | | | | | | -9.03 | 125 ± 5 | 20.5 ± 0.9 | | | |
| 45 | HD 100213 | 314±5 | 191±5 | 1310 ⁺¹⁰⁰ ₋₈₅ | 2230 ⁺²²² ₋₁₈₆ | 4590 | M | M | M | -17.38 | 179 ± 4 | 28.1 ± 0.6 | w-CN | a | |
| " | | | | | | | | | | 6.12 | 305 ± 4 | 44.1 ± 0.6 | | | |
| 46 | HD 101008 | 295±8 | 177±7 | 1195 ⁺¹⁵² ₋₁₂₃ | 3703 ⁺⁶⁶⁷ ₋₄₉₇ | 3580 | M | M | S | 8.69 | 203 ± 8 | 32.3 ± 1.2 | w-CN | a | |
| 47 | HD 104565 | 491±15 | 372±11 | 3620 ⁰ ₋₅₂₀ | 5181 ⁺¹⁵⁴ ₋₈₂₈ | 4615 | M | S | M | -17.06 | 375 ± 4 | 51.9 ± 0.5 | c+CN | a | |
| " | | | | | | | | | | 9.49 | 75 ± 4 | 12.6 ± 0.6 | w-CN | a | |
| 48 | HD 108927 | 62±3 | 41±3 | 375 ⁺¹⁰⁴ ₋₆₅ | 338 ⁺⁵ ₋₅ | 450 | S | S | S | 11.56 | 462 ± 4 | 61.7 ± 0.5 | c+CN | a | |
| 49 | HD 110336 | 60±3 | 37±3 | 320 ⁺⁸⁰ ₋₇₀ | 314 ⁺⁴ ₋₄ | 305 | M | S | S | 12.04 | 638 ± 7 | 77.0 ± 0.9 | c+CN | a | |
| 50 | HD 110715 | 98±3 | 63±3 | 504 ⁺⁵⁰ ₋₅₄ | 532 ⁺¹² ₋₁₂ | 267 | S | S | S | 4.78 | 960 ± 7 | 116.6 ± 0.8 | c+CN | a | |
| 51 | HD 110863 | 340±9 | 208±9 | 1430 ⁺²⁰⁰ ₋₁₇₀ | 1944 ⁺¹⁶² ₋₁₄₀ | 1770 | M | M | M | -30.36 | 536 ± 6 | 68.4 ± 0.7 | c+CN | a | |
| " | | | | | | | | | | -9.84 | 142 ± 8 | 23.6 ± 1.3 | w-CN | a | |
| " | | | | | | | | | | 7.52 | 297 ± 6 | 45.2 ± 1.0 | | | |
| 52 | HD 110946 | 288±12 | 180±8 | 1280 ⁺²³⁰ ₋₁₅₀ | 2078 ⁺¹⁶⁴ ₋₁₆₂ | 1480 | M | M | S | 3.13 | 755 ± 16 | 103.1 ± 2.1 | c+CN | a | |
| 53 | HD 111973 | 426±13 | 242±8 | 1510 ⁺³⁹⁰ ₋₁₉₀ | 2171 ⁺²⁶² ₋₂₁₂ | 2340 | M | M | M | -14.20 | 70 ± 5 | 11.9 ± 0.8 | w-CN | a | |
| " | | | | | | | | | | 7.55 | 160 ± 4 | 25.6 ± 0.7 | | | |
| 54 | HD 111990 | 435±15 | 256±8 | 1660 ⁺²⁰⁰ ₋₁₆₀ | 3643 ⁺⁵⁹¹ ₋₄₅₂ | 1800 | M | M | M | -14.10 | 87 ± 6 | 14.5 ± 1.0 | c+CN | a | |
| " | | | | | | | | | | 7.86 | 205 ± 6 | 31.9 ± 1.0 | | | |
| 55 | HD 112607 | 86±4 | 54±4 | 430 ⁺¹²⁰ ₋₆₄ | 592 ⁺¹⁵ ₋₁₄ | 633 | S | S | S | 5.38 | 730 ± 7 | 90.1 ± 0.9 | c+CN | a | |
| 56 | HD 112954 | 72±3 | 53±2 | 556 ^l ₋₆₁ | 387 ⁺⁶ ₋₇ | 172 | S | S | S | 4.18 | 1176 ± 7 | 124.8 ± 0.8 | c+CN | a | |
| 57 | HD 122669 | 343±15 | 223±12 | 1650 ⁺⁴⁰⁰ ₋₂₇₀ | 2258 ⁺¹⁷² ₋₁₅₀ | 1610 | M | M | M | 18.14 | 163 ± 4 | 26.1 ± 0.7 | w-CN | a | |
| " | | | | | | | | | | -3.30 | 40 ± 5 | 6.9 ± 0.8 | | | |
| " | | | | | | | | | | 2.18 | 146 ± 6 | 24.1 ± 1.0 | | | |
| 58 | HD 123008 | 594±19 | 383±11 | 2750 ⁺³⁶⁵ ₋₂₉₀ | 4115 ⁺⁷⁸⁰ ₋₅₇₅ | 5191 | M | M | M | -15.74 | 177 ± 8 | 28.3 ± 1.3 | w-CN | a | |
| " | | | | | | | | | | -4.45 | 95 ± 7 | 15.8 ± 1.2 | | | |
| " | | | | | | | | | | 0.16 | 93 ± 7 | 15.4 ± 1.2 | | | |
| " | | | | | | | | | | 5.14 | 41 ± 7 | 7.0 ± 1.2 | | | |
| 60 | HD 125288 ^{LR} | 37±1 | 16±1 | 150 ⁺¹² ₋₇ | 239 ⁺⁵⁷ ₋₃₉ | 271 | S | S | S | 2.00 | 262 ± 7 | 42.2 ± 1.1 | - | a | |
| 61 | HD 129557 | 60±2 | 26±2 | 200 ⁺¹² ₋₁₀ | 430 ⁺¹¹ ₋₁₁ | 295 | S | S | S | -1.00 | 0 ± 0 | -1.0 ± -1.0 | - | a | |
| 63 | HD 141318 | 111±4 | 62±4 | 440 ⁺⁷⁰ ₋₆₀ | 589 ⁺³³ ₋₃₀ | 660 | M | M | M | -1.82 | 132 ± 4 | 21.3 ± 0.7 | - | a | |
| " | | | | | | | | | | 2.53 | 99 ± 6 | 16.5 ± 1.0 | | | |
| 64 | HD 141926 | 285±7 | 172±5 | 1191 ⁺²⁸⁷ ₋₁₇₄ | 1345 ⁺⁸⁸ ₋₇₈ | 1110 | M | M | M | -15.82 | 165 ± 10 | 27.1 ± 1.7 | - | c | |
| " | | | | | | | | | | -5.72 | 548 ± 20 | 74.8 ± 1.3 | | | |
| " | | | | | | | | | | 2.30 | 138 ± 8 | 22.6 ± 1.4 | | | |
| 65 | HD 143054 | 215±9 | 147±9 | 1210 ⁺²²⁰ ₋₁₆₀ | 290 ⁺⁵⁰ ₋₃₈ | 1070 | M | M | M | -23.97 | 241 ± 7 | 36.5 ± 1.1 | - | b | |
| " | | | | | | | | | | -15.81 | 183 ± 8 | 29.1 ± 1.3 | | | |
| " | | | | | | | | | | -7.24 | 141 ± 9 | 23.2 ± 1.5 | | | |
| " | | | | | | | | | | 0.10 | 232 ± 7 | 35.5 ± 1.1 | | | |
| 66 | HD 146284 | 61±3 | 33±2 | 260 ⁺⁴⁰ ₋₃₀ | 205 ⁺³ ₋₂ | 250 | M | M | S | -7.48 | 372 ± 4 | 51.0 ± 0.5 | - | b | |
| 67 | HD 146285 | 69±4 | 41±4 | 326 ⁺⁸⁸ ₋₅₄ | 156 ⁺² ₋₂ | 275 | M | S | S | -5.39 | 137 ± 5 | 22.2 ± 0.8 | w-CN | b | |
| 68 | HD 147165 | 55±1 | 30±1 | 247 ⁺¹⁶ ₋₁₄ | 103 ⁺¹⁴ ₋₁₁ | 130 | S | S | S | -5.89 | 143 ± 6 | 22.9 ± 0.9 | - | c | |
| 69 | HD 147196 | 32±4 | 20±3 | 213 ⁺⁵² ₋₃₈ | 139 ⁺² ₋₂ | 220 | M | S | S | -6.46 | 359 ± 5 | 50.0 ± 0.7 | c+CN | a | |
| 71 | HD 147701 | 50±2 | 40±1 | 139 ⁺¹ ₋₁ | 140 | 140 | S | S | S | -6.70 | 862 ± 4 | 93.1 ± 0.4 | c+CN | b | |
| 72 | HD 147888 | 66±2 | 53±2 | 92 ⁺¹ ₋₁ | 185 | 185 | S | S | S | -8.57 | 828 ± 5 | 86.7 ± 0.5 | c+CN | a | |
| 73 | HD 147889 | 43±2 | 37±2 | 138 ⁺³ ₋₂ | 140 | 140 | S | S | S | -7.73 | 675 ± 4 | 72.6 ± 0.5 | c+CN | a | |
| 74 | HD 147933 | 65±4 | 49±3 | 140 ⁺⁴ ₋₄ | 155 | 155 | S | S | S | -8.17 | 685 ± 3 | 88.0 ± 0.4 | c+CN | a | |
| 75 | HD 148579 | 55±5 | 33±4 | 290 ⁺¹²⁰ ₋₆₅ | 139 ⁺⁵ ₋₃ | 165 | S | S | S | -5.79 | 344 ± 3 | 49.3 ± 0.5 | w-CN | a | |
| 76 | HD 148594 | 64±5 | 38±4 | 310 ⁺¹¹⁵ ₋₆₀ | 192 ⁺⁴ ₋₄ | 285 | M | S | S | -4.62 | 255 ± 4 | 38.5 ± 0.6 | w-CN | a | |
| 77 | HD 149038 | 238±3 | 147±2 | 1040 ⁺⁵⁰ ₋₄₅ | 1032 ⁺¹⁷⁴⁶ ₋₄₂₅ | 980 | M | - | M | -8.97 | 42 ± 6 | 7.1 ± 1.1 | w-CN | a | |
| " | | | | | | | | | | -5.35 | 76 ± 5 | 12.4 ± 0.8 | | | |
| " | | | | | | | | | | -2.32 | 115 ± 6 | 18.5 ± 1.0 | | | |
| " | | | | | | | | | | 1.46 | 140 ± 5 | 21.6 ± 0.8 | | | |
| 78 | HD 149757 | 49±1 | 27±1 | 230 ⁺⁸ ₋₆₄ | 182 ⁺⁵³ ₋₄₄ | 230 | M | M | S | -14.23 | 474 ± 4 | 58.4 ± 0.5 | c+CN | a | |
| 80 | HD 152096 | 439±25 | 296±14 | 2300 ⁺³⁹⁰ ₋₃₆₀ | 1434 ⁺¹⁰⁰ ₋₈₈ | - | M | M | M | -4.58 | 142 ± 6 | 22.8 ± 1.0 | w-CN | a | |
| " | | | | | | | | | | 1.27 | 102 ± 6 | 16.9 ± 1.1 | | | |
| 81 | HD 152245 | 406±18 | 252±14 | 1740 ⁺³⁹⁰ ₋₂₇₀ | 1776 ⁺²⁸² ₋₂₁₆ | 1765 | M | M | M | -12.95 | 81 ± 4 | 13.4 ± 0.6 | w-CN | a | |
| " | | | | | | | | | | -5.60 | 217 ± 6 | 34.7 ± 1.0 | | | |
| " | | | | | | | | | | 0.65 | 107 ± 4 | 17.5 ± 0.6 | | | |
| " | | | | | | | | | | 4.71 | 42 ± 4 | 7.1 ± 0.7 | | | |

Table A.3. – continued –

| 1 | 2 | 3 | 4 | 5 | 6 | 7 | 8 | 9 | 10 | 11 | 12 | 13 | 14 | 15 |
|-----|-------------------------|---------------|---------------|--------------------------------------|---------------------------------------|------|------------|------|-----|--------------------------|--|-------------|----------------|----------------|
| ID | Target | Ca II | | Distance | | | Components | | | K I | | | Environ. | WISE |
| | | EW(K) (mÅ) | EW(H) (mÅ) | Ca II | GAIA (pc) | Sp/L | Ca II K | Na I | K I | v _∞ (km/s) | log N (10 ⁹ /cm ²) | EW (mÅ) | class | class |
| 82 | HD 152247 | 430±34 | 291±15 | 2270 ⁺⁸²⁰ ₋₃₂₀ | 1850 ⁺²²⁰ ₋₁₇₉ | 1960 | M | M | M | -8.17 | 174 ± 35 | 29.8 ± 6.1 | - | a |
| " | | | | | | | | | | 2.14 | 532 ± 15 | 80.2 ± 2.2 | | |
| 83 | HD 152560 | 411±14 | 283±9 | 2280 ⁺³⁸⁰ ₋₁₀₀ | 1754 ⁺²⁴⁹ ₋₁₉₅ | 2340 | M | - | M | -4.26 | 69 ± 2 | 11.4 ± 0.4 | - | a |
| " | | | | | | | | | | 1.09 | 456 ± 4 | 63.2 ± 0.5 | | |
| 84 | HD 152667 | 399±13 | 267±9 | 2055 ⁺³³⁰ ₋₂₅₀ | 1584 ⁺¹⁷⁷ ₋₁₄₅ | 1760 | M | M | M | -1.41 | 490 ± 4 | 66.2 ± 0.5 | c+CN | - ^e |
| " | | | | | | | | | | 3.29 | 304 ± 4 | 45.0 ± 0.5 | | |
| 85 | HD 155756 | 718±22 | 494±14 | 3910 ⁺⁵⁹⁵ ₋₄₅₀ | 3307 ⁺⁸²³ ₋₅₆₁ | 6870 | M | M | M | -14.88 | 358 ± 5 | 49.7 ± 0.7 | c+CN | b |
| " | | | | | | | | | | 4.20 | 165 ± 6 | 26.4 ± 0.9 | w-CN | |
| 86 | HD 156247 | 73±3 | 46±3 | 390 ⁺⁸⁰ ₋₁₀₀ | 266 ⁺¹⁰ ₋₁₀₀ | 425 | M | S | S | -15.73 | 206 ± 6 | 31.8 ± 0.9 | w+CN | b |
| 87 | HD 161653 | 243±6 | 147±5 | 1020 ⁺¹⁰⁰ ₋₁₀₀ | 1418 ⁺¹⁸² ₋₁₅₂ | 1230 | M | M | S | -4.28 | 254 ± 4 | 38.5 ± 0.6 | w-CN | a |
| 88 | HD 162978 | 200±6 | 122±5 | 870 ⁺¹¹⁰ ₋₁₀₀ | 1082 ⁺¹⁵² ₋₉₉ | 1220 | M | M | S | -5.17 | 229 ± 4 | 35.4 ± 0.7 | w-CN | a |
| 89 | HD 163181 | 262±10 | 168±7 | 1240 ⁺²²⁰ ₋₁₆₀ | 1879 ⁺²⁴⁰ ₋₁₉₂ | 1710 | M | M | M | -9.41 | 135 ± 3 | 21.6 ± 0.4 | w+CN | a |
| 90 | HD 164536 | 274±13 | 167±9 | 1155 ⁺²⁴⁰ ₋₁₇₀ | 1402 ⁺¹⁴⁵² ₋₄₈₈ | 1980 | M | M | S | -5.07 | 293 ± 6 | 43.5 ± 0.9 | w-CN | d |
| 91 | Hershel 36 | 211±1 | 129±1 | 910 ⁺²⁹⁰ ₋₂₉₀ | 1110 ⁺¹⁰⁸ ₋₁₀₈ | - | M | S | S | -5.00 | 616 ± 6 | 82.9 ± 0.8 | - | - ^e |
| 92 | HD 164816 | 182±10 | 111±10 | 790 ⁺²⁶⁰ ₋₁₆₀ | 1155 ⁺¹⁰⁸ ₋₉₀ | 1020 | M | M | S | -4.73 | 311 ± 30 | 49.7 ± 4.8 | - | a |
| 93 | HD 164863 | 169±6 | 102±4 | 730 ⁺¹⁰⁰ ₋₈₀ | 2747 ⁺²¹⁴ ₋₆₇₄ | 1270 | M | M | M | -8.92 | 74 ± 4 | 12.4 ± 0.7 | w-CN | a |
| 94 | HD 164906 | 222±4 | 133±4 | 900 ⁺¹⁰⁰ ₋₅₈₈ | 1170 ⁺⁶⁰⁹ ₋₃₀₁ | 940 | M | M | S | -5.40 | 459 ± 5 | 58.7 ± 0.6 | - | d |
| 95 | HD 164947A | 262±14 | 138±9 | 830 ⁺¹⁵⁰ ₋₁₅₀ | 1264 ⁺⁵⁴ ₋₅₄ | 1490 | M | M | S | -4.95 | 290 ± 13 | 43.3 ± 1.9 | w-CN | a |
| 95 | HD 164947B | 238±23 | 149±15 | 1075 ⁺⁴⁴⁰ ₋₂₄₀ | 1225 ⁺⁸⁹ ₋₇₈ | 1810 | M | M | S | -4.96 | 292 ± 11 | 43.5 ± 1.6 | w-CN | a |
| 96 | HD 167771 | 299±13 | 193±10 | 1430 ⁺³³⁰ ₋₃₃₀ | 1833 ⁺¹⁵⁹ ₋₁₅₂ | 3030 | M | S | S | -6.30 | 603 ± 6 | 79.2 ± 0.8 | c+CN | a |
| 97 | HD 168750 | 317±24 | 193±15 | 1320 ⁺⁴⁷⁰ ₋₂₈₀ | 1670 ⁺¹⁷¹ ₋₁₄₂ | 1750 | M | M | M | -3.83 | 501 ± 10 | 72.5 ± 1.5 | - | - ^e |
| 98 | HD 168941 | 423±36 | 255±28 | 1700 ⁺⁸⁵⁰ ₋₄₅₀ | 2394 ⁺⁶³⁷ ₋₄₂₁ | 6940 | S | M | M | -2.21 | 387 ± 24 | 62.5 ± 3.9 | - | c |
| " | | | | | | | | | | 19.41 | 27 ± 23 | 4.7 ± 3.9 | | |
| 99 | HD 169582 | 624±22 | 484±13 | - | 1681 ⁺¹⁹⁷ ₋₁₆₀ | 3500 | M | M | S | -10.17 | 1422 ± 12 | 166.3 ± 1.4 | c+CN | a |
| 100 | HD 170634 | 153±7 | 122±6 | - | 417 ⁺⁹ ₋₉ | 420 | S | S | M | -11.89 | 2436 ± 14 | 220.8 ± 1.3 | c+CN | c |
| 101 | HD 170740 | 69±1 | 42±1 | 350 ⁺¹⁷ ₋₁₃ | 230 ⁺⁷ ₋₇ | 320 | M | S | M | -10.83 | 567 ± 4 | 77.2 ± 0.6 | - | b |
| 104 | HD 172175 | 658±22 | 488±13 | 4480 ⁺⁹⁹⁰ ₋₉₉₀ | 2147 ⁺³⁰⁰ ₋₂₃₆ | 4200 | M | M | M | -16.00 | 273 ± 6 | 40.7 ± 0.9 | c+CN | a |
| " | | | | | | | | | | -9.12 | 2051 ± 15 | 181.9 ± 1.3 | c+CN | |
| 105 | HD 177989 ^{LR} | 281±26 | 170±13 | 1100 ⁺⁵²⁰ ₋₄₁₉ | 2398 ⁺⁴⁰⁵ ₋₃₀₅ | - | | | | -1.86 | 640 ± 29 | 91.4 ± 4.2 | - | - ^e |
| 106 | HD 180968 | 102±6 | 67±6 | 560 ⁺¹³⁰ ₋₁₃₀ | 561 ⁺³⁴ ₋₃₄ | 400 | S | S | S | -11.64 | 569 ± 28 | 82.8 ± 4.1 | - | a |
| 107 | HD 185418 | 154±4 | 112±3 | 1050 ⁺¹⁵⁰ ₋₁₂₀ | 740 ⁺²¹ ₋₂₀ | 1050 | S | - | M | -11.23 | 406 ± 5 | 52.9 ± 0.6 | - ^v | a |
| 108 | HD 185859 | 233±4 | 179±3 | 1830 ^l ₋₁₆₀ | 1086 ⁺⁴⁹ ₋₂₃₈ | 1350 | M | S | S | -7.38 | 1090 ± 5 | 114.8 ± 0.6 | c+CN | b |
| 109 | HD 198478 ^{LR} | 203±10 | 149±8 | 1390 ^l ₋₂₉₀ | 1164 ⁺¹⁷¹ ₋₁₇₁ | 1260 | S | S | S | -13.99 | 868 ± 17 | 129.5 ± 2.6 | - | c |
| 110 | HD 200775 ^{LR} | 80±3 | 52±2 | 445 ⁺⁶⁵ ₋₆₅ | 357 ⁺⁶ ₋₆ | 400 | S | S | S | -13.30 | 112 ± 3 | 18.8 ± 0.6 | c+CN | c |
| 111 | HD 203532 | 50.5±1 | 30.5±1 | 270 ⁺⁵⁰ ₋₁₇ | 289 ⁺⁴ ₋₄ | 250 | S | S | S | 14.55 | 968 ± 4 | 108.6 ± 0.4 | c+CN | a |
| 112 | HD 204827 | 280±12 | 208±8 | 1960 ^l ₋₃₄₀ | 1269 ⁺¹⁸³ ₋₁₄₃ | 1630 | M | - | M | -17.29 | 2672 ± 23 | 279.6 ± 2.4 | c+CN | a |
| 113 | HD 206267 | 249±17 | 159±8 | 1170 ⁺³²⁰ ₋₂₀₀ | 1191 ⁺⁷⁵¹ ₋₃₃₇ | 1030 | M | - | M | -7.74 | 222 ± 9 | 35.7 ± 1.4 | - ^v | a |
| " | | | | | | | | | | -17.77 | 401 ± 8 | 56.5 ± 1.1 | | |
| 114 | HD 207198 ^{LR} | 316±18 | 226±9 | 1970 ^l ₋₁₀₀ | 999 ⁺⁵⁸ ₋₃₂ | 1185 | S | - | S | -13.32 | 1930 ± 21 | 241.3 ± 2.6 | c+CN | b |
| 115 | HD 209975 ^{LR} | 241±13 | 173±7 | 1530 ⁺²⁷⁰ ₋₂₇₀ | 857 ⁺¹⁰¹ ₋₁₃₂ | 1210 | S | - | S | -13.40 | 680 ± 14 | 105.2 ± 2.2 | - | a |
| 116 | HD 210121 | 93±2 | 56±2 | 430 ⁺⁴⁵ ₋₃₀ | 339 ⁺¹⁶ ₋₁₄ | 475 | M | S | S | -14.57 | 896 ± 3 | 98.8 ± 0.3 | c+CN | a |
| 117 | HD 218376 | 150±3 | 97±3 | 760 ⁺⁸⁰ ₋₇₀ | 375 ⁺⁴¹ ₋₃₄ | 470 | M | - | M | -16.87 | 238 ± 14 | 38.5 ± 2.3 | - | a |
| " | | | | | | | | | | -9.38 | 265 ± 9 | 40.3 ± 1.4 | | |
| " | | | | | | | | | | -2.88 | 16 ± 6 | 2.8 ± 1.1 | | |
| 118 | HD 259105 | 271±7 | 189±5 | 1580 ⁺²¹⁰ ₋₁₅₅ | 1471 ⁺¹⁹¹ ₋₁₅₃ | 1800 | M | M | M | 17.89 | 131 ± 8 | 21.5 ± 1.4 | w-CN | d |
| " | | | | | | | | | | 24.22 | 392 ± 9 | 56.8 ± 1.3 | | |
| 119 | HD 281159 ^{LR} | 95±8 | 67±6 | 620 ^l ₋₁₆₀ | 1062 ⁺⁸²⁶ ₋₄₀₁ | 370 | S | S | S | 13.28 | 1044 ± 19 | 143.4 ± 2.6 | c+CN | c |
| 120 | HD 284839 | 202±8 | 145±5 | 1300 ⁺¹⁹⁰ ₋₁₉₀ | 648 ⁺¹⁷ ₋₁₆ | 680 | S | S | M | 14.35 | 250 ± 6 | 37.4 ± 1.0 | c+CN | a |
| 121 | HD 284841 | 187±7 | 131±6 | 1130 ⁺²⁶⁰ ₋₁₈₀ | 606 ⁺¹⁵ ₋₁₄ | 557 | S | - | M | 15.14 | 289 ± 5 | 42.7 ± 0.8 | c+CN | a |
| 122 | HD 287150 | 174±9 | 127±6 | 1116 ^l ₋₂₅₀ | 432 ⁺⁹ ₋₈₈ | 377 | M | S | S | 20.45 | 1364 ± 11 | 145.1 ± 1.1 | - | |
| 123 | HD 292167 | 587±22 | 422±15 | 3640 ⁺⁵⁶⁰ ₋₅₆₀ | 4782 ⁺¹³⁷⁸ ₋₉₂₇ | 5000 | M | M | M | 26.37 | 916 ± 10 | 115.9 ± 1.2 | c+CN | b |
| 124 | HD 294264 | 137±8 | 89±6 | 705 ⁺²¹⁵ ₋₁₃₀ | 445 ⁺⁹ ₋₉ | 870 | M | S | M | 26.10 | 97 ± 7 | 16.3 ± 1.2 | w-CN | d |
| " | | | | | | | | | | 29.42 | 239 ± 4 | 35.7 ± 0.6 | | |
| 125 | HD 294304 | 177±9 | 122±9 | 1030 ^l ₋₂₃₀ | 802 ⁺³¹ ₋₃₂ | 940 | M | - | S | 22.03 | 557 ± 10 | 77.8 ± 1.4 | c+CN | d |
| 126 | HD 315021 | 209±15 | 131±13 | 955 ⁺²²⁵ ₋₂₃₀ | 1259 ⁺¹³⁴ ₋₁₁₁ | 870 | M | - | S | -5.35 | 196 ± 9 | 30.9 ± 1.4 | - | d |
| 127 | HD 315023 | 229±17 | 127±11 | 810 ⁺²⁴⁰ ₋₁₆₀ | 1095 ⁺⁷⁵ ₋₆₆ | 1135 | M | - | M | -25.27 | 80 ± 8 | 13.3 ± 1.4 | - | d |
| " | | | | | | | | | | -4.47 | 315 ± 10 | 45.5 ± 1.4 | | |
| 128 | HD 315024 | 212±13 | 131±9 | 940 ⁺²⁷⁰ ₋₁₈₀ | 1326 ⁺¹⁰⁷ ₋₉₂ | 1225 | M | M | S | -4.80 | 382 ± 5 | 42.7 ± 0.9 | w-CN | d |
| 129 | HD 315031 | 229±9 | 138±6 | 975 ⁺¹²⁵ ₋₁₂₅ | 1407 ⁺¹³² ₋₁₆₁ | 1650 | M | M | S | -4.51 | 382 ± 5 | 54.1 ± 0.7 | w-CN | d |
| 130 | HD 315032 | 260±11 | 170±9 | 1290 ⁺²⁰⁰ ₋₁₉₀ | 996 ⁺⁸⁷ ₋₇₄ | 1835 | M | M | S | -5.18 | 438 ± 11 | 60.4 ± 1.5 | w-CN | d |
| 131 | HD 315033 | 261±13 | 161±8 | 1133 ⁺²³⁸ ₋₁₆₀ | 1578 ⁺¹⁴⁶ ₋₁₃₄ | 1354 | M | M | S | -4.57 | 402 ± 6 | 55.9 ± 0.9 | w-CN | d |
| 132 | HD 326309 | 518±54 | 333±34 | 2390 ⁺⁶⁹⁰ ₋₆₉₀ | 1599 ⁺¹⁵² ₋₁₂₈ | 1600 | M | M | M | -3.54 | 270 ± 16 | 41.4 ± 2.4 | c+CN | a |
| " | | | | | | | | | | 3.29 | 512 ± 14 | 66.3 ± 1.9 | | |

Table A.3. – continued –

| 1 | 2 | 3 | 4 | 5 | 6 | 7 | 8 | 9 | 10 | 11 | 12 | 13 | 14 | 15 |
|-----|-----------|---------------|---------------|--------------------------------------|--------------------------------------|------|------------|------|-----|--------------------------|--|---------------------------------------|----------|-------|
| ID | Target | Ca II | | Distance | | | Components | | | K I | | | Environ. | WISE |
| | | EW(K) (mÅ) | EW(H) (mÅ) | Ca II | GAIA (pc) | Sp/L | Ca II K | Na I | K I | v _∞ (km/s) | log N (10 ⁹ /cm ²) | EW (mÅ) | class | class |
| 133 | HD 326330 | 417±15 | 264±14 | 1870 ⁺³⁹⁰ ₋₂₈₀ | 1774 ⁺²¹⁷ ₋₁₇₅ | 2050 | M | M | M | -12.55 -5.74 2.09 | 19 ± 8 192 ± 9 706 ± 11 | 3.3 ± 1.4 30.5 ± 1.5 87.1 ± 1.4 | w-CN | a |
| " | | | | | | | | | | 1.74 | 587 ± 17 619 ± 14 | 83.8 ± 2.4 81.9 ± 1.8 | | |
| 134 | HD 326332 | 403±35 | 246±18 | 1670 ⁺⁶³⁰ ₋₃₆₀ | 1575 ⁺¹⁴³ ₋₁₂₁ | 1380 | M | M | M | -10.85 | 237 ± 12 | 39.1 ± 1.9 | c+CN | a |
| " | | | | | | | | | | 1.64 | 570 ± 7 | 76.9 ± 0.9 | w-CN | a |
| 135 | HD 326333 | 391±16 | 260±13 | 1980 ⁺⁴⁶⁰ ₋₂₂₀ | 1500 ⁺¹³⁴ ₋₁₁₄ | 1960 | M | M | M | -10.64 -8.67 1.69 | 437 ± 7 945 ± 8 | 64.3 ± 1.2 106.9 ± 0.9 | c+CN | a |
| " | | | | | | | | | | | | | w-CN | |
| 136 | HD 326364 | 378±23 | 196±13 | 1597 ⁺³⁷⁹ ₋₂₃₃ | 1679 ⁺¹⁴⁹ ₋₁₂₇ | 1859 | M | M | M | | | | | |
| " | | | | | | | | | | | | | | |

Notes: ^LRlow resolution spectrum has insufficient resolving power for classification as single-cloud sight-line, ^t saturated line, ^v: ignored because lines have different velocities, ^e: WISE image shows artifact.

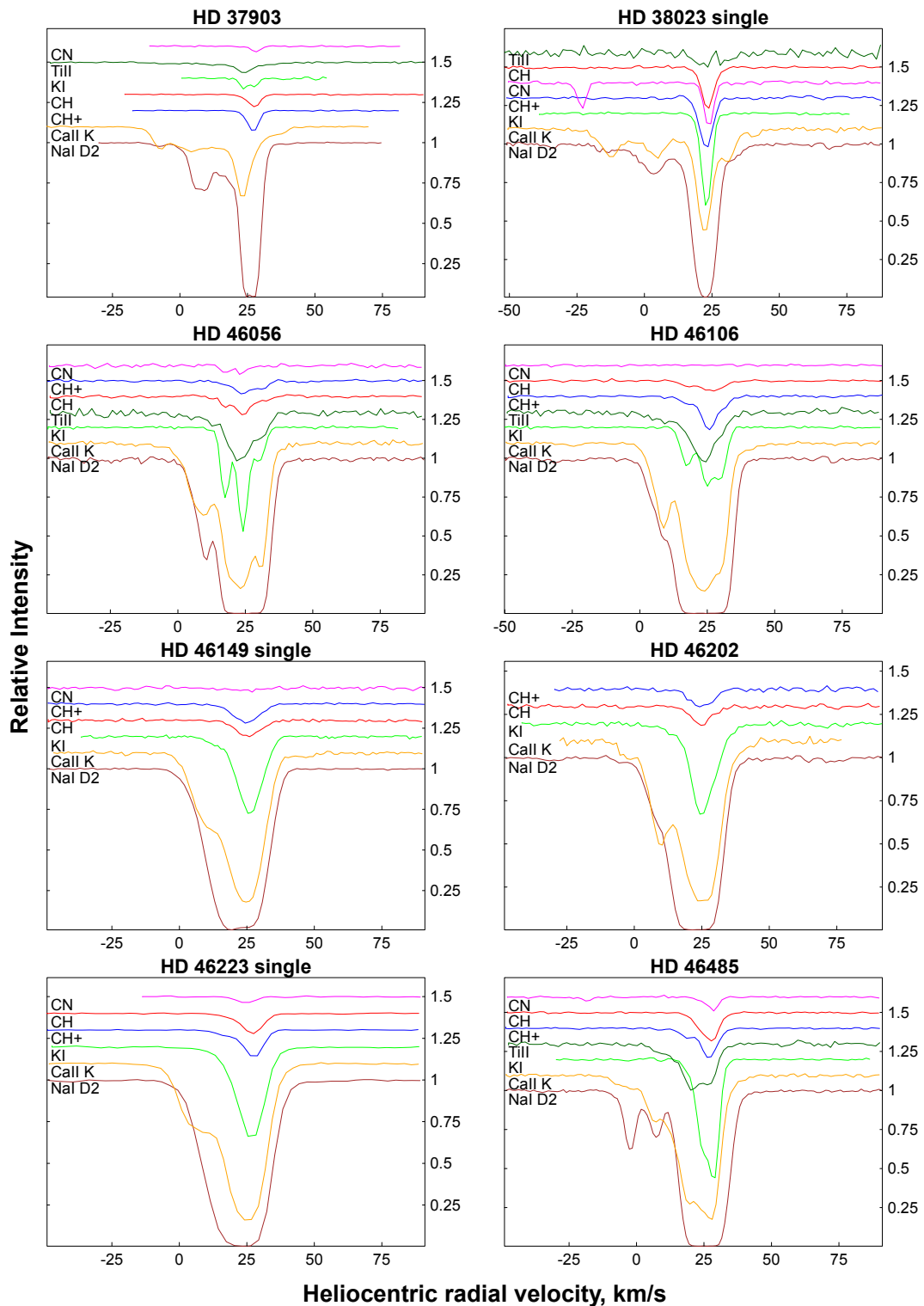


Fig. A.1. Heliocentric velocity profiles of Ti II 3383.8 Å (dark green), CN 3874.6 Å (magenta), CH 4300.3 Å (red), CH^+ 4232.5 Å (blue), K I 7699 Å (green), Ca II K 3933.7 Å (orange), Na I D2 5889 Å (brown). Single-cloud sightlines are marked “single”.

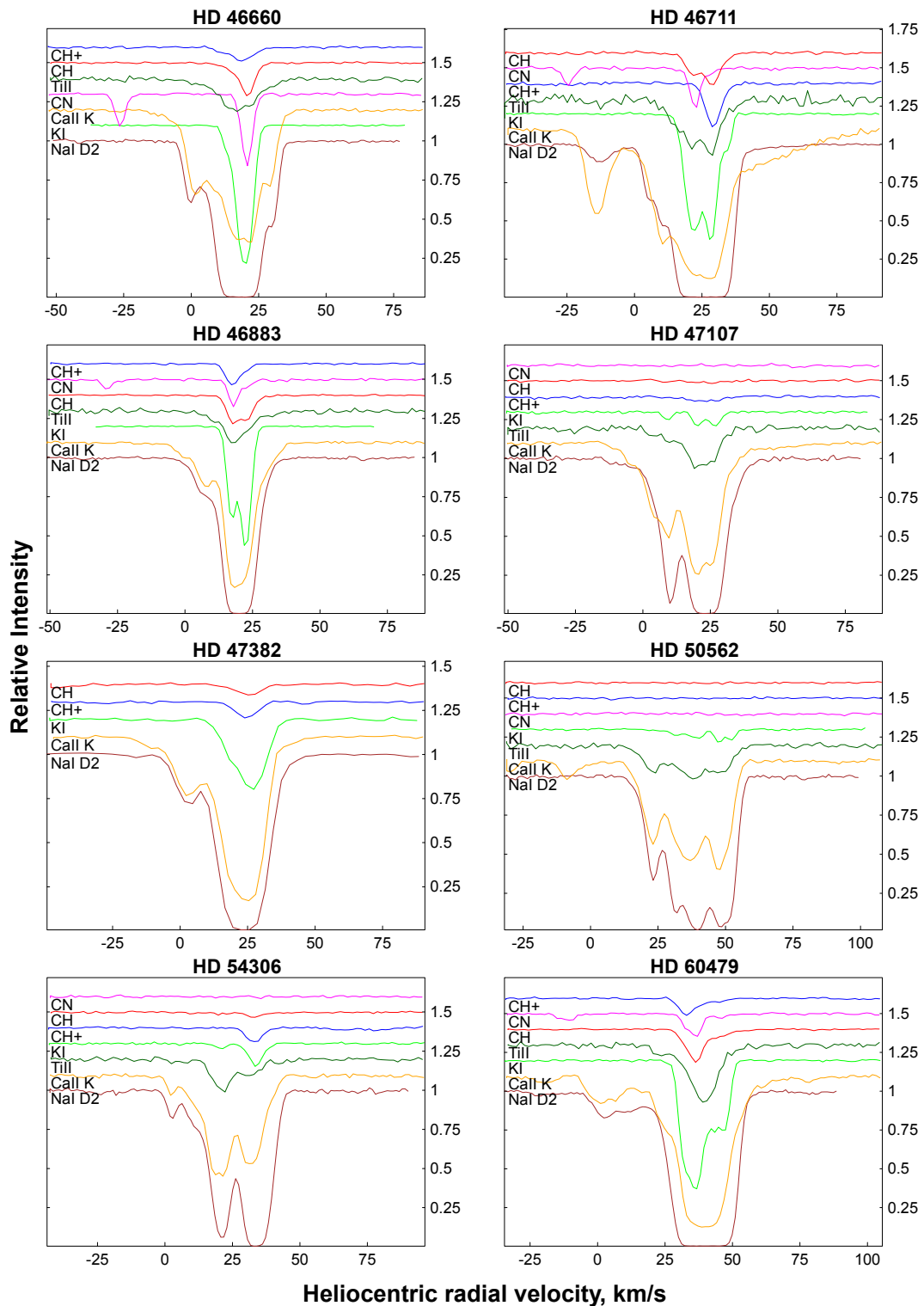


Fig. A.2. Velocity profiles of Ti II 3383.8 Å (dark green), CN 3874.6 Å (magenta), CH 4300.3 Å (red), CH⁺ 4232.5 Å (blue), K I 7699 Å (green), Ca II K 3933.7 Å (orange), Na I D2 5889 Å (brown).

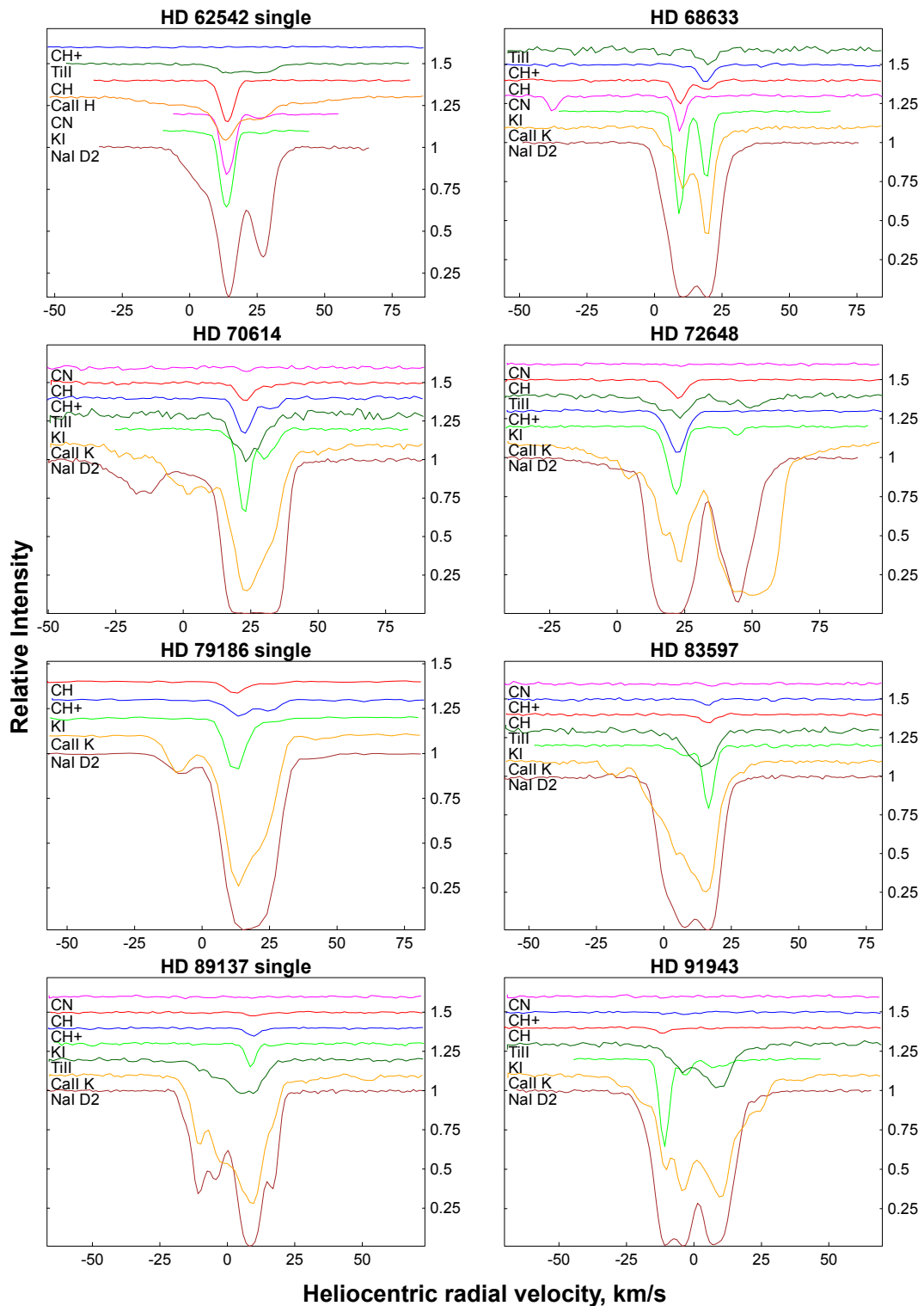


Fig. A.3. Velocity profiles of Ti II 3383.8 Å (dark green), CN 3874.6 Å (magenta), CH 4300.3 Å (red), CH^+ 4232.5 Å (blue), K I 7699 Å (green), Ca II K 3933.7 Å (orange), Na I D2 5889 Å (brown). Single-cloud sightlines are marked “single”.

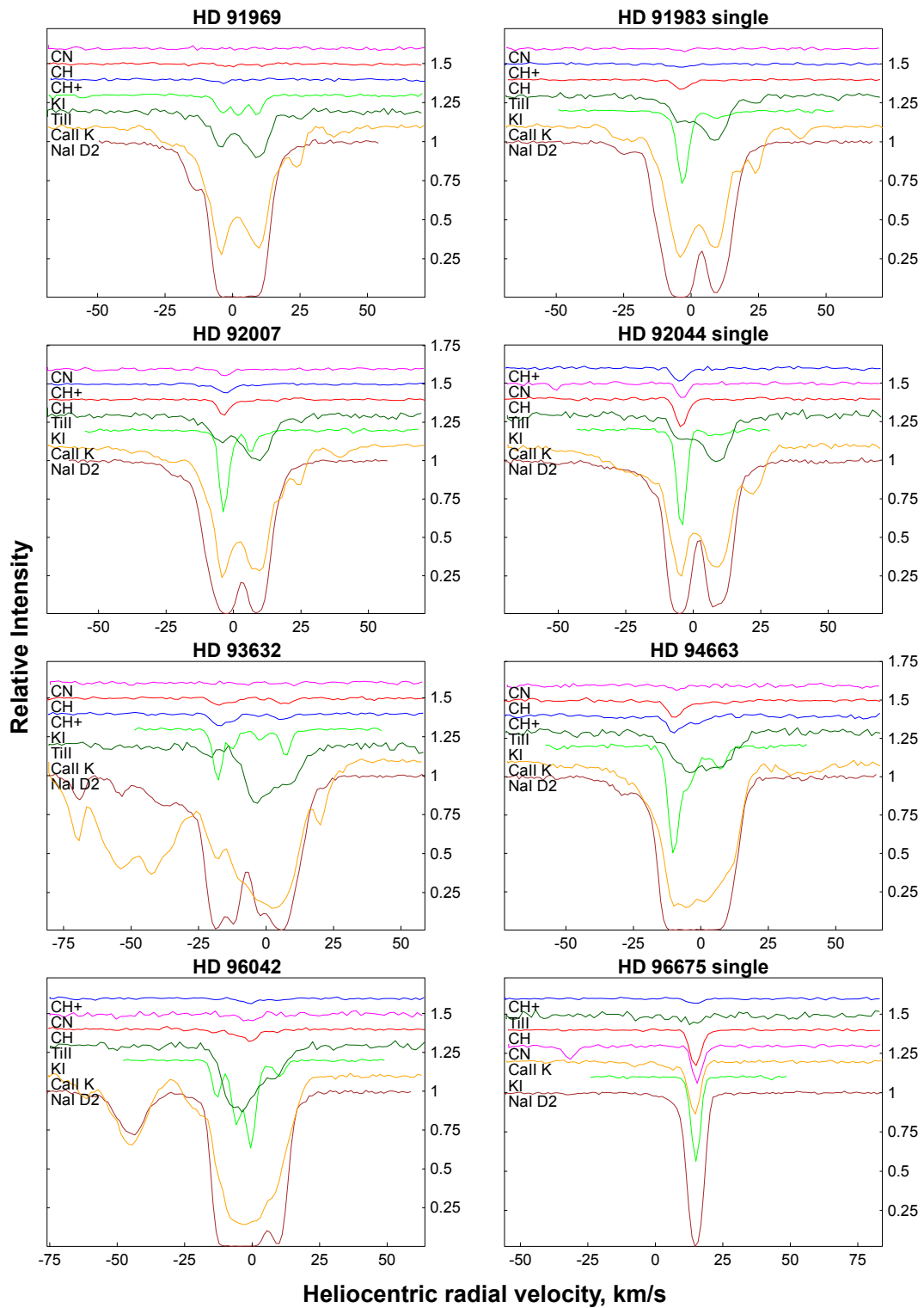


Fig. A.4. Velocity profiles of Ti II 3383.8 Å (dark green), CN 3874.6 Å (magenta), CH 4300.3 Å (red), CH^+ 4232.5 Å (blue), KI 7699 Å (green), Ca II K 3933.7 Å (orange), Na I D2 5889 Å (brown). Single-cloud sightlines are marked “single”.

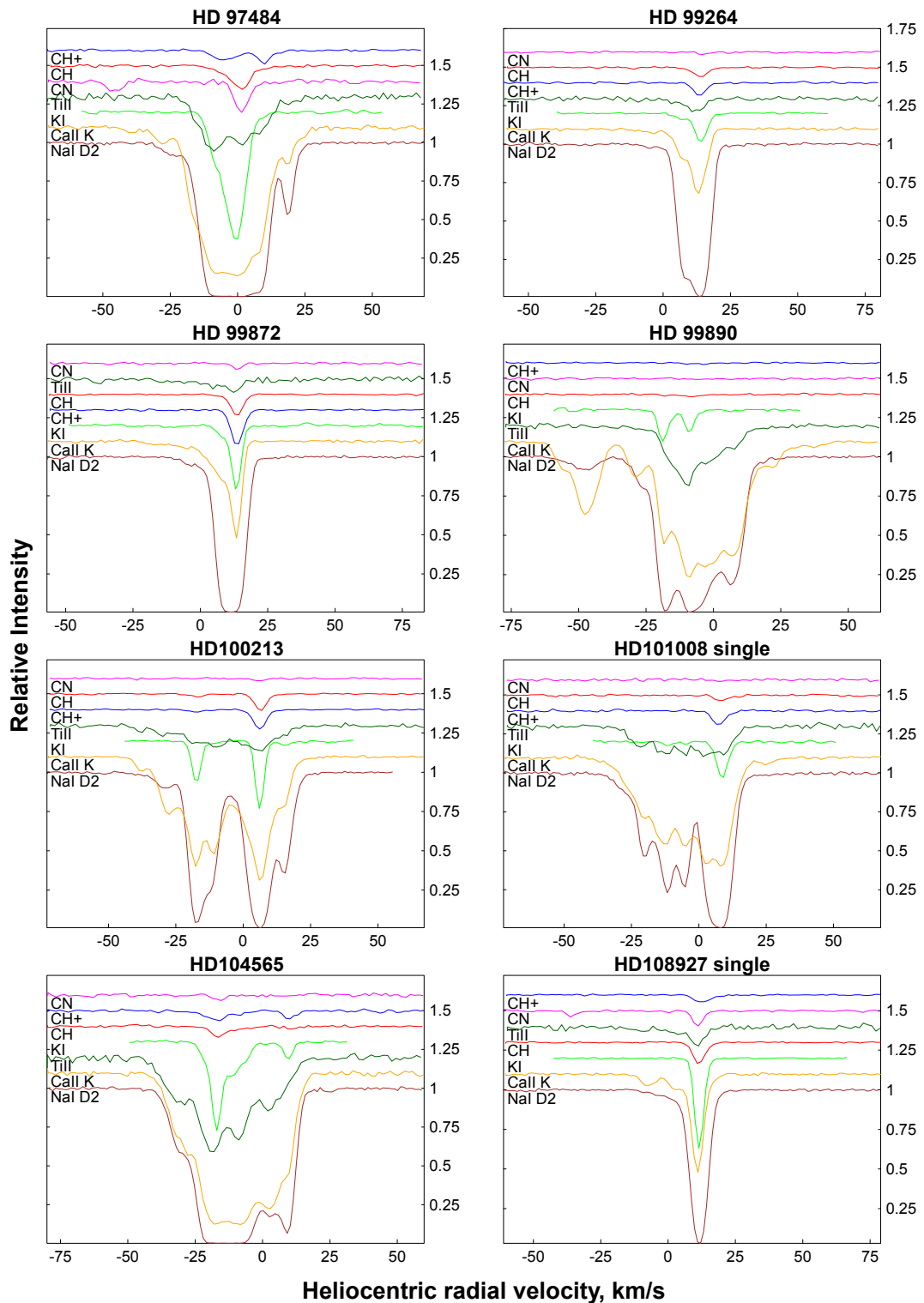


Fig. A.5. Velocity profiles of Ti II 3383.8 Å (dark green), CN 3874.6 Å (magenta), CH 4300.3 Å (red), CH^+ 4232.5 Å (blue), KI 7699 Å (green), Ca II K 3933.7 Å (orange), Na I D2 5889 Å (brown). Single-cloud sightlines are marked “single”.

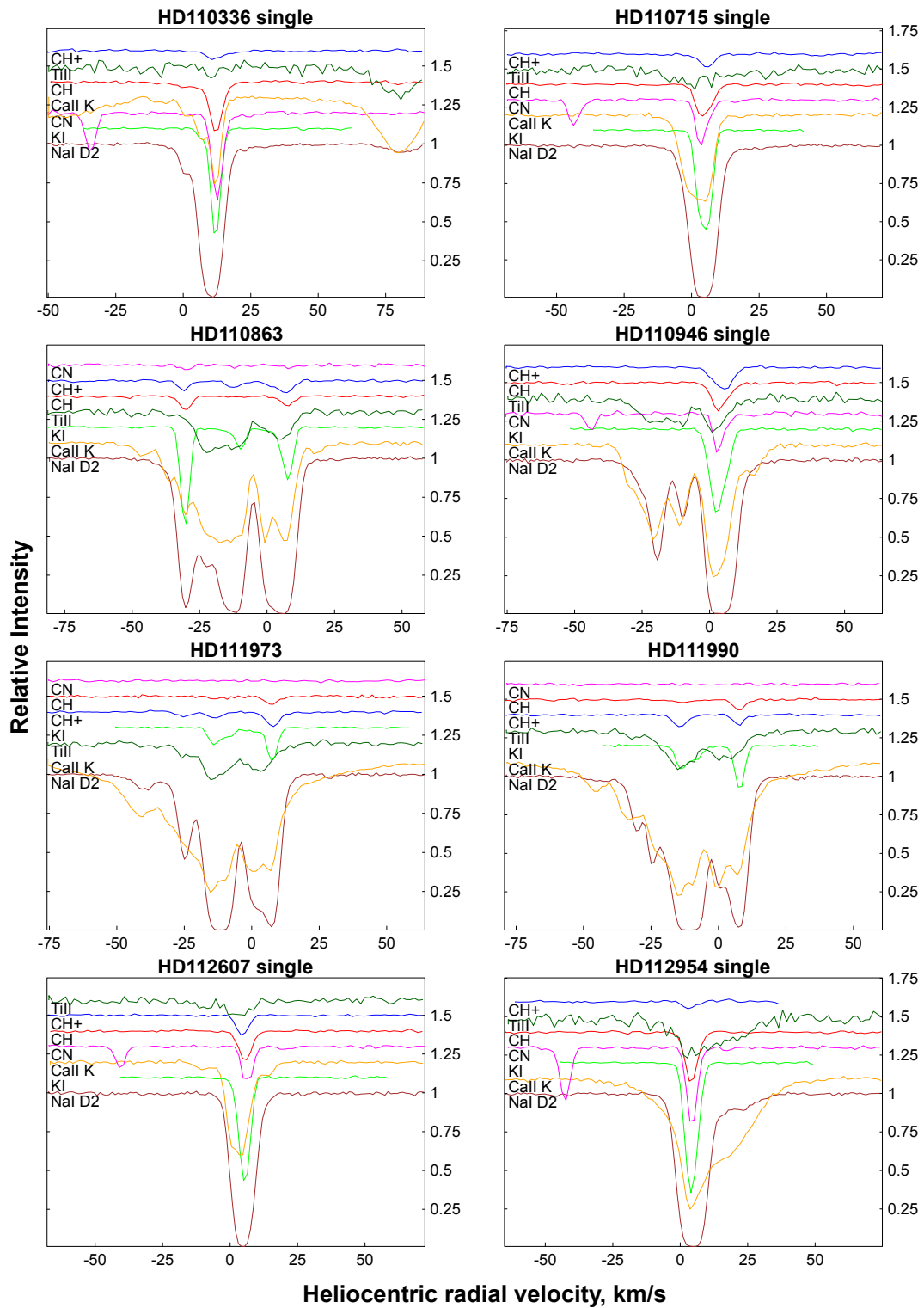


Fig. A.6. Velocity profiles of Ti II 3383.8 Å (dark green), CN 3874.6 Å (magenta), CH 4300.3 Å (red), CH^+ 4232.5 Å (blue), K I 7699 Å (green), Ca II K 3933.7 Å (orange), Na I D2 5889 Å (brown). Single-cloud sightlines are marked “single”.

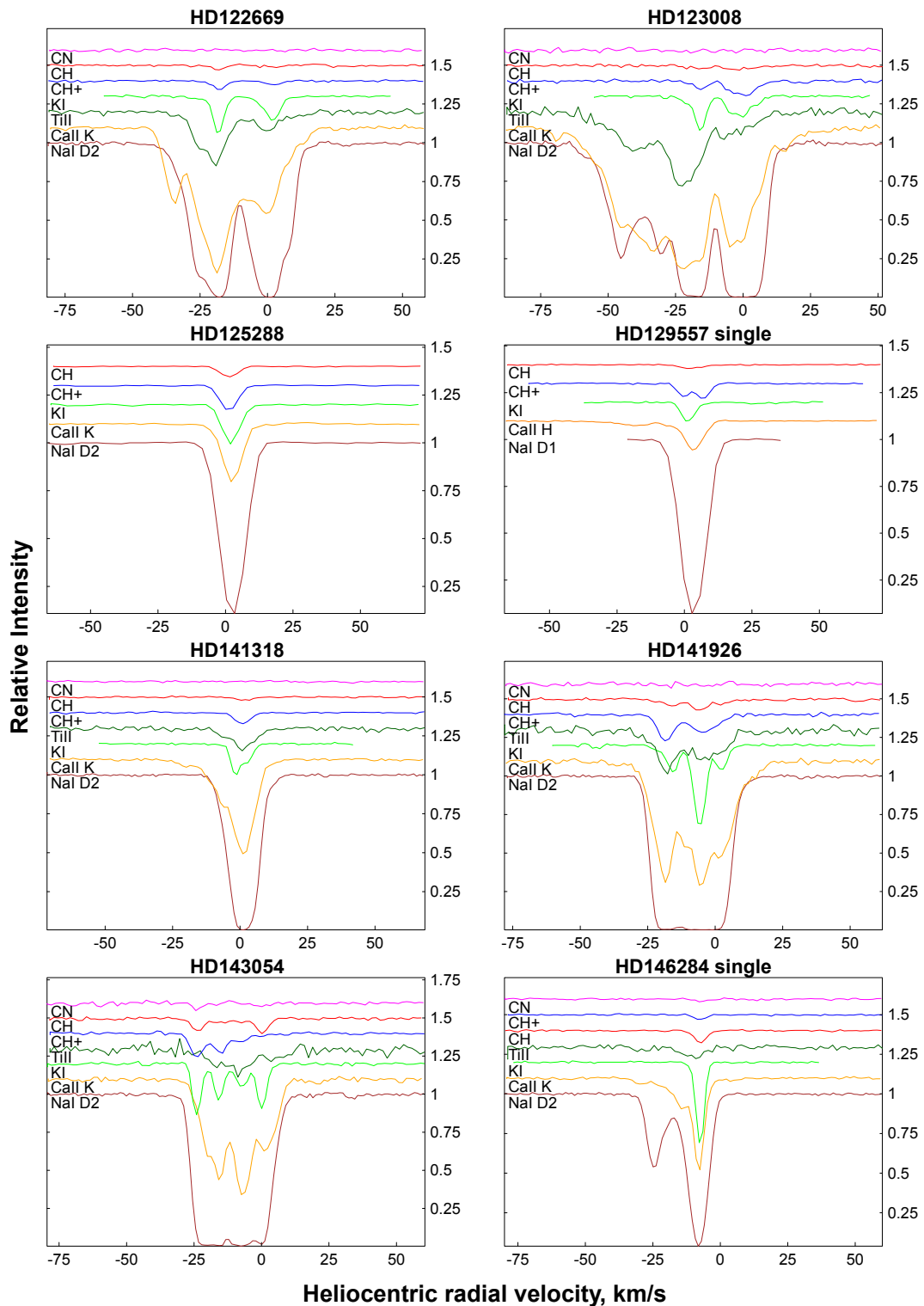


Fig. A.7. Velocity profiles of Ti II 3383.8 Å (dark green), CN 3874.6 Å (magenta), CH 4300.3 Å (red), CH^+ 4232.5 Å (blue), KI 7699 Å (green), Ca II K 3933.7 Å (orange), Na I D2 5889 Å (brown). Single-cloud sightlines are marked “single”.

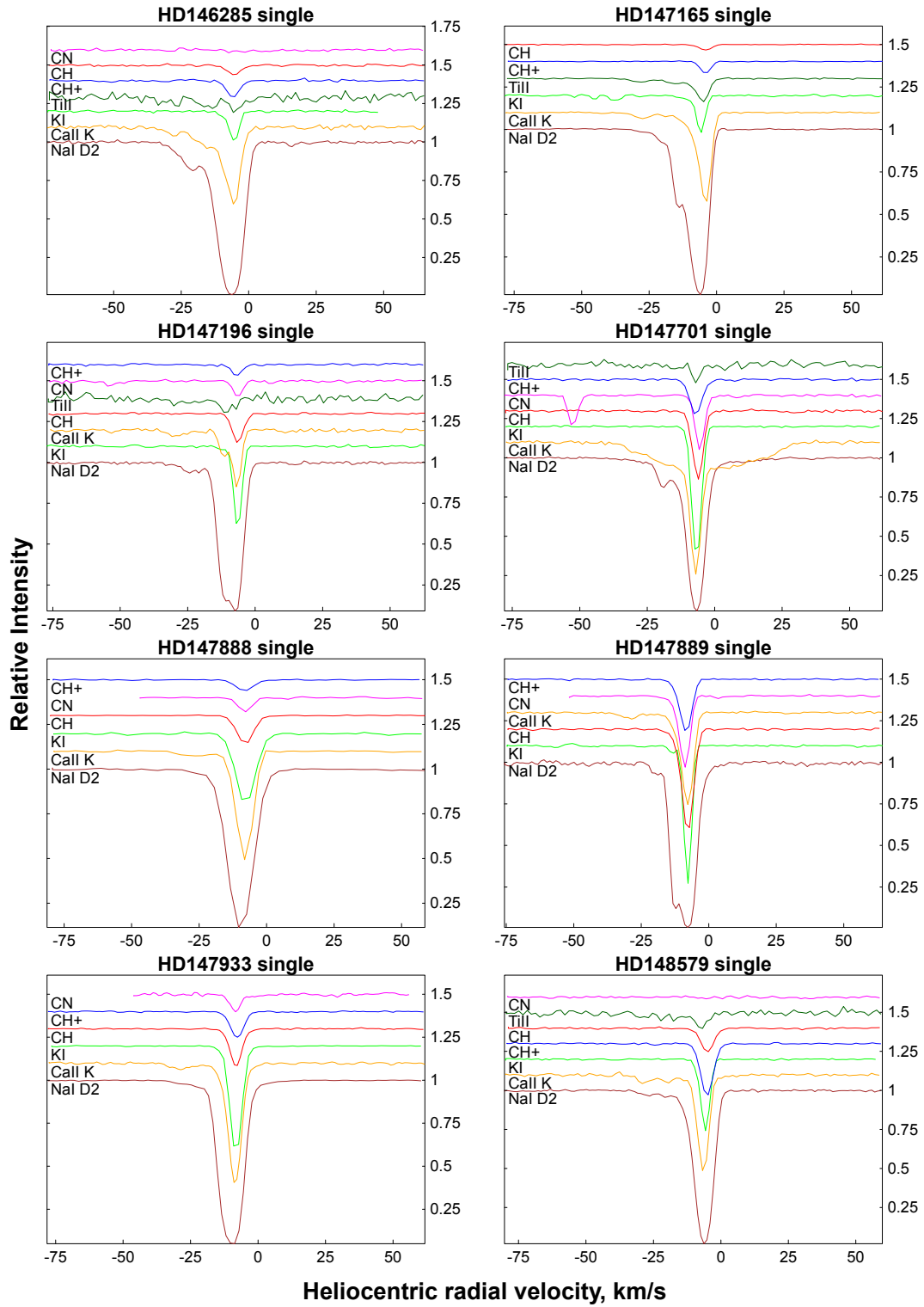


Fig. A.8. Velocity profiles of Ti II 3383.8 Å (dark green), CN 3874.6 Å (magenta), CH 4300.3 Å (red), CH^+ 4232.5 Å (blue), K I 7699 Å (green), Ca II K 3933.7 Å (orange), Na I D2 5889 Å (brown). Single-cloud sightlines are marked “single”.

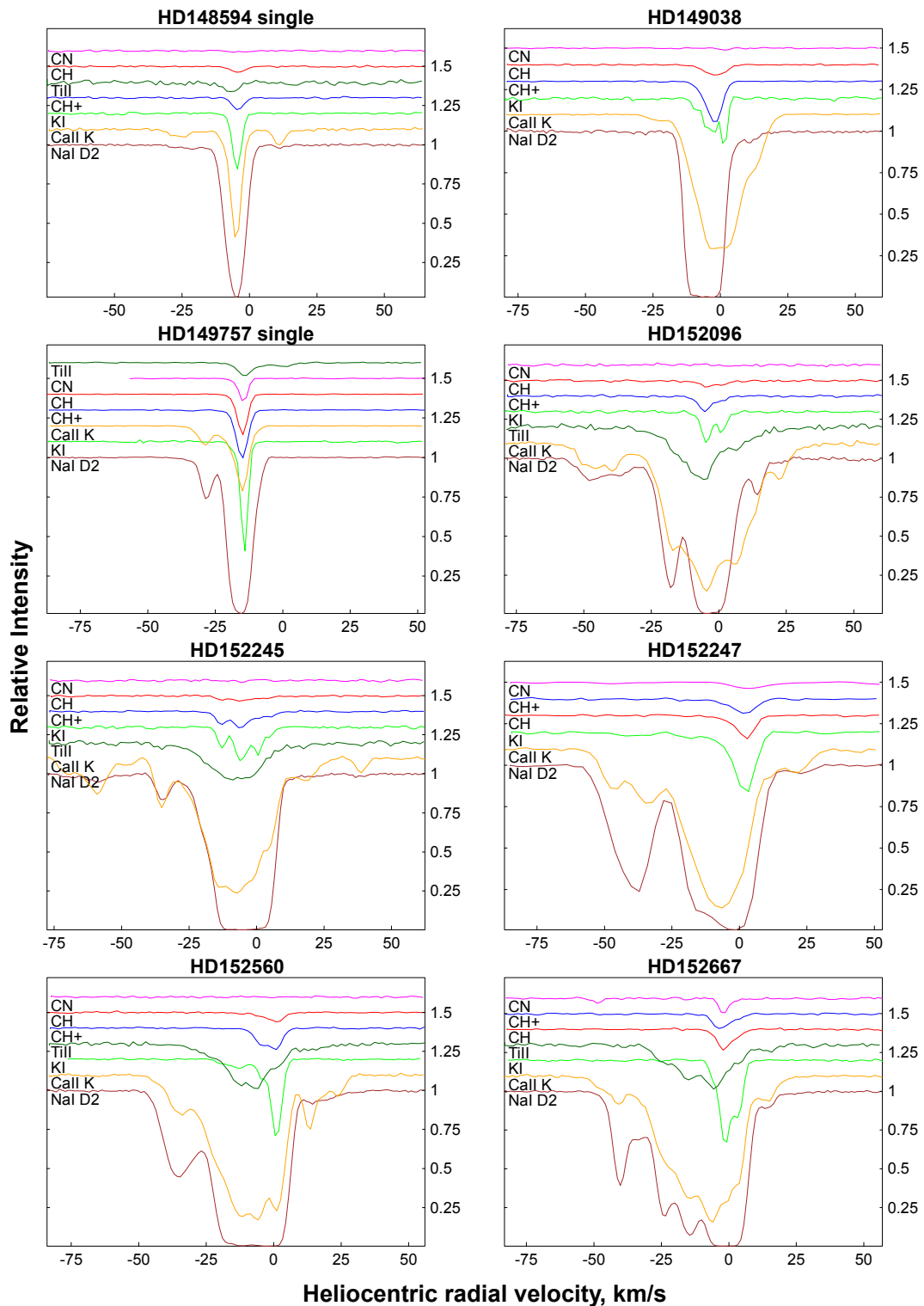


Fig. A.9. Velocity profiles of Ti II 3383.8 Å (dark green), CN 3874.6 Å (magenta), CH 4300.3 Å (red), CH⁺ 4232.5 Å (blue), K I 7699 Å (green), Ca II K 3933.7 Å (orange), Na I D2 5889 Å (brown). Single-cloud sightlines are marked “single”.

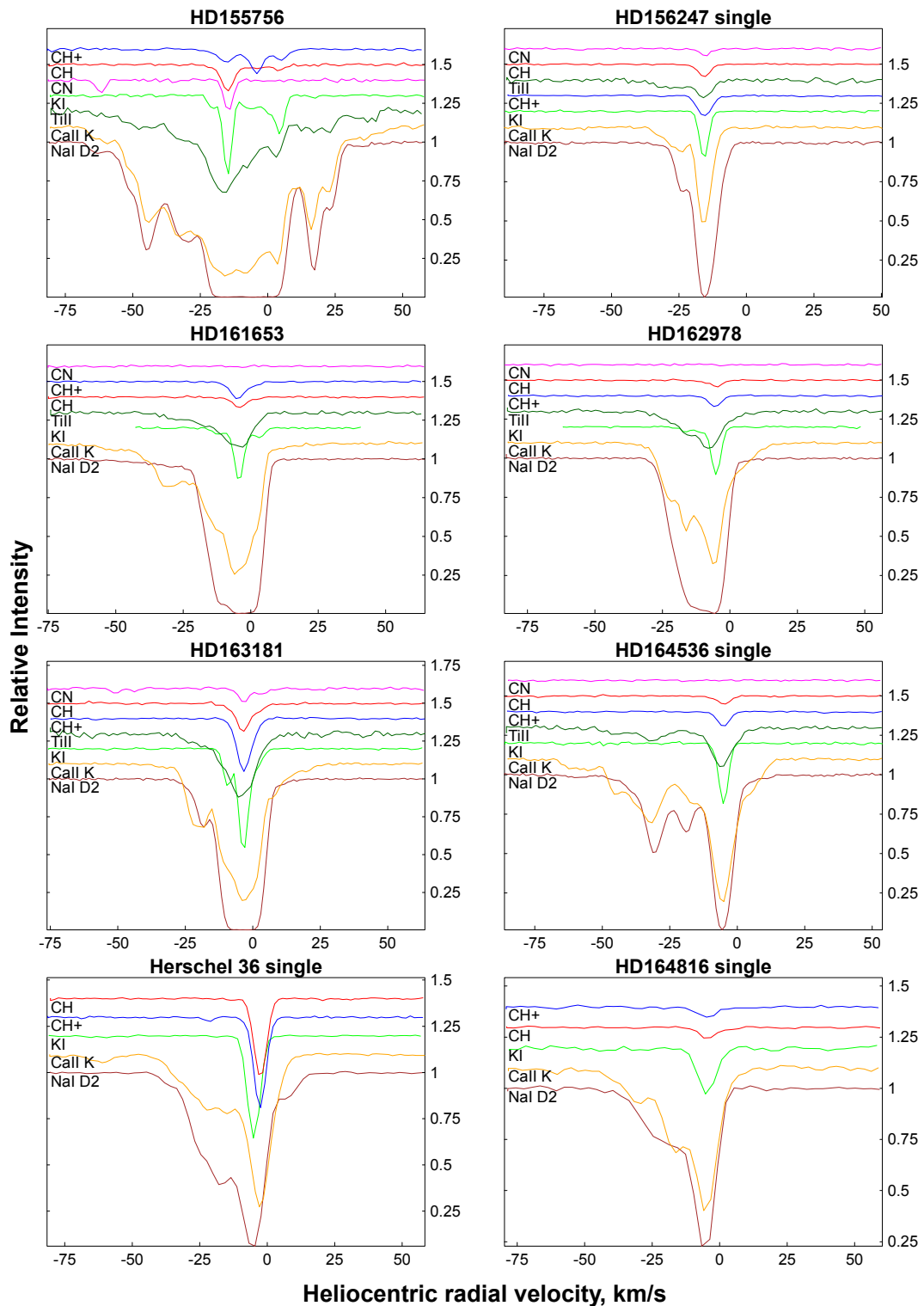


Fig. A.10. Velocity profiles of Ti II 3383.8 Å (dark green), CN 3874.6 Å (magenta), CH 4300.3 Å (red), CH^+ 4232.5 Å (blue), KI 7699 Å (green), Ca II K 3933.7 Å (orange), Na I D2 5889 Å (brown). Single-cloud sightlines are marked “single”.

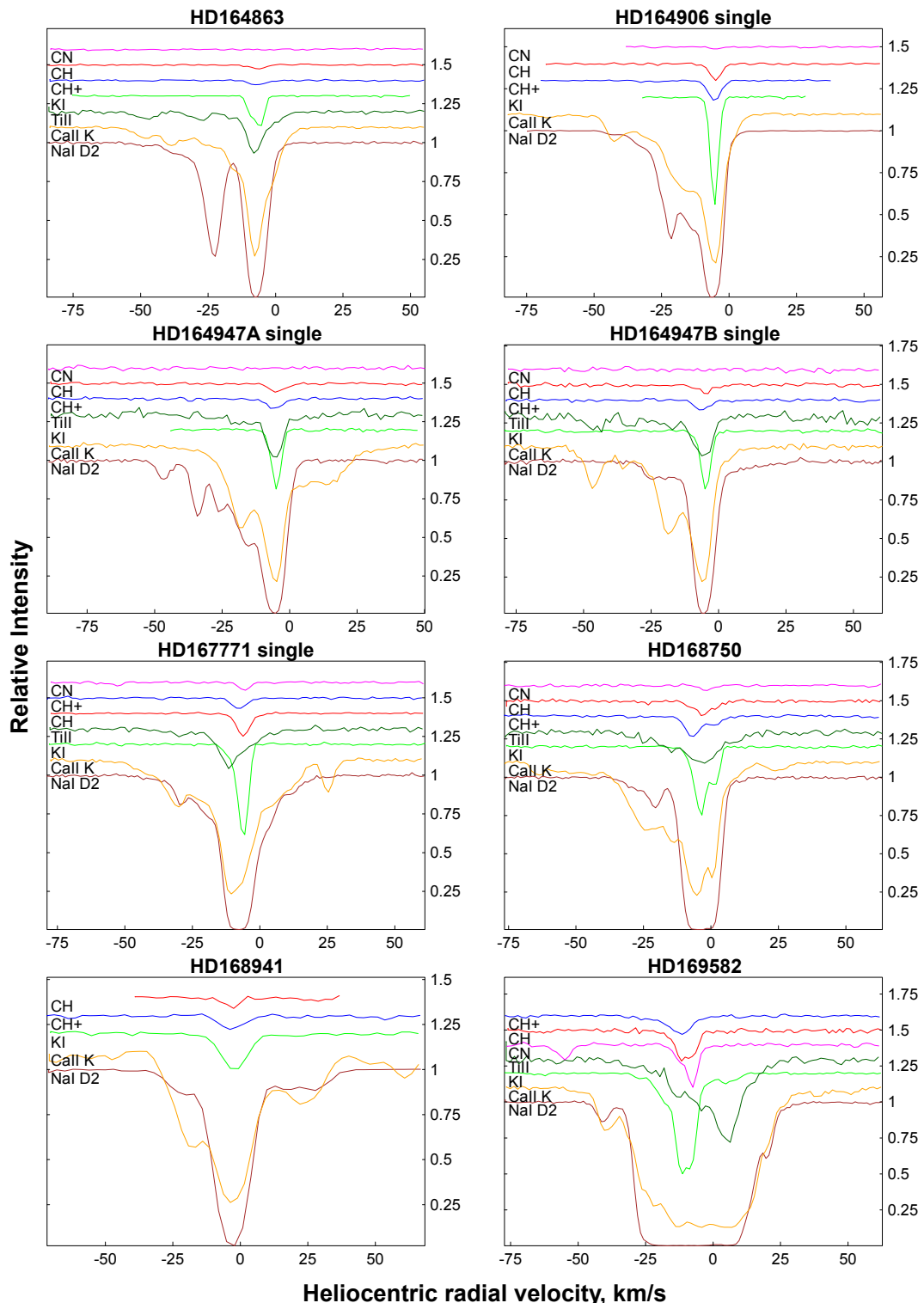


Fig. A.11. Velocity profiles of Ti II 3383.8 Å (dark green), CN 3874.6 Å (magenta), CH 4300.3 Å (red), CH⁺ 4232.5 Å (blue), KI 7699 Å (green), Ca II K 3933.7 Å (orange), Na I D2 5889 Å (brown). Single-cloud sightlines are marked “single”.

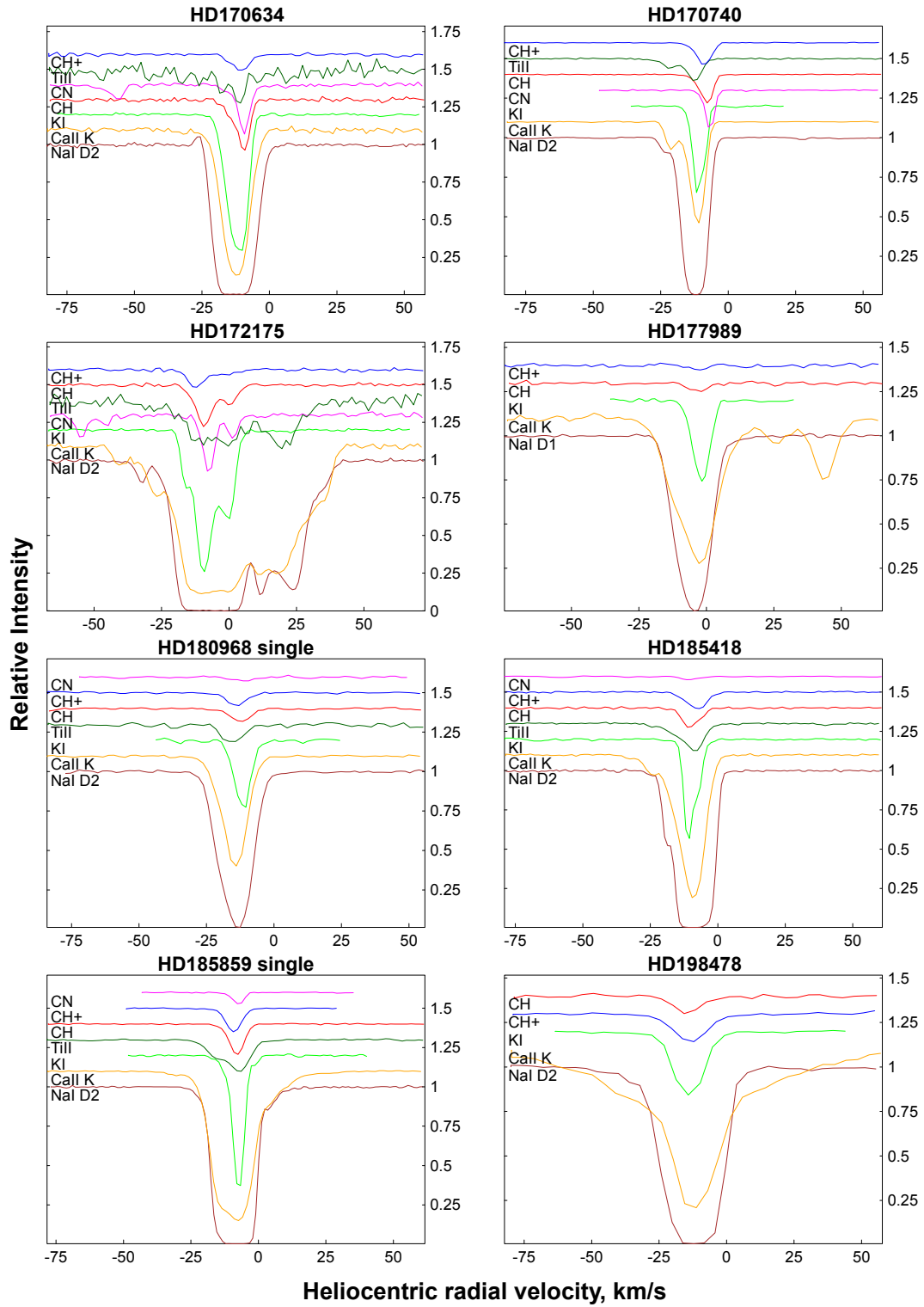


Fig. A.12. Velocity profiles of Ti II 3383.8 Å (dark green), CN 3874.6 Å (magenta), CH 4300.3 Å (red), CH^+ 4232.5 Å (blue), KI 7699 Å (green), Ca II K 3933.7 Å (orange), Na I D2 5889 Å (brown). Single-cloud sightlines are marked “single”.

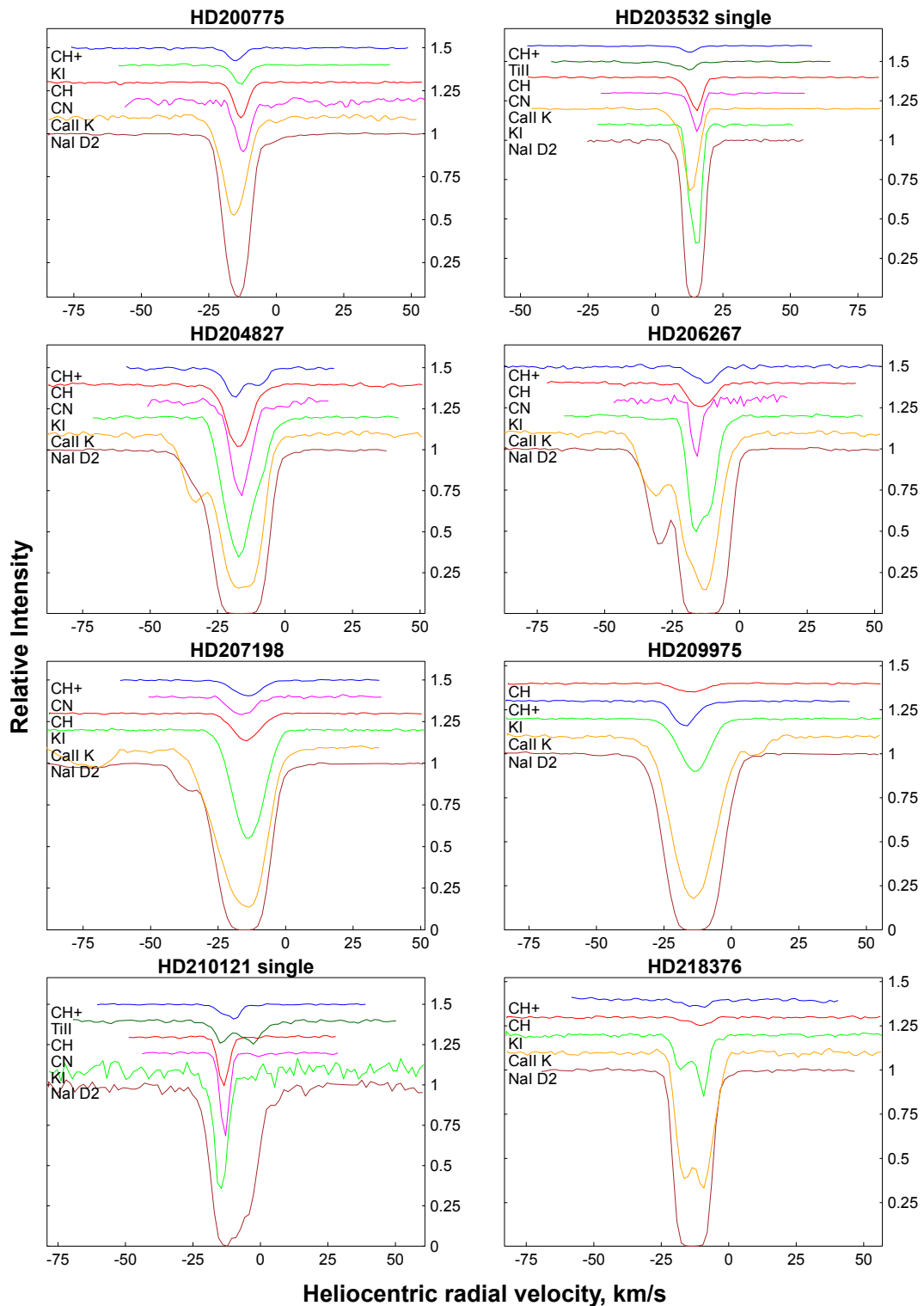


Fig. A.13. Velocity profiles of Ti II 3383.8 Å (dark green), CN 3874.6 Å (magenta), CH 4300.3 Å (red), CH⁺ 4232.5 Å (blue), K I 7699 Å (green), Ca II K 3933.7 Å (orange), Na I D2 5889 Å (brown). Single-cloud sightlines are marked “single”.

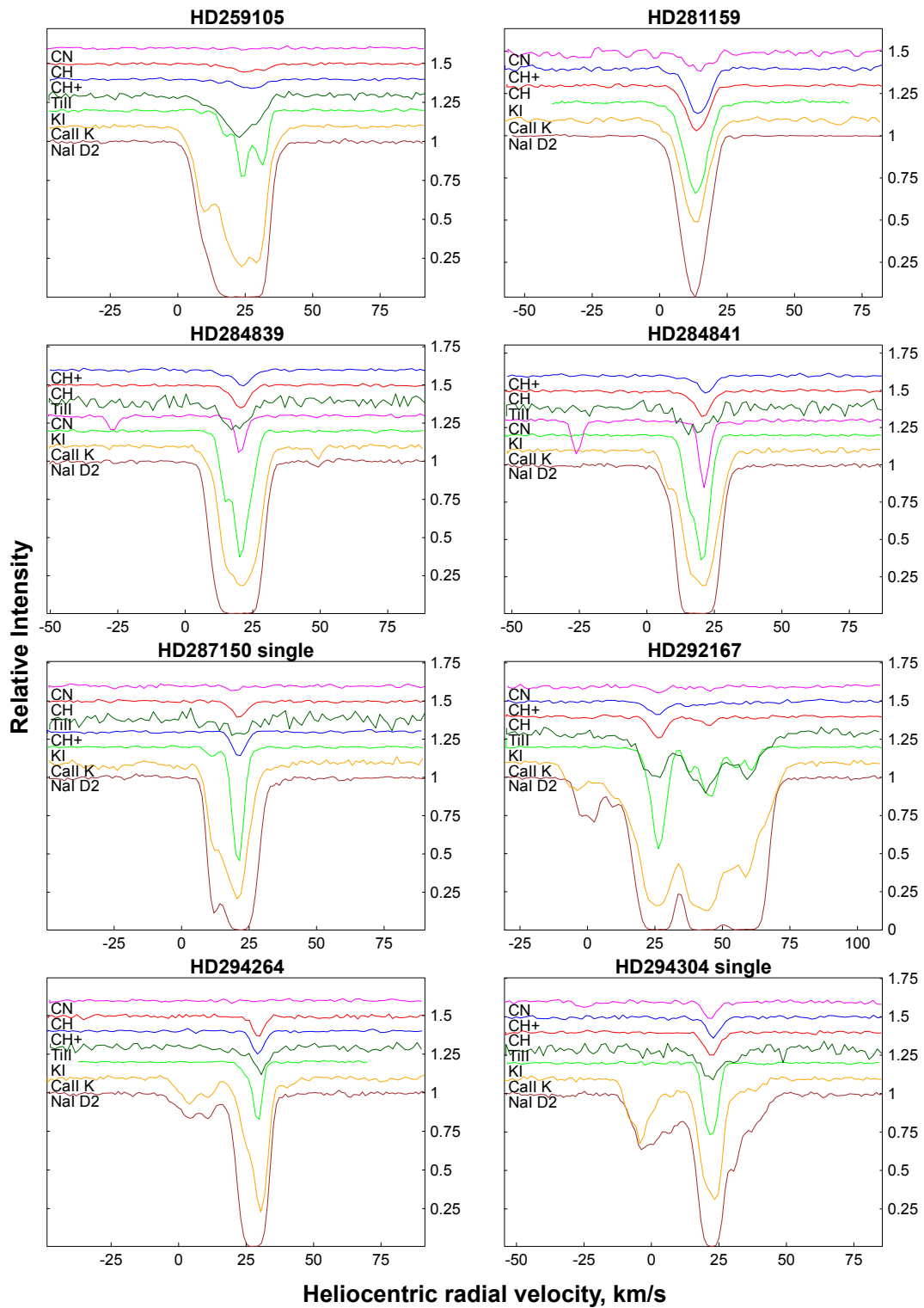


Fig. A.14. Velocity profiles of Ti II 3383.8 Å (dark green), CN 3874.6 Å (magenta), CH 4300.3 Å (red), CH^+ 4232.5 Å (blue), KI 7699 Å (green), Ca II K 3933.7 Å (orange), Na I D2 5889 Å (brown). Single-cloud sightlines are marked “single”.

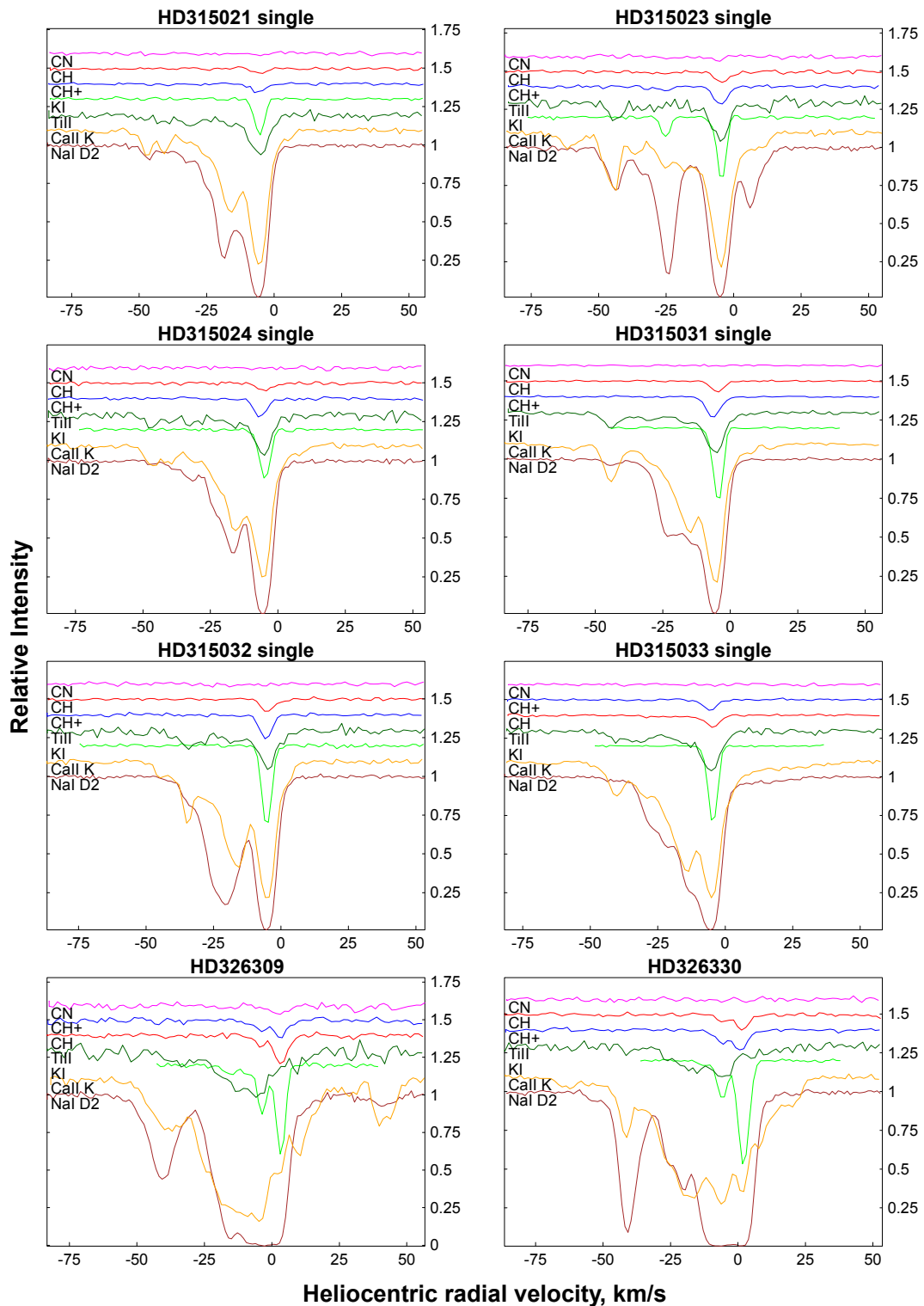


Fig. A.15. Velocity profiles of Ti II 3383.8 Å (dark green), CN 3874.6 Å (magenta), CH 4300.3 Å (red), CH⁺ 4232.5 Å (blue), K I 7699 Å (green), Ca II K 3933.7 Å (orange), Na I D2 5889 Å (brown). Single-cloud sightlines are marked “single”.

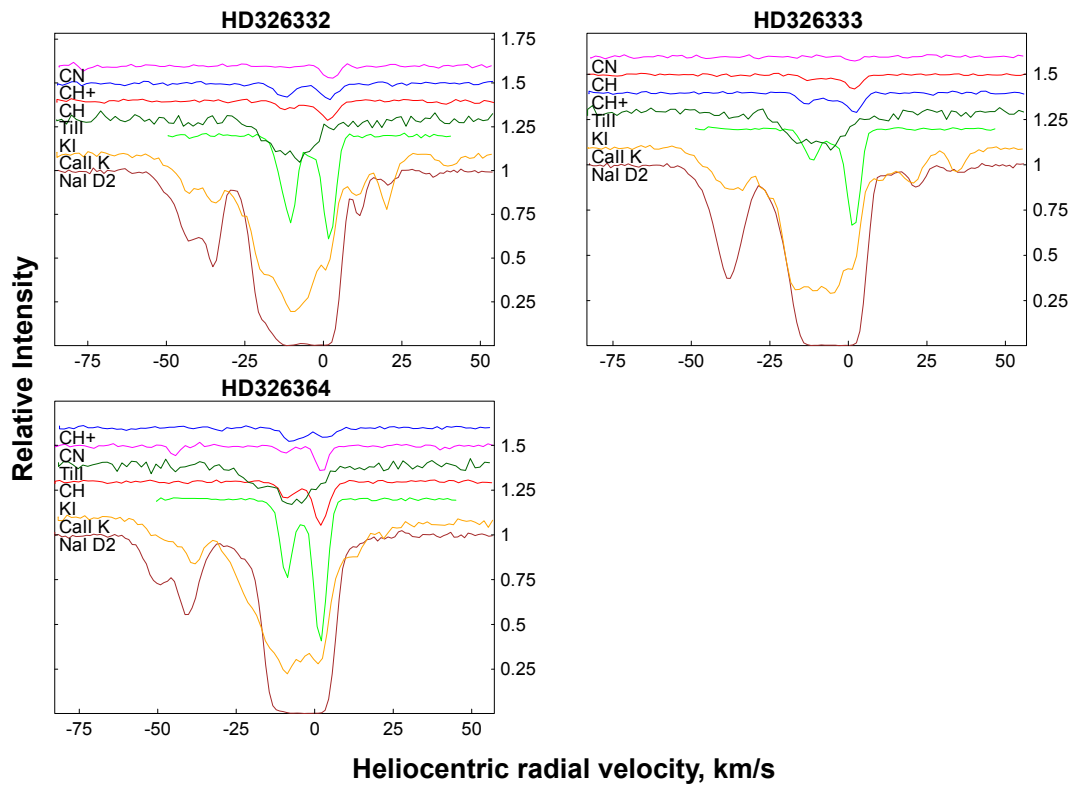


Fig. A.16. Velocity profiles of Ti II 3383.8 Å (dark green), CN 3874.6 Å (magenta), CH 4300.3 Å (red), CH⁺ 4232.5 Å (blue), K I 7699 Å (green), Ca II K 3933.7 Å (orange), Na I D2 5889 Å (brown).